Shibaura Institute of Technology

Graduate School of Engineering and Science

Doctor thesis

# Hysteresis Modeling and Adaptive Model Predictive Control of Tap-Water Driven McKibben Muscles

Wataru Kobayashi

Student ID: NB12102

Major: Functional control system

Supervisor: Prof. Kazuhisa Ito

# Abstract

This dissertation is concerned with tap-water driven McKibben muscles, especially modeling and displacement control of them. Tap-water driven McKibben muscles can improve environmental friendliness of systems because water hydraulics is 100% oil-free. In addition, tap-water can remove driving sources such as compressors and hydraulic pumps. On the other hand, the control performance of them is a considerable problem, which is a same problem as conventional McKibben type muscles, and then it should be solved to expand their application.

To improve the control performance of the muscles, we propose two model-based control methods, which are MRAC and MPC because conventional PI control cannot compensate the nonlinearities of the muscles such as hysteresis. Although there are some muscle models used in model-based control, there exists some problems. For examples, model structure is complex to be used as nominal models of the muscle, they require lots of measurements of muscle physical parameters, and simple models cannot take account of the nonlinearities. For these problems, combination of linear system identification method and Bouc-Wen hysteresis model is applied to obtain muscle models because it can be easily possible to obtain the linear muscle model with system identification. Moreover it is reasonable to combine the Bouc-Wen hysteresis model with the obtained linear model due to the structure of the linear model.

Accuracy of the model is shown by experiments. As a result, the model can express the characteristics of the muscle under not only no-load condition but also loaded condition. However, the model must be derived under loaded condition because difference between the loaded and no-load conditions are huge. In addition, the structure of the model is simple and then it can be used for not only the static analysis such as hysteresis analysis but also a nominal model of model-based controls. Proposed model is used as a nominal muscle model of some model-based controls. The model-based controls applied here are model reference adaptive control (MRAC) and model pre-

dictive control (MPC). Although the control performance of MPC is the best, the difference of them are small for under no-load condition. Under loaded condition (3.5 kg), the performance of MPC becomes worst due to accuracy of the nominal model. Note that the performance of MRAC under loaded condition can be improved because MRAC has adaptive parameter estimation algorithm. However, the characteristics of the muscle consistently change and then the adaptive algorithm consistently work. It means that the muscle parameters are updated under transient response at all times. This leads degradation of the control performance because MRAC cannot ensure transient response.

To solve the problem of MPC under loaded condition, recursive least squares (RLS) algorithm is applied to the control method. RLS algorithm can update the parameters of the muscle on real-time basis. In addition, its convergence is faster than the speed of MRAC. Hence, adaptive model predictive control (AMPC) can control the muscle displacement under loaded condition. Additional improvement is the use of multiple coincident points for MPC and AMPC. When prediction horizon is set to 5 steps, which means 0.5 s here, the control performance of both control methods, which use only one coincident point, is degraded because of failure of prediction. For this problem, the use of multiple coincident points and evaluation function are proposed. This can take into account of all predicted error in prediction horizon.

We also propose predictive On/Off control to improve the control performance of On/Off control when only On/Off valves are used in muscle systems because the performance of the valves is lower than the performance of the servo and proportional valves, although On/Off valves are generally cheaper than the servo and proportional valves. The proposed On/Off control is based on the concept of MPC, which are one-step-ahead estimation and evaluation function. The proposed control method can consider the predicted muscle displacement and then can reduce the undesirable switching of the valves. Hence, it is shown that the On/Off control can be improved by using the concept of MPC.

Two estimation methods without stroke sensors and rotary potentiometers are proposed: 1) Estimation method I with a flex sensor and 2) Estimation method II with a flowmeter. Although the method I can estimate the muscle displacement, there exists some problems such as position of the flex sensor, repetitive operation, and torsion of the flex sensor covered with rubber tube. On the other hand, the method II is reasonable for estimation of the displacement of tap-water driven McKibben

muscles because it can be easily possible to implement. In addition, the control performance of the displacement control with estimation method II is shown by experiment and then it is shown that the maximum steady-state error is less than 5 mm.

Finally, achievements of this dissertation are as follows: 1) Modeling of the muscles with system identification method and application of Bouc-Wen hysteresis model, 2) Application of MPC with RLS algorithm and validation of its control performance, and 3) Estimation methods with flex sensors and flowmeters. The structure of the derived model is simple and the muscle paremeters including hysteresis paramenters can be easily tuned. Hence, the model is reasonable to use in model-based control. AMPC can control the muscle displacement under not only no-load but also loaded conditions. It is a great benefit that compensation of loads can be achieved because it is one of considerable problems of the muscles. Moreover, the proposed control method can improve the control performance, although the control performance of the muscle in general is lower than cases using any other actuators. The proposed estimation methods are useful for systems that require high flexibility and user friendliness such as rehabilitation devices.

# Acknowledgments

I wish to express my deepest gratitude to my supervisor Professor Kazuhisa Ito of Department of Machinery and control Systems, Systems Engineering and Science, Shibaura Institute of Technology, for his enthusiastic guidance, numerous useful advices, and helpful technical support.

I would like to thank Professor Pierluigi Beomonte Zobel of Department of Industrial and Information Engineer and Economics, University of L'Aquila, Italy, for not only technical support but also his hospitality during my stay in Italy for exchange program.

I would also like to thank Professor Shin-ichirou Yamamoto of Department of Bioscience and Engineering, Systems Engineering and Science, Shibaura Institute of Technology.

My special thanks are to all members of Environment and System Control Laboratory. Special thanks to Takashi Okamoto, Kouichi Teraoka, and Keiichiro Yasumori. Without their contribution and support, this work would not have been possible.

By virtue of the above supports, the dissertation has been successfully accomplished.

# Contents

# List of Figures

# List of Tables

# Notation

| | | | |
|---|---|---|---|
| $A, n, \alpha, \beta, \gamma$ | : | Hysteresis parameters | [·] |
| $D(k)$ | : | Outer diameter of muscle | [m] |
| $F(k)$ | : | Normal function | [·] |
| $G_i(z)$ | : | Transfer function of muscle ($i = 1, 2, 3, 4$) | [·] |
| $H_p$ | : | Prediction horizon | [step] |
| $J(k)$ | : | Evaluation function | [·] |
| $L(k)$ | : | Muscle length | [m] |
| $L_0$ | : | Natural length of muscle | [m] |
| $P(k)$ | : | Covariance matrix | [·] |
| $Q(k)$ | : | Weight matrix of error | [·] |
| $R(k)$ | : | Weight matrix of input | [·] |
| $S(H_p)$ | : | Step response | [·] |
| $T_s$ | : | Sampling period | [s] |
| $U(z)$ | : | Applied voltage | [V] |
| $V(k)$ | : | Volume of muscle | [$m^3$] |
| $a(k)$ | : | Gain constant | [·] |
| $b$ | : | Thread length | [m] |
| $e(k)$ | : | Error | [m] |
| $k_i$ | : | Integral gain | [V/m] |
| $k_p$ | : | Proportional gain | [V/m] |
| $l(k)$ | : | Muscle displacement | [m] |
| $p(k)$ | : | Supply pressure | [MPa] |
| $q(k)$ | : | sum of flow | [L] |

| | | | |
|---|---|---|---|
| $r_0$ | : | Diameter of inner tube | [m] |
| $u(k)$ | : | Input | [V] |
| $x(t)$ | : | Displacement | [m] |
| $w(k)$ | : | Hysteresis state variable | [·] |
| $y(k)$ | : | Output | [m] |
| $\gamma_m$ | : | Angle between axis and a thread | [rad] |
| $\eta$ | : | Contraction rate | [·] |
| $\theta(k)$ | : | Parameter vector | [·] |
| $\hat{\theta}(k)$ | : | Estimated parameter vector | [·] |
| $\phi(k)$ | : | Regression vector | [·] |

Subscript

0 : Initial condition

# Acronyms

| | |
|---|---|
| ADL | Activities of daily living |
| AMPC | Adaptive model predictive control |
| ARX | Auto-regressive ex-ogenous |
| BIBO | bounded input - bounded output |
| BWSTT | Body weight support treadmill training |
| KAFO | Knee-ankle-foot orthosis |
| MPC | Model predictive control |
| MRAC | Model reference adaptive control |
| QOL | Quality of life |
| RLS | Recursive least squares |
| WBC | Weight bearing control |

# Chapter 1

# Introduction

## 1.1 Background and motivation

Engineering technology for medical and welfare fields has been strongly required year by year because elderly society is one of the critical issues all over the world. In particular, it is a serious problem in Japan as seen in Fig. 1.1[1]. Its population under 15 years old is 16,803 thousand (13.2% of the total population), the population from 15 to 64 years old is 81,032 thousand (63.8%), and the population over 65 years old is 29,246 thousand (23.0%) in 2010. The population under 15 years old have decreased by 718 thousand from 2005 but its over 65 years old increased by 3,574 thousand.

Decrease of younger people means decrease of workers in these fields, on the other hand, increase of elderly people means increase of people who need medical helps. Thus, substitution of human resources by engineering technology is essential for the situation.

Development of rehabilitation systems demands various knowledge of rehabilitation. In other words, medical and welfare systems without consideration of users or patients have no sense. It has often been a wall between engineers and users. Rehabilitation engineering is not only diversion of industrial mechanical engineering. Important priorities requiring for rehabilitation engineering are safeness and human friendliness, although performance and efficiency are also important factors. Thus, rehabilitation systems must be developed with special attention to humans.

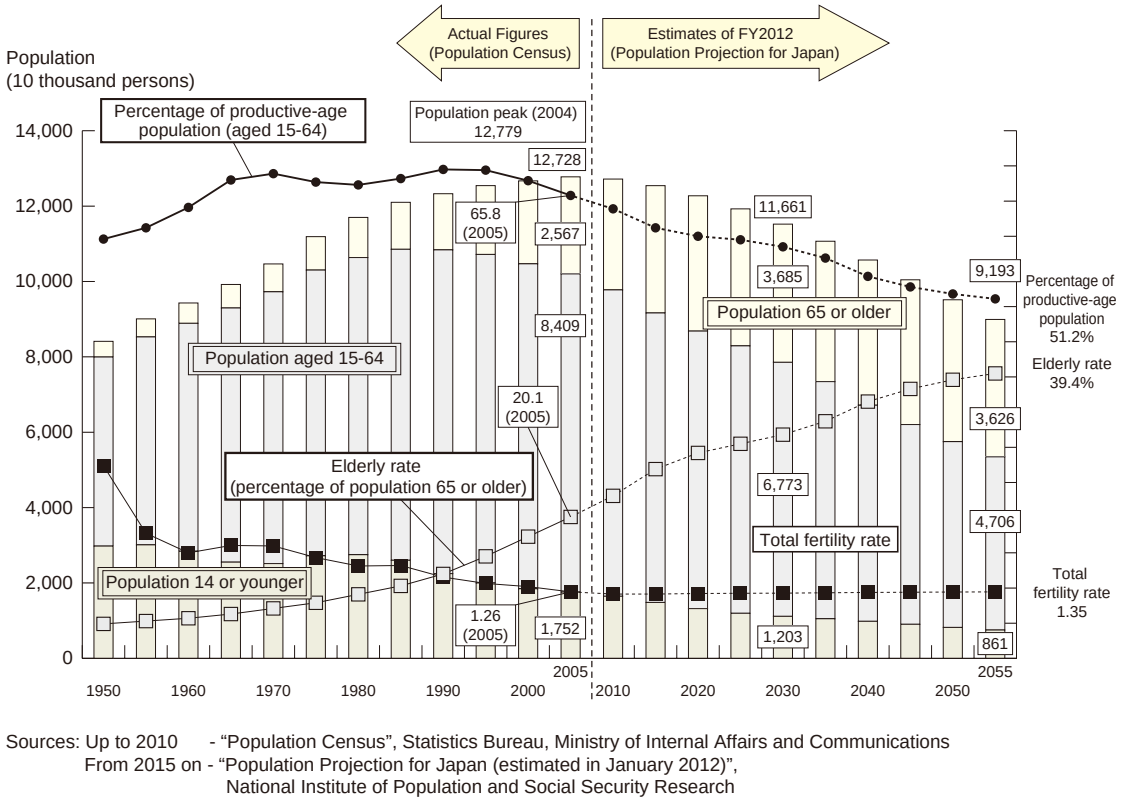


Sources: Up to 2010 - "Population Census", Statistics Bureau, Ministry of Internal Affairs and Communications
From 2015 on - "Population Projection for Japan (estimated in January 2012)",
National Institute of Population and Social Security Research

Fig. 1.1: Change of population composition by age group-Japan: 1950 to 2055[1]

This study is concerned with McKibben muscles as actuators for such systems. Figure 1.2 shows a photo of a McKibben muscle. McKibben muscles, in general, consist of inner rubber tube and outer nylon sleeve[2]. The muscles have some advantages as actuators of rehabilitation systems: 1) Light weight, 2) High power-to-weight ratio, 3) High flexibility, and 4) Low cost[3]. In particular, 1) and 3) are suitable for rehabilitation. Inherent redundancy attributed their structures is also preferable.

On the other hand, there are two problems: The one is driving source and the other is the control performance. In fact, the muscles require compressors as driving sources in pneumatics. Notice that there are only narrow spaces for rehabilitation devices in hospitals. In addition, compressors make noise and vibration, which give discomfortable feelings to patients.

It is well known that the muscles have low control performance because the muscles have strong nonlinearities such as hysteresis and saturation characteristics[4]. Moreover, shorter lifetime of the

muscles due to components such as rubber tube and nylon sleeve should be a problem.

From these backgrounds, we focus on water hydraulic McKibben muscles, especially tap-water driven McKibben muscles. The muscles use tap-water as a driving source because it is no need to use certain power source devices such as compressors or hydraulic pumps.

Application of tap-water can solve the problem mentioned above, that is, installation spaces in hospitals. This also has additional effects on rehabilitation. It is suitable for patients to use water hydraulics, which have 100% oil-free characteristics[5], especially for underwater rehabilitation. Moreover, faster response than the one of pneumatic McKibben muscles is expected when water is used as working fluid because water is incompressible fluid. Thus, tap-water driven McKibben muscles have lots of advantages for rehabilitation.

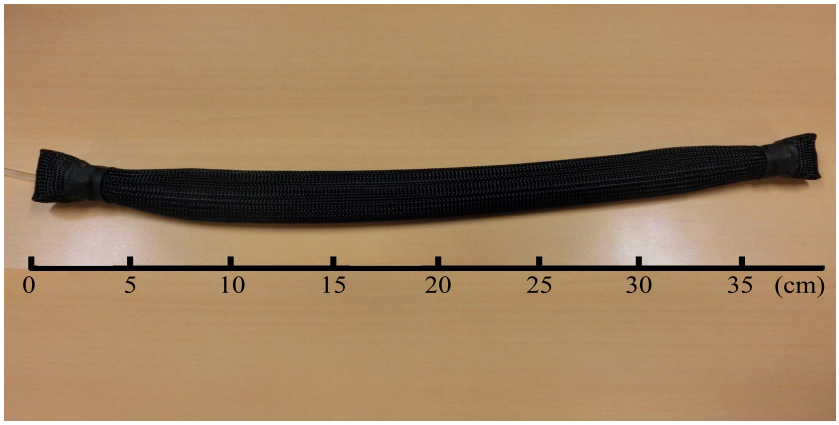


Fig. 1.2: McKibben artificial muscles

## 1.2 Modeling of tap-water driven McKibben muscles

As mentioned above, there still exists the problem of control. In general, PID control has been used for control of McKibben muscles[6]. Its control performance, however, is not enough, and then the gains of the controller have to be tuned by trial and error when some loads exist. This is caused by the characteristics of McKibben muscles, which are drastically affected by loads. There is few situation without loads in practice and loads are usually changed from situation to situation. To solve this problem, many control laws have been applied and examined so far [7]-[9]. In particular, model-based controls have been taken notice. The control performance of these controls depends

on accuracy of nominal models, which can express behavior of plants.

On the other hand, modeling of McKibben muscles is difficult because the muscles have strong nonlinearities. In pneumatic McKibben muscles, compressibility has also to be taken into consideration. If complexity of models is allowed, we can derive precise models but control laws generally require simple models. The important point here is how to get simple models of the muscles. Unfortunately, there is no such an appropriate model with simple structure and high accuracy.

## 1.3 Load compensation for McKibben muscles

Load compensation is another considerable point in control[10], especially the applied controls are model-based controls because loads can easily degrade the control performance. Figure 1.3 shows the experimental results with three types of loads: 50N, 100N, and 150N.

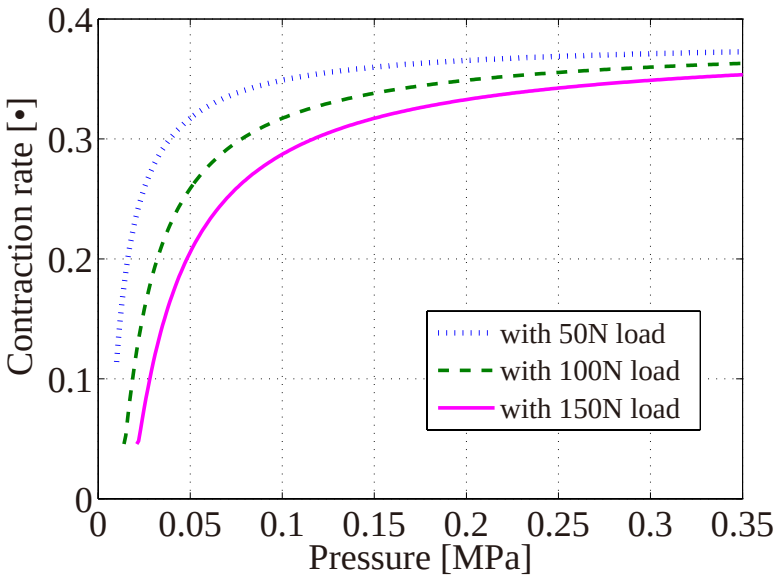


Fig. 1.3: Comparison of contraction rate with loads

As shown in Fig. 1.3, contraction rate - supply pressure characteristics change for loads. It means that the parameters of the McKibben muscles are drastically changed by loads. Thus, load compensation mechanism is necessary for the muscles to achieve high control performance. Sufficient verification for this matter has not been discussed yet while it is a critical problem of the

muscles.

## 1.4 Research objectives

This study is concerned with tap-water driven McKibben muscles as actuators of rehabilitation systems. “Tap-water driven” here means systems driven by tap-water pressure. The main purposes of this study are modeling of the muscles for the model-based controller and design of model-based controllers. Then they includes methods to figure out the characteristics, that is contraction rate - supply pressure characteristics, of tap-water driven McKibben muscles. Note that there is additional purpose of this study: It is an application of the muscles to gait-training orthoses. Some of research objectives are concerned with the orthoses.

The detail of research objectives are as follows.

1. Derivation of precise and simple models of the muscles

   Linear system identification method, which is based on only relationship between inputs (supply pressure or applied voltage for control valves) and outputs (displacement of the muscles), is applied to derivation of the muscle models. This method is expected to simplify muscle models because water as working fluid is incompressible and temperature dynamics can be neglected. In pneumatic McKibben muscles, it is required to take account of compressibility and also temperature dynamics. This is, however, only linear theory and it is obvious that nonlinearities of the muscles such as hysteresis are neglected.

2. Application of Bouc-Wen hysteresis model

   To compensate the nonlinearities neglected in the derived simple linear model of the muscles, we propose combination of a hysteresis model, which is widely used in various fields. As the simple model can be obtained by system identification method, the hysteresis model can easily be applied. The modified model can be used for not only a nominal model of model-based control but also static analyses such as hysteresis analysis.

3. Controller design

   We propose applications of adaptive control and model predictive control with the proposed muscle model as a nominal model. The control performances of these controller are com-

pared with conventional PID controller. In particular, experiment with some loads show considerable problem of the muscle.

4. Adaptive parameter estimation

   Load compensation by adaptive parameter estimation is proposed, specifically recursive least squares (RLS) algorithm is applied to the system. In addition, modeling error can be compensated by the algorithm in real-time basis. The effectiveness of the proposed method is shown by some experiment with/without loads.

5. Displacement estimation method

   A gait-training orthosis is assumed as an application of tap-water driven McKibben muscles. We propose simplification of the orthosis by elimination of potentiometers on the hip and knee joints of the orthosis. To this end, two displacement estimation methods are applied: 1) Measurement method with a flex sensor, and 2) Measurement method with a flowmeter.

# Chapter 2

# Composition of the dissertation

This dissertation is structured as follows:

In Chap. 3, contraction force - supply pressure and contraction rate - supply pressure characteristics of tap-water driven McKibben muscles are shown and some applications of conventional McKibben muscles are introduced. In particular, the applications, for which the tap-water driven muscles should be used, are suggested. In addition, conventional rehabilitation systems are introduced and then some advantages and disadvantages of them are also presented.

In Chap. 4, models of the muscles are proposed and validity of the models is confirmed by analyses of contraction rate - supply pressure and hysteresis characteristics. The proposed model consists of a simple model derived by system identification method and Bouc-Wen hysteresis model. Then discussion about loads is made because they significantly effect on the response of the muscles. Note that there is few consideration about loads, although muscle models including Bouc-Wen hysteresis model have been already proposed.

In Chap. 5, two experimental setups are constructed: The one consists of proportional valves and another consists of only On/Off valves. For the setup with proportional valves, three control laws are applied to the muscles. The one is PID control, which is a conventional control for the muscle displacement control. The others are model reference adaptive control (MRAC) and model predictive control (MPC), which are model-based control methods. The control performances of these controllers are examined by experiment. In particular, MPC assumes that nominal models are completely identified plants but the models surely have modeling errors in practice. This leads inevitable degradation of the control performance of MPC. An adaptive parameter estimation al-

gorithm, which is recursive least squares method, is combined to overcome the error caused by modeling. Moreover, the number of coincident points is considered in MPC at design steps and the results are compared with the results of PID, MRAC, and conventional MPC.

On the other hand, for the setup with On/Off valves, conventional On/Off control and predictive On/Off control, which is based on a concept of MPC, are applied and compared.

In Chap. 6, displacement estimation methods are discussed to achieve displacement control of the muscle without potentiometer measuring the displacement directly. This chapter shows two estimation methods: 1) Estimation method I (flex sensor), and 2) Estimation method II (flowmeter). Experiment of displacement controls, which combine the results of Chap. 5 and displacement estimation methods, are conducted. These results can be used for the application of gait-training orthosis, which is introduced in Chap. 3.

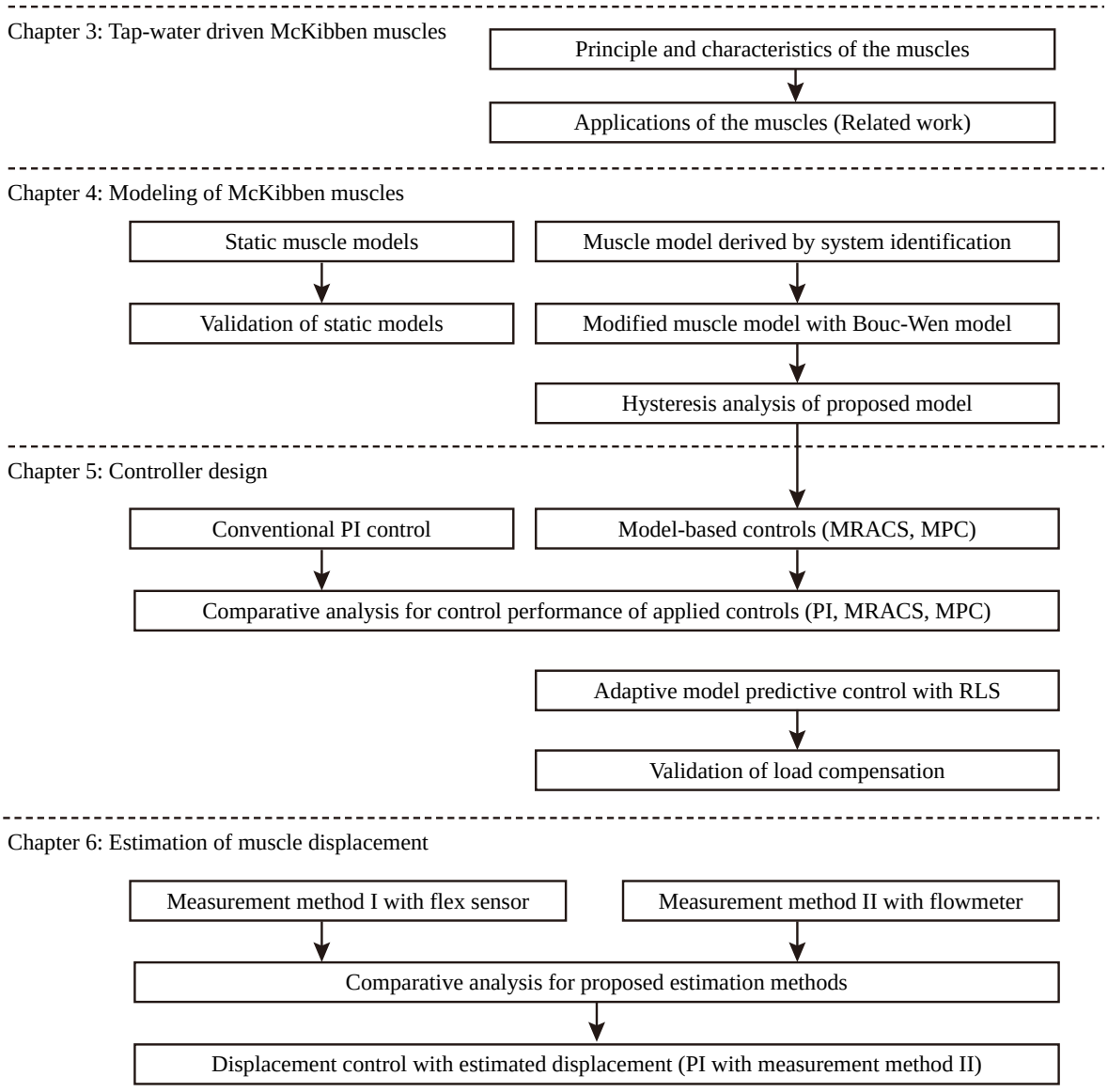


Fig. 2.1: Flow chart of the dissertation

# Chapter 3

# Tap-water driven McKibben muscles

## 3.1 Introduction

McKibben muscles are one of the feasible actuators for medical and welfare systems. Advantages of the muscles are following: 1) Light weight, 2) High power-to-weight ratio, 3) High flexibility, and 4) Low cost. These are suitable for such systems because human friendliness is the most important factor and highly required. Generally, electric motors, pneumatic compressors, or hydraulic pumps are used as driving sources but they are unsuitable in that sense. The muscles were invented in the 1950s by Joseph L. McKibben[11], [12] to motorize arm orthoses and help handicapped hands. They consist of an inner rubber tube and outer braided sleeve (Fig. 3.1) and are closed by two joints. They are usually driven by pneumatics, and when the inner tube is pressurized, gas inside the tube pushes inner surface of the tube and then increases its volume. The muscles can shorten due to non-extensibility of the sleeve. This is almost same motion as human skeletal muscles.

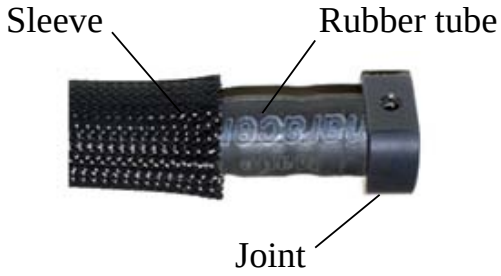


Fig. 3.1: Inner tube and braided sleeve of McKibben muscle

Relationship between supply pressure, muscle displacement, and contraction force are major characteristics of the muscles. Human skeletal muscles also have particular characteristics: 1) Convex shape active tension - length relationship, 2) Nonlinear passive tension - length relationship, and 3) Hyperbolic tension - velocity relationship[13]. Although the characteristics of the McKibben muscles are completely same characteristics as human skeletal muscles, this should be emphasized because most of actuators cannot have the characteristics and be important for medical and welfare systems.

A conventional driving source of these kind of muscles is pneumatics. As that is well known, pneumatics is an easy-to-use driving source because pressure medium is air. Pressure range of pneumatics covers rated pressure range of the muscles. If compressed air leaks from the muscles or pneumatic circuits, they slightly damage environment and also humans. In addition, compressibility of air helps system softness. On the other hand, compressibility of air degrades system response. Pneumatics requires compressors and their installation spaces. In general, compressors make noise and vibration and then these aspects critically come to problems.

A solution of these problems is water hydraulics, especially tap-water here. Water hydraulics has faster response than the one of pneumatics due to characteristics of water as working fluid. Moreover, water hydraulics has a unique characteristics, which is 100% oil-free. This means that water hydraulics has higher human friendliness than pneumatics. More importantly, tap-water driven McKibben muscles need no driving source devices such as compressors or hydraulic pumps when tap water, whose pressure level is approximately less than 0.3 MPa, can generally be available. Although the pressure level of tap-water is less than the level of pneumatics, the omission of driving source devices is attractive for medical and welfare fields. In other words, the tap-water driven McKibben muscles are available for anywhere with a tap. This leads to wider applications of them. Thus, it is useful to create synergy effects between advantages of the McKibben muscles and advantages of water hydraulics.

Notice that there are also disadvantages of the tap-water driven muscles. Water as a working fluid is heavier than air as pressure medium. This means the muscles are also heavier when water is supplied to the muscles. Thereby, when the muscles are attached to rehabilitation systems or power-assist suits, the weights may be troubles.

In addition, the most considerable disadvantage is leak of water. There is no problem in pneu-

matics whenever compressed air is leaked. In water hydraulics, however, leaked water swamps the systems and also environment. Moreover, McKibben muscles in general are breakable because the main material of the muscles is synthetic rubber and the rubber may burst during operation.

There are other types of water hydraulic McKibben muscles[14], [15]. In particular, the muscles can be used in higher pressure range, which is more than 1 MPa, because pneumatics is less than 1 MPa basically and there is no way to apply such a high pressure range. These types of muscles have been applied to industrial machineries and robotics[16]. The structures, materials, and production methods of the muscles have been improved in order to withstand the high pressure and enhance life cycle of the muscles. In contrast with that types of the muscles, water hydraulic muscles driven by tap-water have same structure, materials, and production methods of the pneumatic muscles because the pressure range of a tap is almost same level as the pneumatic muscles. Thus, the water hydraulic muscles can be classified by pressure range or driving sources (hydraulic pumps or tap-water).

For the purposes of modeling and control, it is required to simplify muscle models. There are many models describing the muscle characteristics but each model has trade-off between accuracy and simplicity, especially the pneumatic muscles have some considerable characteristics such as compressibility and temperature dynamics. On the other hand, the water hydraulic muscles have no such characteristics and should be simplified. The details are discussed in Chap. 4.

## 3.2 Working principle of McKibben muscles[17]

This section shows the description and working principle of McKibben muscles. The sleeve of the muscles consists of braided threads, which have biased angle to allow expansion of the pressurized inner tube as illustrated in Fig. 3.2. Then dynamic pantograph shaped by braided threads open up when the inner tube is pressurized. This flexible pantograph can convert circumferential pressure forces into axial contraction force because inner tube is cylindrical shape as seen in Fig. 3.2. This working principle is ensured when the muscles contract due to their structures, which are always cylindrical shapes.

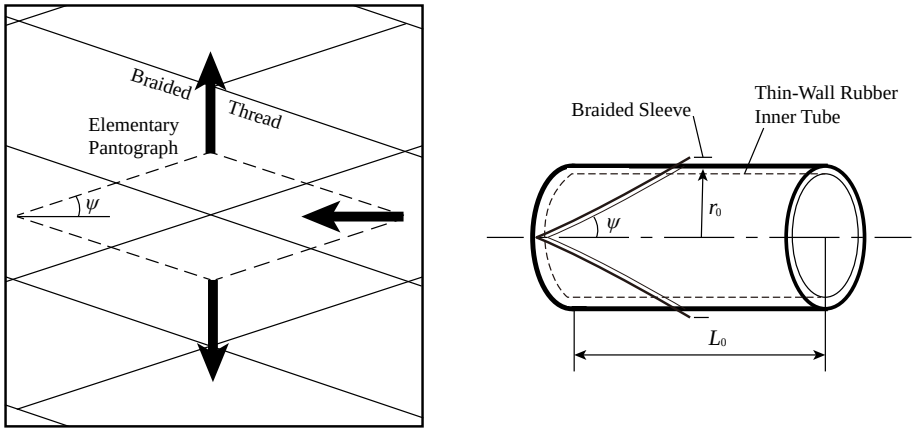


Fig. 3.2: Braided sleeve of the muscles [17]

Parameters characterizing the shapes of the muscles are initial braid angle $\gamma_m$ and initial muscle length $L_0$. The initial braid angle $\gamma_m$ and the initial muscle length $L_0$ are defined as the angle between the muscle axis and the braided thread before expansion and the initial length of the sleeve of the muscles, respectively. The other is initial muscle radius noted $r_0$, which is defined as the radius of the inner rubber tube. Note that this definition involves a consideration of a thin inner tube and then the radius $r_0$ indicates the initial internal radius of the muscle sleeve.

In these geometrical parameters of the muscles, the following are neglected: 1) Conic shapes at the ends of the muscle, and 2) Intrinsic mechanical aspects of the braided threads and inner tube. To take into consideration of conic shapes is particularly complex for modeling of the muscles. For second point in detail, the braided thread is assumed to be unstretchable and without any distortions.

## 3.3 Characteristics of McKibben muscles

The characteristics of the muscles are shown here; specifically contraction force - supply pressure and displacement - supply pressure characteristics are examined by experiments because there is no such results for water hydraulic McKibben muscles. Note that the muscle here is driven by tap-water but its structure is same as pneumatic muscles, which means that it is not specialized for water hydraulics. Thereby, verification of applicability of tap-water for the muscle is another purpose of these experiments and also comparison of the characteristics with pneumatic muscles is a considerable point here.

### 3.3.1 Experimental conditions

Figure 3.3 shows an experimental setup for tap-water driven McKibben muscles. The setup consists of the muscle, two proportional valves, pressure sensor, load cell, linear potentiometer, and PC. The details of them are listed in Tables 3.1 to 3.4. Note that a pair of the proportional valves used in this setup, which are two-port two-position valves, is applied to construct a three-port three-position proportional valve in Fig. 3.3 in order to simplify the symbol because no commercialized three-port three-position proportional valves are available and we use the combination of the valves with same function as a three-port three-position valves. Plastic tubes are used for the experimental circuit to connect components. Maximum pressure of tap-water as a driving source is approximately 0.25 to 0.3 MPa but it is depends on situations. Applied voltage source for each instruments is PC with MATLAB and dSPACE, which is a real-time control system including AD/DA converters.

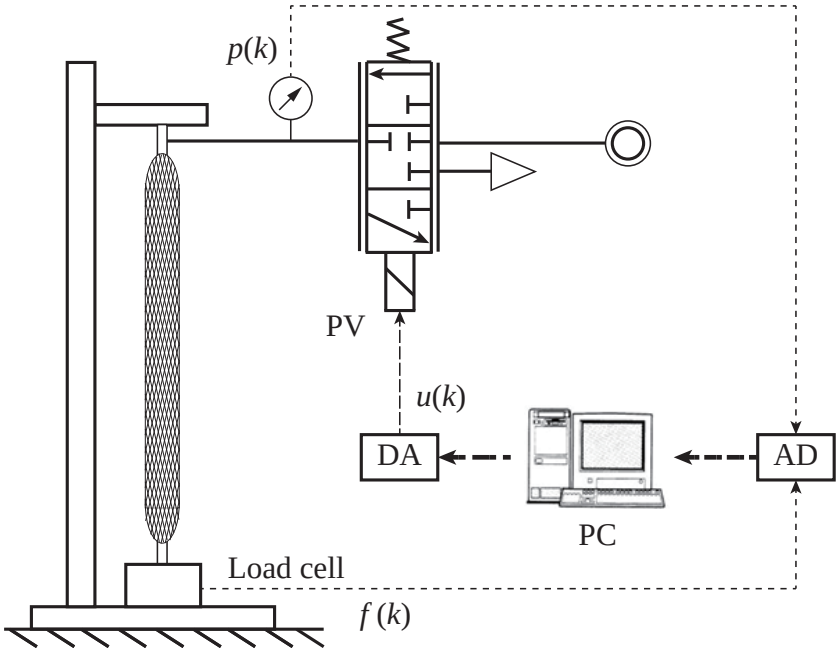


Fig. 3.3: Experimental setup

Table 3.1: Proportional valve: PV (KFPV300, Koganei Corporation)

| | |
|---|---|
| Working fluid | Air, neutral gas, and water |
| Structure | 2 ports and 2 positions |
| Operation type | Direct action type |
| Circuit configuration | Normally closed |
| Operation pressure range | 0.1 to 0.3 MPa |
| Cv value | 1.60 |
| Range of temperature | -10 to 90 °C (no freezing allowed) |
| Water proof | IP65 equivalent |

Table 3.2: Pressure sensor (PVL10KD, KYOWA ELECTRONIC INSTRUMENTS CO., LTD.)

| | |
|---|---|
| Rated pressure | 1 MPa |
| Output signal | 0 to 5 V |
| Material of body | SUS |
| Range of temperature | -10 to 60 °C |
| Applied voltage | 12 V DC |
| Water proof | IP61 |

Table 3.3: Load cell (LUX-B-2KN-ID, KYOWA ELECTRONIC INSTRUMENTS CO., LTD.)

| | |
|---|---|
| Rated force | $\pm$ 20 kN |
| Input resistance | 375 $\Omega \pm$ 1.5% |
| Rated output | $\pm$ 1.3 mV/V |
| Range of Temperature | -20 to 80 °C |
| Range of applied voltage | 1 to 10 V AC or DC |
| Water proof | IP67 |

Table 3.4: Potentiometer (SR1A-62, Celesco Transducer Products, Inc.)

| | |
|---|---|
| Range of measurement | 0 to 1575 mm |
| Rated applied voltage | 30 V |
| Range of Temperature | -40 to 85 °C |
| Rated velocity | 2000 mm/s |
| Tensional force of wire | 6.4 N $\pm$ 30% |
| Water proof | IP67 |

### 3.3.2 Contraction force - pressure characteristics

This section shows the relationship between supply pressure and contraction force of the muscles. In these isometric experiments, the muscle is 540 mm in natural length, and the supply pressure by tap-water is approximately 0.27 MPa. The load cell fixed bottom of the setup is connected with the muscle in series. Calibration of the load cell is shown in Table 3.5 by Eq. (3.1).

$$F_{\mathrm{l}} = y_{\mathrm{o}} \times h \tag{3.1}$$

where $F_{\mathrm{l}}$ is an external force, $y_{\mathrm{o}}$ output of load cell (mV/V), and $h$ calibration coefficient: 0.0006496 kN/1.0 $\times 10^{-6}$, which is given by manufacturer.

Table 3.5: Calibration of load cell

| | | | | | | |
|---|---|---|---|---|---|---|
| Weight [kg] | 1.01 | 2.50 | 4.97 | 7.47 | 9.95 | 14.97 |
| Indicated force [N] | 10.6 | 25.5 | 48.4 | 75.5 | 99.5 | 148.4 |

Figures 3.4 - 3.9 show the transient response of the supply pressures and the contraction force of the muscle in 5% increments from natural length of the muscle. Input signal 10 V (rated voltage) for the valve are applied at 10 s and the load cell connected with the bottom of the muscle measures the contraction force. Note that contraction rate of the muscle is adjusted by changing positions of the top end of the muscle fixed on the setup.

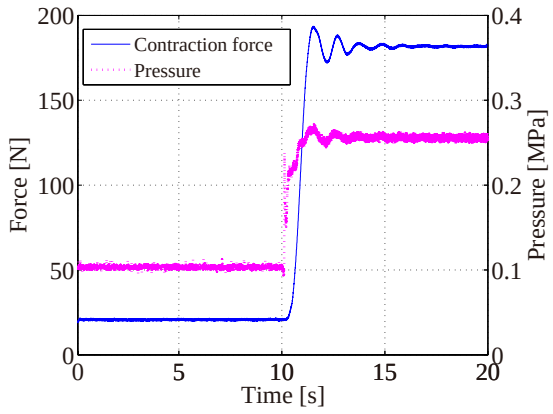


Fig. 3.4: Contraction force (length: 540 mm)

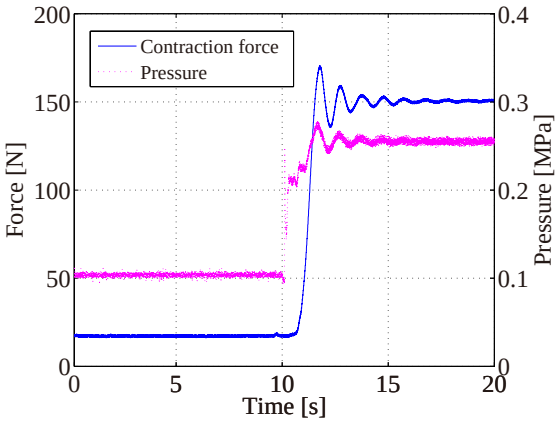


Fig. 3.5: Contraction force (length: 513 mm)

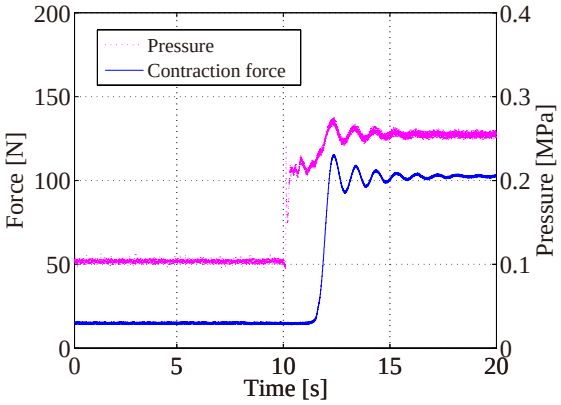


Fig. 3.6: Contraction force (length: 486 mm)

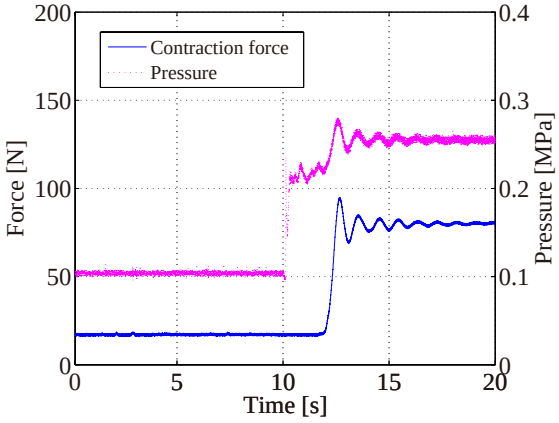


Fig. 3.7: Contraction force (length: 459 mm)

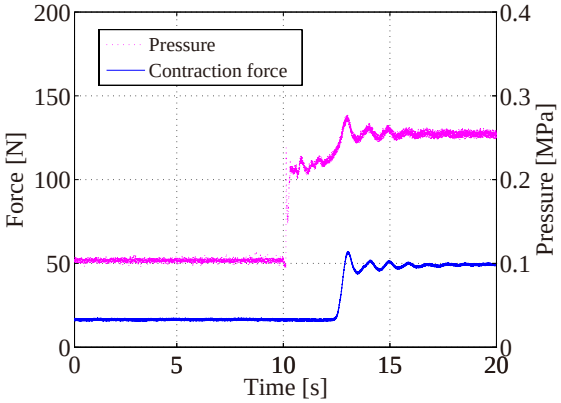


Fig. 3.8: Contraction force (length: 432 mm)

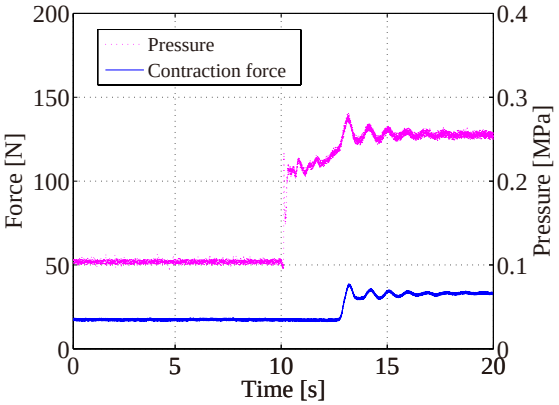


Fig. 3.9: Contraction force (length: 405 mm)

### 3.3.3 Discussion

It is obvious that the pressure inside the muscle can reach the maximum pressure 0.25 MPa for all experiments. Then contraction forces of each experiments depend on the initial condition of muscle length. Contraction force in natural length is the largest and it decreases in proportion to contraction rate. Braid angle of the muscle is attributed to the difference of maximum contraction forces. The larger the contraction rate is, the thinner pantograph shaped by braided threads is. Thereby, vertical force acting the pantograph is smaller than horizontal force acting the pantograph.

Figure 3.4 shows the experimental result in natural length and there is a time delay less than 1 s after applying the input for the valve. The time delays of other results increase in proportion to

contraction rate because contraction times, which indicate the time to contract 5% to 25%, increase in proportion to contraction rate. However, steady-state values of contraction force are constant and then we can compare these results and characterize the contraction force - pressure relation as shown in Fig. 3.10. These results and related experimental results [18] for pneumatic muscles have same tendency for this aspect. Thus water hydraulic McKibben muscles have same contraction force level as pneumatic one. Note that maximum pressure of tap-water is less than conventional maximum pressure of pneumatics. In addition, dynamics comparison between water hydraulic and pneumatic muscles is difficult from these results because the transient response depends on experimental circuits and components.

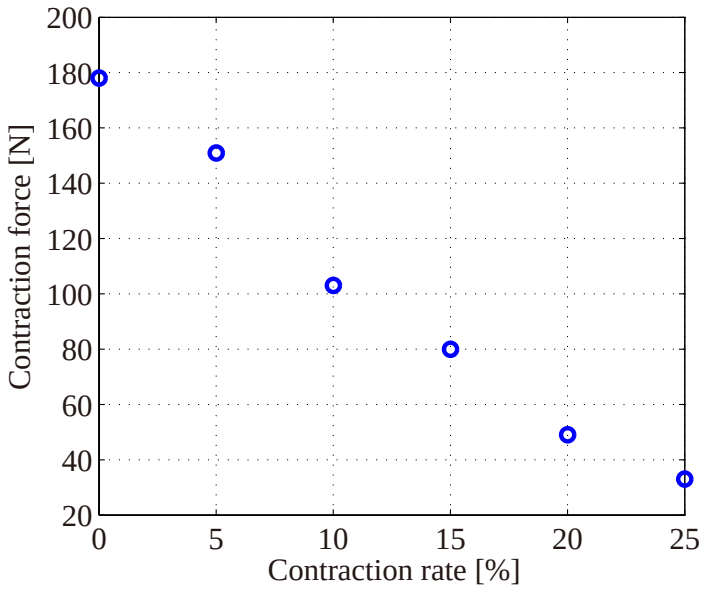


Fig. 3.10: Experimental results of contraction force - pressure characteristics

### 3.3.4 Displacement - pressure characteristics

The relationship between supply pressure and displacement of the muscle is also important characteristics of the muscles. The experimental setup is almost same as previous one in Fig. 3.3 but the load cell connected with the bottom of the muscle in series is replaced with linear potentiometer to measure displacement of the muscles. Displacement of the muscle indicates amount of length change of the muscle. Figures 3.11 and 3.12 show experimental results of displacement.

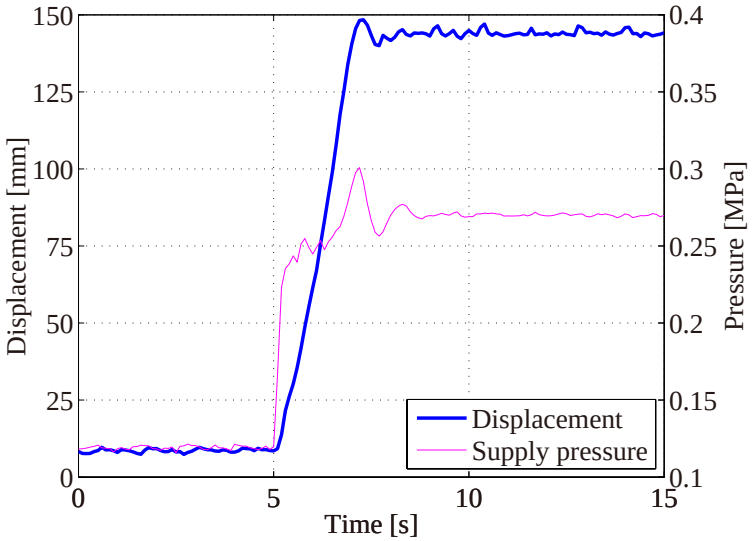


Fig. 3.11: Experimental result (0.27 MPa)

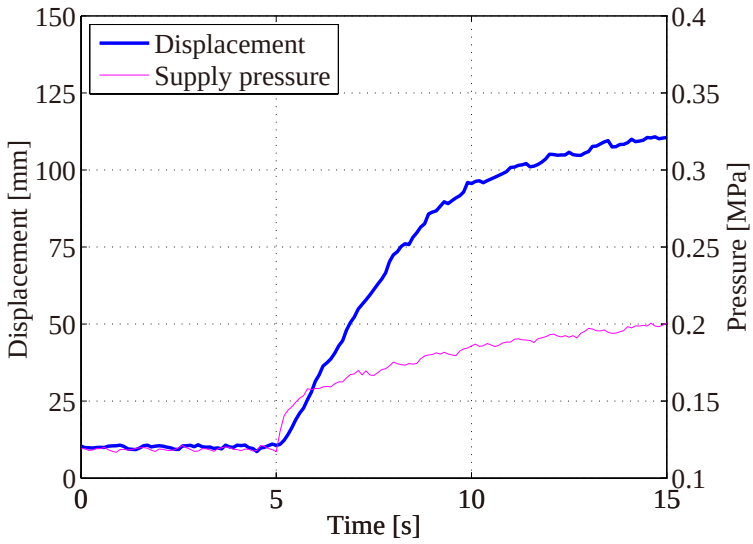


Fig. 3.12: Experimental result (0.2 MPa)

By merging all experimental results, the displacement - pressure characteristics can be shown in Fig. 3.13. This figure shows only static state of the muscle.

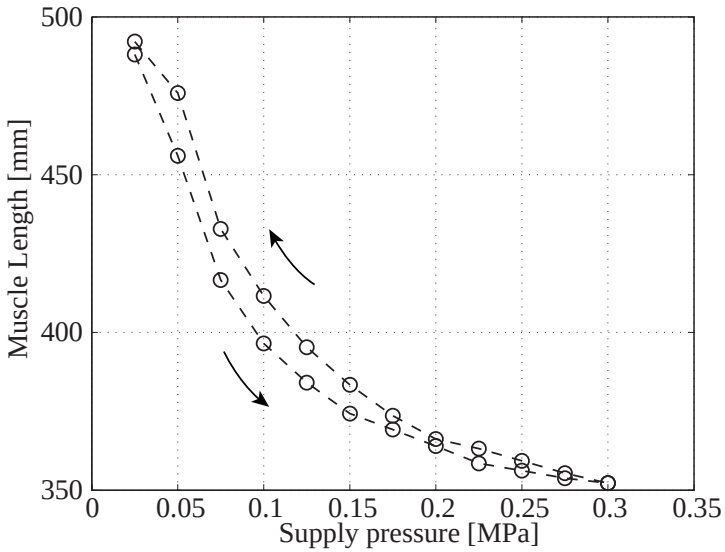


Fig. 3.13: Displacement - pressure characteristics

### 3.3.5 Discussion

Displacement of McKibben muscles may be changed by natural length of the muscles and in general contraction rate, which indicates ratio of displacement to natural length of the muscles, is introduced. The contraction rate $\eta$ is defined as

$$\eta = \frac{L_0 - L}{L_0} \tag{3.2}$$

where $L$ is length of the muscle, and $L_0$ natural length of the muscle.

In these experiments, proportional valves are controlled to set supply pressure as 0 to 0.26 MPa in 0.02 MPa increments. When supply pressure is 0.26 MPa, which is almost maximum pressure, the contraction rate $\eta_{\max}$ is obtained by

$$\eta_{\max} = \frac{L_0 - L_{\max}}{L_0} = 0.25 \tag{3.3}$$

The result shown in Fig. 3.13 is similar to the result of pneumatic muscles[18]. In addition, water hydraulic circuit, which consists of a hydraulic pump, an accumulator and an On/Off valve is used to examine the maximum contraction rate of the muscle because it is impossible to supply higher pressure than 0.3 MPa by tap-water. As a result, the muscle can be contracted more than 30% and

has the same statics as pneumatic muscles. Thus water hydraulic McKibben muscles have same characteristics as pneumatic McKibben muscles.

## 3.4 Applications of McKibben muscles

Pneumatic McKibben muscles have already been applied to various systems such as rehabilitation devices[19]-[23], body-support suits[24], [25], and robotics[26], [27], as illustrated in Figs. 3.14 to 3.17. These developments show the applicability of the muscles. Suitably the muscles have been used for the satisfaction of human friendliness.

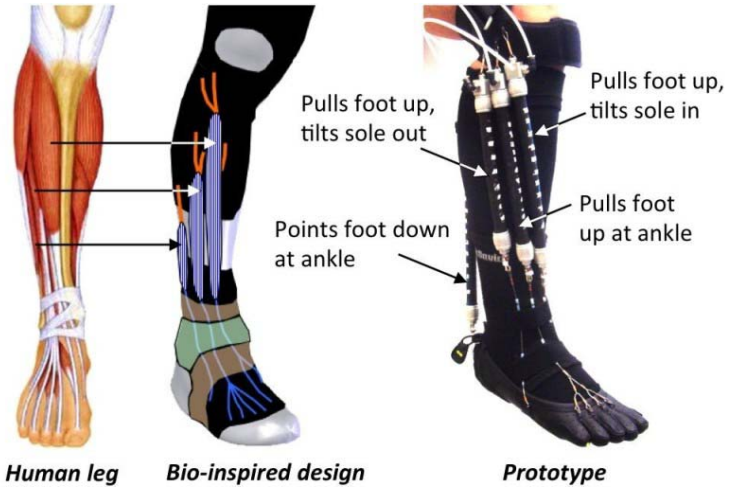


Fig. 3.14: Rehabilitation devices using McKibben muscles[19]

Fig. 3.15: Rehabilitation devices using McKibben muscles[22]

Fig. 3.16: Robotics using McKibben muscles[26]

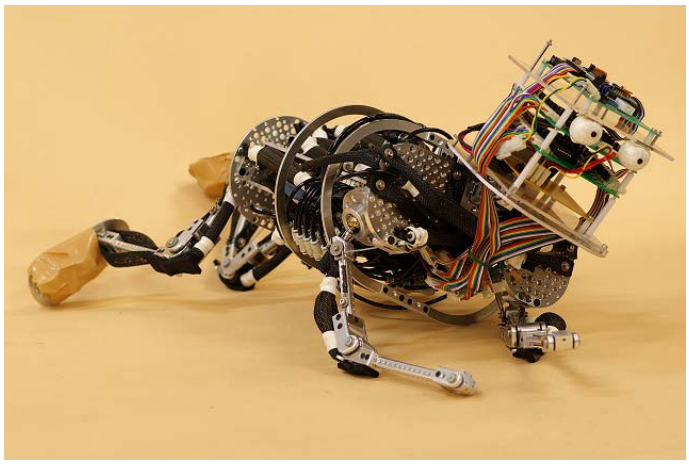

Fig. 3.17: Robotics using McKibben muscles[27]

### 3.4.1 Rehabilitation engineering

Rehabilitation engineering is essential for rehabilitation in practice. It can replace a part of PT's work and carry out effective rehabilitation. Originally, rehabilitation intends to recover radical abilities, which were lost by accidents or diseases and to compensate for irreversibly-disabled abilities by

using auxiliary component, for instance, artificial limbs, prosthetic orthoses, and wheelchairs[28]. Thereby, it aims to achieve domestic and social independence of patients. Rehabilitation engineering contributes on multiple roles: 1) Development of auxiliary and training equipment, 2) Quantitative analyses of training and clinical test data, 3) Systemization of rehabilitation programs, and 4) Maintenance of network systems and rehabilitation institutions. In particular, training equipment can reduce strain of PTs making patients rehabilitate themselves. In addition, high-intensity and long-term repetitive action pattern exercises can be possible by using training equipment. Then benefits from applications of training equipment are to be able to quantitatively adjust loads depending on knowledge of PTs and to store and analyze training data to evaluate effectiveness of rehabilitation methods and assessment of repeatability.

In particular, this study is also concerned with gait-training, which is rehabilitation for motor function, as an application of tap-water driven McKibben muscles. Reduction of motor function caused by accidents or diseases and loss of motor function with aging leads to cause loss of activities of daily living (ADL)[29] and quality of life (QOL)[30]. ADL, which introduces a new perspective on the medical community, is a key concept for adaptation from daily life. In the 1980s, the key concept of rehabilitation was changed once from ADL to QOL. Although QOL is mainstream now, ADL has not lost its importance. In fact, from “Improvement the level of ADL for QOL”, ADL has not only its importance but also connection with QOL. The recovery of gait disorder is particularly useful in ADL and QOL because gait movement, which is well known as means of migration, is one of the important elements of daily living.

### 3.4.2 Gait-training orthosis

Underwater gait-training is one of gait-training in rehabilitation. This is a suitable application of the muscles because water hydraulics, which has 100% oil free is desirable in the gait-training, not oil hydraulics and pneumatics. In addition, as buoyant force reduces patient’s weight under water, smaller and lighter system without any body weight support devices can be realized. This has great impact to the conventional rehabilitation systems.

According to an investigation conducted on disabled people in 2006 by Japan Ministry of Health, Labour and Welfare[31], it figures out that there were 58,500 people with damaged spinal cords, 273,000 people with cerebral vascular disease in Japan. Spinal cords, which are in cen-

tral nervous systems, have never been recovered and repaired again if nerve cells were damaged once. Although some cases depend on regions of damaged spinal cords, reduction of locomotion is caused by functional loss of spinal cords. In conventional rehabilitation, an assumption that lost functions never recovered were accepted, and its purpose was to obtain compensation by using residual function. In other words, rehabilitation based on conventional methods means exercises for residual function to compensate lost function. However, an opinion for this tradition is changing tremendously because animal experiment proves plastic adaptation of central nerve and possibility of recovery by reconstruction of neural networks. A lot of researcher actively are now carrying out studies on neurorehabilitation[32].

In general, there are some gait-training with parallel bars, walkers, and sticks for PTs to make a choice on training methods according to levels of patient's torpor and movement function. On the other hand, a new gait-training called body weight support treadmill training (BWSTT) gains much attention as seen in Fig. 3.18. In 1980s, Barbeau[12] reports on recovery of muscle activities and joint motion patterns of cats damaged spinal cord by making the cat exercise on a treadmill. BWSTT builds on a concept and apply results to practical situation. Wernig[33] reports that BWSTT is effective against a large number of cases. Then availability of BWSTT against complete/incompetence spinal injury is shown and it is indicated that BWSTT has effects on recovery of walk function[34]-[37]. About BWSTT, however, harness suspending patients to compensate their body weight is needed and couple of PTs are required to move patient's legs, and thereby these give excessive burdens for the PTs. For this reason, it is difficult to carry out effective training with BWSTT for a long time. Nevertheless, there are poorly-reproducible results because effects of training depend on experiences and subjective opinion of PT who make choices of training methods. Colombo[38] developed a training system that can support gait-training automatically and Dietz[39] reports on the effect and precautions of using the system. As seen from the above, studies on neurorehabilitation are actively made around the West. In Japan, however, these new approaches are not at bedside stage because of the restriction of Pharmaceutical Affairs Act and its cost.

On the other hand, there is a lot of studies on neurorehabilitation in Japan and are various training systems for research step. Most of training systems have postural maintenance and walk mechanism in practice and build on activation of central pattern generator (CPG)[40]. Nakazawa suggests a possible beneficial effect of gait-training with weight bearing control (WBC) and stick

by encouraging reorganization of neural network. Kojima[41] carried out experimental tests with WBC and reports paralyzed muscle activities are induced same as BWSTT by exciting lower-limb. Kakou[42] developed a walking support robot and used it in clinical practice. This consists of gait-training device, low limb function recovery system, and upper limb training support system. In particular, low-limb function recovery system is to help biped walk movement for patients who have gait disorder caused by stroke. In fact, in clinical practice, both subacute and chronic paralyzed persons have improved their gait speed and low-limb muscle strength by training with this system twenty minutes at once in five days a week and during three weeks. In addition, physical strain of PTs and enough securement of training and safe management are also referred in these studies. On the other hand, this training had little effect on activities of daily living and the severity of paralysis and spasticity[43].

Fig. 3.18: Body weight support treadmill training[33]

Yamamoto[44] has carried out research and development regarding gait-training orthosis based on nuerorehabilitation. The orthosis consists of knee-ankle-foot orthosis (KAFO), which supports body trunk, hip, knee, and ankle joints, and applies pneumatic McKibben muscles as actuators. This is different from conventional gait-training, which means passive gait-training. As a result,

it is expected to obtain strong effect because patients need to purposely walk on the system. In addition, McKibben muscles can be assigned same as human musculoskeletal structure because the muscles contract same way as human by supplying working air/fluid. Moreover, McKibben muscles are riskless actuator, which is thought of as an important thing in rehabilitation and is suitable for human support like rehabilitation. This gait-training orthosis, however, has risk of falling by patients supporting themselves though the training effect is expected. Hence, a gait-training orthosis, which permits not only passive gait-training but also active one, has been developed as an integrated system combining of treadmill training and gait-training orthosis.

### 3.4.3 Hydrotherapy and underwater gait-training

Underwater gait-training is one of the BWSTT. Hydrotherapy is combination of physical and exercise therapies and intends to following points: 1) Improvement of moving range of joints, 2) Buildup of muscle strength and endurance using viscosity resistance and buoyant force of water, 3) Improvement of muscle cooperativeness using water stream (turbulent or vortex flow), and 4) Adjustment of body using hydrostatic pressure. In addition, hydrotherapy is an effective treatment for respiratory and circulatory function care because gait movement and exercise in water are aerobic exercises that patients can stretch their entire body supported by hydrostatic pressure. Figure 3.19 shows an underwater gait-training orthosis.

Fig. 3.19: Underwater gait-training orthosis[45]

Hydrotherapy has an advantage of buoyant force that no exercises have and can reduce strain on human's joint by reducing their body weight. Because the higher water level is, the stronger buoyant force is, buoyant force that water level is in lumbar and breast reduces 30% and 90%, respectively. Thus, patients can easily keep themselves with muscle strength less than gait-training on ground. However, hydrotherapy requires attention to carry out exercises because there is strong resistance force caused by characteristics of water.

Miyoshi[45],[46] shows that hip joint extension moment increased by gait speed increasing in water though knee joint moment decreased. Then, they suggest the application of gait-training orthosis with pneumatic muscles and develops the system for this task.

# Chapter 4

# Modeling of McKibben muscle

## 4.1 Introduction

McKibben muscles are used in medical and welfare fields as mentioned in the previous chapters. The reasons why the muscles are used are high flexibility, high human friendliness, light weight, and easy to use. In particular, pneumatic muscles are widely used in the fields. As mentioned in Chap. 1, one of the important problems is control performance of the muscles.

In this chapter, we derive muscle models used as nominal models of model-based controls. Many muscle models have been proposed in the past. A well-known static model is derived by Chou[47]. The model is based on equilibrium of supply and release energy and there are related works dealing with improvements of the model[48]-[50]. Although the purposes here are fundamentally to obtain dynamic models for control, we once review the static model when the model is applied to tap-water driven McKibben muscles. It is useful to evaluate the model because static models are used in feedforward controls, which are often applied to rehabilitation devices with the McKibben muscles. Dynamic muscle models have also been proposed and can be classified by purposes: analysis and control. For analysis, muscle models require high accuracy and usually have complex structure. In other words, it is impossible to use these models as nominal models of model-based controls because nominal models should be simple for calculation and usually sampling period may become problems in practice.

Specific muscle models are as follows except for the static models mentioned above: 1) Muscle model based on motion equation taking into consideration of inertial and viscous loads[4], 2) Mus-

cle model using the Maxwell-slip model[52], [53], 3) Muscle model using Preisach model[54], 4) Empirical nonlinear muscle model[55], and 5) Muscle model taking into consideration of hysteresis caused by friction[56]. Common considerable points of these models are frictions and hysteresis caused by frictions. Some of them describe friction or hysteresis models such as Maxwell-slip model and Preisach model proposed in other fields. On the other hand, the others empirically obtain the relation between inputs (supply pressure or applied voltage for valves) and outputs (displacement or contraction force of muscles). Thus nonlinearities such as friction and hysteresis are important factors to derive precise muscle models. Although these models have high accuracy, it is unsuitable to use the models for control as mentioned before.

Consider hysteresis characteristics of the muscles. Hysteresis characteristics is defined as "the lag in a variable property of a system with respect to the effect producing it as this effect varies". Hysteresis is one of complex nonlinearities with memory. Then it is known as interference for control and is included in several types of actuators such as electromagnetic actuators[57], piezoelectric actuators[58]. In pneumatic McKibben muscles, the hysteresis characteristics can be examined by experiments[59], [60], which indicate contraction force - displacement and displacement - pressure hysteresis, respectively. The hysteresis of the McKibben muscles is examined by [52], in which it is shown that the hysteresis is caused by the inherent characteristics of inner rubber tube, and the friction between the tube and braided threads and between braided threads themselves. In particular, the friction between braided threads is dominant. Hysteresis usually invites energy loss and then degrade the system performance. This leads complex structure of controller for the system. Thereby, it is difficult to control the system using the model without consideration of hysteresis.

We propose modeling of the muscles by using system identification method, which is based on the experimental data. system identification method is based on statistical method and assumes that objectives are black-boxes. For linear system identification, it has been theoretically systematized. In contrast, there is the first principle modeling based on motion equation, circuit equation, chemical equation, and law of conservation of energy. The first principle modeling can be used in only the cases that structure of objectives are obviously known, and then derived models accurately express the behavior of objectives. On the other hand, physical parameters may not be able to be measured, for instance, friction coefficients. In general, although the precise model can be used for analyses and simulations, it is impossible to use the precise models directly as nominal models of model-

based controls.

McKibben muscles have complexity as mentioned above. Therefore, it is unavailable to apply the first principle modeling to the muscles for control purposes. Generally, simple models is obtained by system identification if objectives are complex. This is the motivation that we apply the system identification method to the muscles. Moreover, tap-water driven muscles may have simpler structure than pneumatic muscles for the compressibility and temperature changing. Note that nonlinearities of the muscles should be neglected because this method is only based on linear system identification method.

The obtained muscle model by system identification is simple and can be used as a nominal model of model-based controls. The model, however, cannot express the hysteresis characteristics, which is important for modeling of the muscles. As introduced before, some models such as Maxwell-slip model and Preisach model are available for the model but the muscle model requires simple structure in practice. To overcome this difficulty, Bouc-Wen hysteretic model[61] is combined with the identified muscle model. Fortunately, Bouc-Wen model is directly applicable for the identified muscle model because of the structure of the identified muscle model. Although the number of parameters that should be considered in the proposed model including Bouc-Wen model increases and the structure of the proposed model becomes little bit complex compared with the linear identified model, these parameters are easily identified by trial and error and then the model can be used as nominal model.

The accuracy of the proposed models is verified by analyzing the displacement - pressure characteristics and hysteresis characteristics. In the analyses, hysteresis loops of proposed models are compared with actual hysteresis loop obtained by experiment. In addition, effect of loads connected with the muscles is examined. This is important because when loads are connected with the muscles, the characteristics of the muscles are drastically changed and the accuracy of the proposed model may also be degraded.

## 4.2 Static muscle model

Schulte[49] reports the relationship between the axial contraction force and pressure difference between supply pressure and atmospheric pressure. This relationship is based on equilibrium between

the input work in the McKibben muscle when supplied air/fluid works the rubber tube surface and the output work when the actuator shortens associated with the volumetric change without elastic deformation. The geometric structure of the McKibben muscle in Fig.4.1 shows following geometric relationships.

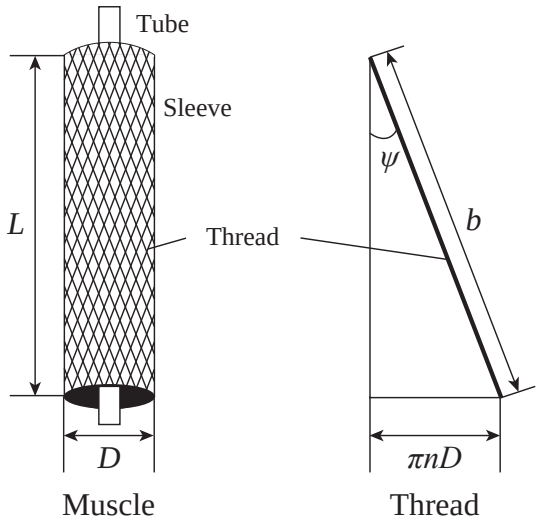


Fig. 4.1: Geometry of McKibben muscle

$$L = b\cos\psi, D = \frac{b\sin\psi}{n\pi} \tag{4.1}$$

where $L$ is the length of the muscle, $D$ the outer diameter of the muscle, $b$ the thread length, $n$ the number of turns of a thread, and $\psi$ the angle between a sleeve and axis.

### 4.2.1 Static model of McKibben muscle

The input work $W_{\text{in}}$ is applied in the muscle when working fluid/air pushes the rubber tube surface and can be expressed for the product of the supply pressure and the volumetric change.

$$dW_{\text{in}} = (p - p_0)dV = p'dV \tag{4.2}$$

where $p$ is the supply pressure, $p_0$ the atmospheric pressure, $p'$ the pressure difference, and $dV$ the volumetric change. The volume of the rubber tube $V$ is

$$V = \frac{1}{4}\pi L D^2 \tag{4.3}$$

with assumption that shape of the rubber tube is a cylinder. Then, from Eq. (4.1),

$$V = \frac{1}{4}\pi L D^2 = \frac{b^3}{4\pi n^2}\sin^2\psi\cos\psi. \tag{4.4}$$

Then $dV/d\psi$ can be expressed as following,

$$\frac{dV}{d\psi} = \frac{b^3}{4\pi n^2}\sin^2\psi(3\cos^2\psi - 1). \tag{4.5}$$

On the other hand, when the actuator contracts by the volumetric change, the output work $W_{\text{out}}$ is given by

$$dW_{\text{out}} = F \times (-dL) \tag{4.6}$$

where $F$ is the axial tension, and $dL$ the axial displacement change. Then $dL/d\psi$ can be expressed as following,

$$\frac{dL}{d\psi} = -b\sin\psi. \tag{4.7}$$

From the assumption that the input work should equal the output work if a system is lossless and without energy storage and Eqs. (4.2), (4.5) - (4.7),

$$F = -p'\frac{dV/d\psi}{dL/\psi} = \frac{\pi p'}{4}\Big(\frac{b}{\pi n}\Big)^2(3\cos^2\psi - 1). \tag{4.8}$$

The tension $F$ is linearly proportional to the pressure difference $p'$ and is a monotonic function of the angle ($0^\circ < \psi < 90^\circ$). When $F$ = 0, the theoretical maximal angle $\psi_{\max}$ can be expressed as

$$\psi_{\max} = \cos^{-1} 1/\sqrt{3} \cong 54.7^\circ. \tag{4.9}$$

Note that, although the tension with the assumption of ideal cylinder is obtained here, the tension can be derived by knowing the $dV/dL$ of any arbitrary shape actuator with Eqs. (4.2) and (4.6) and

the virtual work argument without the assumption.

$$dW_{\text{in}} = dW_{\text{out}} \tag{4.10}$$

$$\therefore F = -p'\frac{dV}{dL}. \tag{4.11}$$

### 4.2.2 Modified static model

A static model of the McKibben muscle can be expressed as Eq. (4.8). However, if the thickness $t_k$ of the sleeve and rubber tube is considered, the volume Eq. (4.3) is modified to

$$V = \frac{1}{4}\pi L(D-2t_k)^2 = \frac{b^3}{4\pi n^2}\sin^2\psi\cos\psi + \frac{bt_k}{2n}\cos\psi(2\pi n t_k - b\sin\psi). \tag{4.12}$$

Then $dV/d\psi$ can also be expressed as following,

$$\frac{dV}{d\psi} = \frac{b^2 t_k}{2n}\Big(\sin^2\psi - \cos^2\psi\Big) - \pi b t_k^2 \sin\psi \tag{4.13}$$

and from Eq.(4.7),

$$\frac{dV}{dL} = \frac{dV/d\psi}{dL/d\psi} = \frac{bt_k}{2n}\Big(\frac{\cos^2\psi}{\sin\psi} - \sin\psi\Big) + \pi t_k^2. \tag{4.14}$$

Therefore, from Eqs.(4.11) to (4.14), a modified static model can be divided as a function of $p'$ and $\psi$,

$$F = -p'\frac{dV}{dL} = \frac{\pi p'}{4}\Big(\frac{b}{\pi n}\Big)^2(3\cos^2\psi - 1) + \pi p' t_k\left[\frac{b}{\pi n}\Big(2\sin^2\psi - \frac{1}{\sin\psi}\Big) - t_k\right]. \tag{4.15}$$

## 4.3 Experimental validation of static models

Contraction rate of the McKibben muscle is examined with 5 and 10 kg weight as loads. The supply pressure is from 0 to 0.3 MPa in increments of 0.05 MPa. The purpose here is to examine the validity of the static model and modified static model of McKibben muscle in Eqs. (4.8) and (4.15).

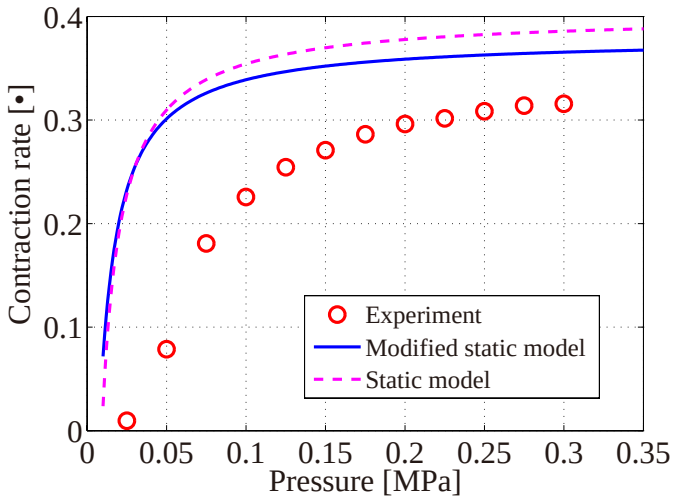


Fig. 4.2: Experimental results of contraction rate with 5 kg load

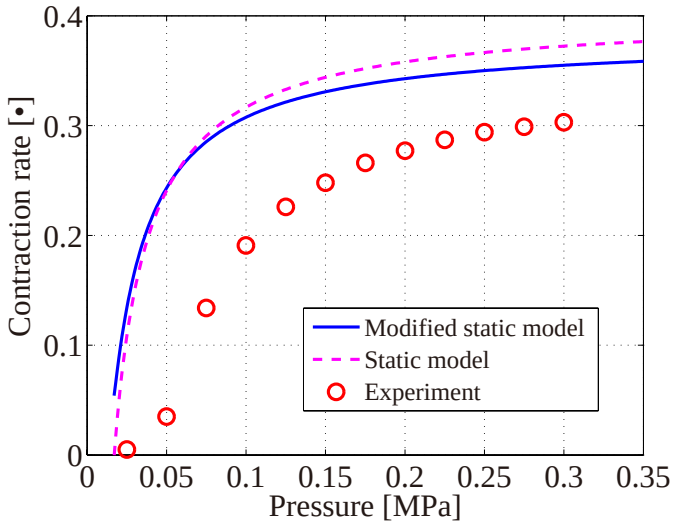


Fig. 4.3: Experimental results of contraction rate with 10 kg load

### 4.3.1 Discussion

From these results, theoretical static models shown in Eqs. (4.8) and (4.15) disagree with experimental results in all cases because theoretical static models take no consideration of all friction force. To obtain better agreement of static model, the following should be considered: 1) Friction force between two thread of sleeve, 2) Friction force between a thread and rubber tube, 3) Bending

moment of a thread, and 4) Rotational resistance by expanding rubber tube. Although theoretical static models may agree with experimental results by taking into consideration of these elements, the models need many parameters and becomes more complex structure than original static models. Moreover, the models lack universality because parameters of the muscle differ from each muscle. In other words, use of the complex static model requires calibration of all physical parameters because a size of muscle can be changed.

## 4.4 Muscle model based on linear system identification

We propose a muscle model derived by linear system identification method[62]. System identification method requires experimental data, which are input and output signals. Moreover, it also requires pre-identification that is experiment of step response to generate appropriate input signal for identification. In this section, we introduce the derivation of muscle model based on linear system identification and improvement of the identified model by use of Bouc-Wen hysteresis model.

### 4.4.1 Experiments of pre-identification

System identification method requires information of objectives, for instance, time constant, settling time, and bandwidth. In addition, time delay of objectives is a considerable point to identify the objectives accurately. Pre-identification, which is experiment of step response in general, is conducted to obtain these data. The experimental setup is same as in Fig. 3.3. Note that input voltage range of the proportional valves is -10 to 10 V. Figure 4.4 shows the step response of the muscle, of which natural length is 540 mm. The experimental result indicates the settling time of the muscle $T_r$ is 1.83 s. Then sampling period $T_s$ for generating identified input signal is chosen in general to put eight sampling points into settling time, that is

$$T_s = \frac{T_r}{7} = \frac{1.83}{7} \qquad \therefore T_s = 0.25. \tag{4.16}$$

However, this basic derivation of the sampling period should not be used in the muscle because the derivation focuses on only the dynamic characteristics near the bandwidth of the muscle. A reliable identified bandwidth of system identification method is 1 hundredth times of a sampling period (frequency) as shown in Fig. 4.5. Then the sampling period of the muscle is chosen again to

involve whole operation range of the muscle: it is 12 s.

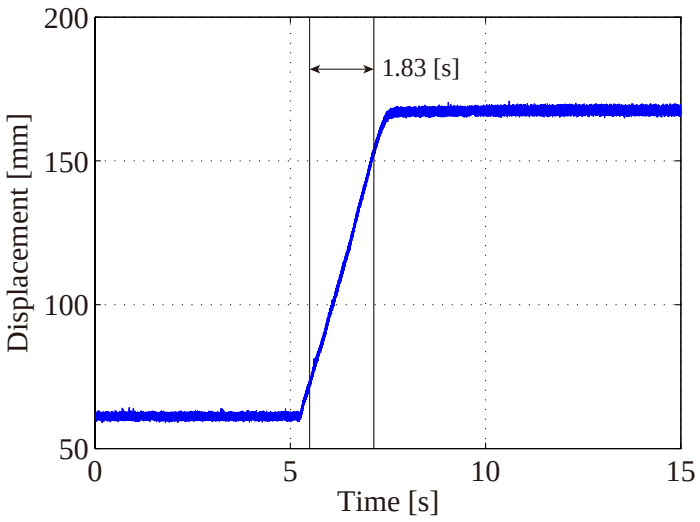


Fig. 4.4: Experiment of step response (pre-identification)

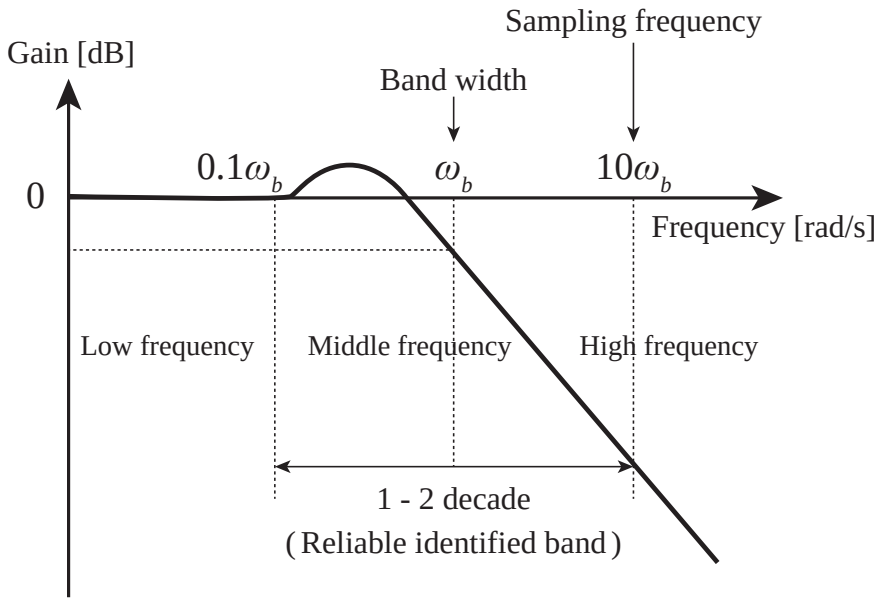


Fig. 4.5: Reliable identified bandwidth

### 4.4.2 Experiments of identification

Based on the allocated sampling period, an input signal (supply pressure) for identification can be generated. Figure 4.6 shows the input signal and an output signal (muscle displacement) when the input signal is applied to the muscle. Note that the input signal for the valve is maximum-length linear shift register sequence, which is one of pseudo random binary signal, and then the supply pressure can be generated as in Fig. 4.6, where the sampling period of the data is 0.1 s.

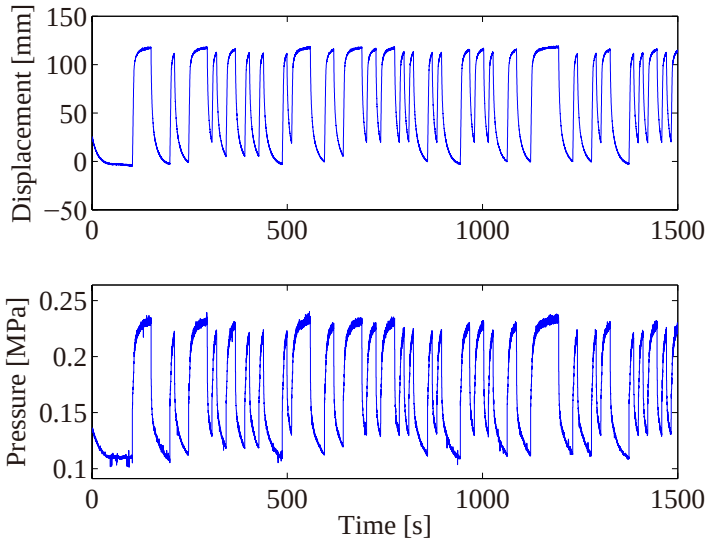


Fig. 4.6: Input and output singnal for identification

Next, a structure of the identified model is selected. In this identification, Auto-regressive exogenous (ARX) model is applied because ARX model is suitable for least squares method and is usually used for system identification. A specific method to identify the muscle is use of system identification toolbox provided with MATLAB. The identified muscle model $G(z)$ has first-order denominator and zero-order numerator polynomials, and relative degree one as expressed as Eq. (4.17).

$$G(z) = \frac{L(z)}{P(z)} = \frac{67.22}{z - 0.9356} \tag{4.17}$$

where $L(z)$ is $z$-transformation of muscle displacement, and $P(z)$ $z$-transformation of supply pressure. Thus the identified model has simple structure; first-order system. Having good agreement

with experimental result in transient response, the model has some difference in steady-state response in Fig. 4.7.

Nonlinearities of the muscle such as hysteresis characteristics can not be modeled because the introduced model is only linear model as mentioned above. Moreover, hysteresis characteristics of the muscle is strong as shown in Fig. 4.8. Note that the hysteresis loop can be measured and analyzed by contraction and extension operations of five cycles and the all loops trace the same trajectory.

Although this model can be used for control purpose, it is difficult to use the model for analysis purpose, for instance, analysis of displacement - pressure characteristics because the model is only linear model and cannot express nonlinearities such as hysteresis, which is an important factor for static analysis.

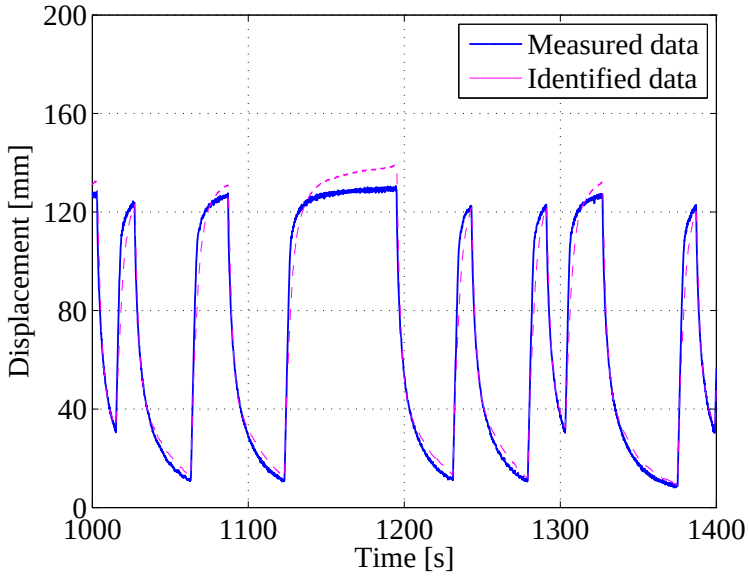


Fig. 4.7: Comparison of identified and measured data

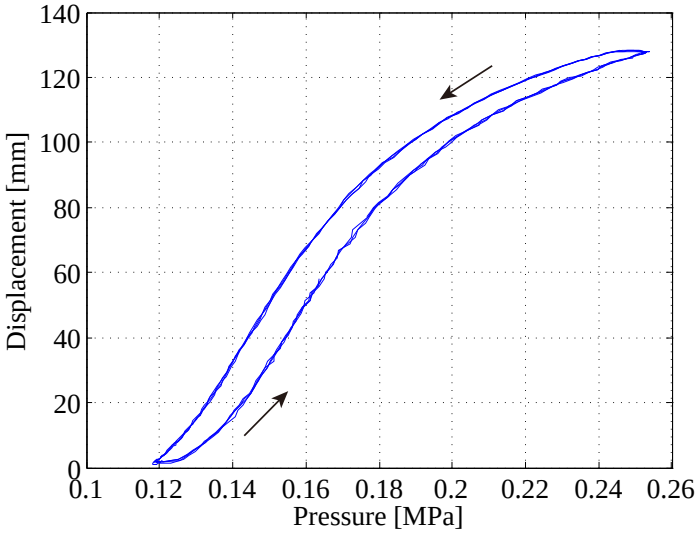


Fig. 4.8: Hysteresis loop of McKibben muscles

## 4.5 Modified model with Bouc-Wen hysteretic model

This section describes modified models of the muscle because the linear identified model cannot express the hysteresis characteristics of the muscle correctly. This means hysteresis analysis cannot be carried out with the model. For this problem, we propose modification of the model by using a well-known hysteresis model.

Hysteresis models for the muscle have been applied, for instance, Preisach model. A hysteresis model proposed here is a model called Bouc-Wen model. Advantages of the model are follows: 1) Easy-to-use, 2) Intuitive for parameter identification, and 3) Suitable for parametric models. Compared with other hysteresis models, the advantages particularly match control purposes. Furthermore, the model has been improved to express various hystereses such as asymmetric hysteresis. Fortunately, the hysteresis of the muscle can be express by general Bouc-Wen model. Bouc-Wen model was first developed by Bouc in 1971[61] and modified by Wen in 1976[63]. Generally, a virtual hysteresis variable is introduced and put it into zero-order term of mathematical models. In addition, the model can take account of dynamics of the virtual hysteresis variable. The detail of the model is described in Appendix A and application for the muscle here is introduced.

The identified model Eq. (4.17) can be rewritten by

$$l(k) - 0.9356l(k-1) = 67.22p(k-1). \tag{4.18}$$

Then a virtual hysteresis variable $w$ is introduced as

$$l(k) - 0.9356\{\alpha l(k-1) + (1-\alpha)w_(k-1)\} = 67.22p(k-1). \tag{4.19}$$

In general, zero-order term can be expressed as

$$\phi_{hys}(l, w) = 0.9356\{\alpha l(k-1) + (1-\alpha)w(k-1)\} \tag{4.20}$$

where the first term indicates elastic effect, the second term indicates hysteretic effect. Then $\alpha(0 \leq \alpha \leq 1)$ is a weight coefficient, and Eq. (4.19) becomes the identified model without hysteresis characteristics when $\alpha = 1$.

The virtual hysteresis variable in general can be expressed in time domain as

$$\dot{w} = A\dot{l} - \beta|\dot{l}||w|^{n-1} - \gamma\dot{l}|w|^n. \tag{4.21}$$

As seen in Eq. (4.21), Bouc-Wen model has five hysteresis parameters such as $A, \alpha, \beta, \gamma, n$. $A$ has relations with an amplitude of hysteresis loop, $n$ indicates behavior of hysteresis, which is either linear or nonlinear, $\alpha$ defines levels of hysteresis, and $\beta$ and $\gamma$ dominantly shape hysteresis loop. Thus the hysteresis characteristics can be expressed by choosing these parameters[64].

Equation (4.21) should be transformed into a discrete-time equation to combine this equation with the identified muscle model because the muscle model is expressed as discrete-time equation in Eq. (4.18). To obtain a forward difference approximation of Eq. (4.21), the following are introduced;

$$\frac{dx}{dt} \approx \frac{x(t+h) - x(t)}{T_s} = \frac{x(k+1) - x(k)}{T_s} \tag{4.22}$$

$$\frac{d^2x}{dt^2} \approx \frac{x(t+2T_s) - 2x(t+h) + x(t)}{T_s^2} = \frac{x(k+2) - 2x(k+1) + x(k)}{T_s^2} \tag{4.23}$$

where $T_s$ is a sampling period. Therefore, the virtual hysteresis variable can be discretized as

$$\begin{aligned}
\frac{w(k+1)-w(k)}{T_s} &= A\Big\{\frac{l(k+1)-l(k)}{T_s}\Big\} - \beta\Big|\frac{l(k+1)-l(k)}{T_s}\Big||w(k)|^{n-1} \\
&\quad -\gamma\Big\{\frac{l(k+1)-l(k)}{T_s}\Big\}|w(k)|^n \\
\therefore w(k+1) &= A\{l(k+1)-l(k)\} - \beta|l(k+1)-l(k)||w(k)|^{n-1} \\
&\quad -\gamma\{l(k+1)-l(k)\}|w(k)|^n + w(k). \qquad (4.24)
\end{aligned}$$

Consequently, the discrete-time muscle model with Bouc-Wen model can be written by

$$\begin{cases}
l(k) &= 67.22p(k-1) - \phi_{hys}(l,y) \\
\phi_{hys}(l,w) &= 0.9356\{\alpha l(k-1) + (1-\alpha)w(k-1)\} \\
w(k) &= A\{l(k)-l(k-1)\} - \beta|l(k)-l(k-1)||w(k-1)|^{n-1} \\
&\quad -\gamma\{l(k)-l(k-1)\}|w(k-1)|^n + w(k-1)
\end{cases} \qquad (4.25)$$

The bounded input - bounded output (BIBO) stability property is important because the model is used for not only analyses but also model-based controls. A classification as in Table 4.1 is introduced to satisfy BIBO stable [65]. Although Classes I to IV satisfy BIBO stable in the table, Class I should be chosen to ensure necessary and sufficient condition for thermodynamic admissibility of Bouc-Wen model[66].

Table 4.1: Classification of Bouc-Wen model

| Class | Parameters |
|---|---|
| I | $A > 0$, $\beta + \gamma > 0$ and $\beta - \gamma \geq 0$ |
| II | $A > 0$, $\beta - \gamma < 0$ and $\beta \geq 0$ |
| III | $A < 0$, $\beta - \gamma > 0$ and $\beta + \gamma \geq 0$ |
| IV | $A = 0$, $\beta + \gamma > 0$ and $\beta - \gamma \geq 0$ |
| V | All other cases |

## 4.6 Evaluation of proposed model

This section evaluates the accuracy of the proposed muscle model Eq. (4.25) by experiment. In general, although an applicable range of McKibben muscles is less than 1 MPa, the range of the tap-water driven muscles is less than 0.3 MPa. Hence we confine the range of experiments and analyses to less than 0.3 MPa. The five hysteresis parameters of the proposed model are chosen by trial and error as shown in Table 4.2. These parameters satisfy Class I in Table 4.1.

Table 4.2: Identified hysteresis parameters of proposed model Eq. (4.25)

| Parameter | Value |
|---|---|
| $A$ | 1 |
| $\alpha$ | 0.9350 |
| $\beta$ | 0.0040 |
| $\gamma$ | -0.0002 |
| $n$ | 1 |

Note that when $n = 1$, the model (4.25) is simplified as following equation and that is confined case of Bouc-Wen model, but BIBO stability of the model can surely be ensured[65].

$$\begin{cases} l(k) &= 67.22p(k-1) - \phi_{hys}(l,w) \\ \phi_{hys}(l,w) &= -0.9356\{\alpha l(k-1) + (1-\alpha)w(k-1)\} \\ w(k) &= A\{l(k) - l(k-1)\} - \beta|l(k) - l(k-1)| \\ & \quad -\gamma\{l(k) - l(k-1)\}|w(k-1)| + w(k-1) \end{cases} \tag{4.26}$$

### 4.6.1 Hysteresis analysis

Displacement - supply pressure characteristics is shown by experimental and simulation results. Linear potentiometer measures actual displacement of the muscle and the proposed model Eq. (4.26) simulates the displacement by supply pressure. Figure 4.9 shows comparison of the experimental and simulation results. Note that the input signal is stepwise and its time interval is five seconds. Figure 4.9 indicates the identified model without Bouc-Wen model has rather error during contraction phase and then the maximum displacement of the model is larger than the mea-

sured maximum displacement. Thus hysteresis loop of the model is different from experimental results and this means that the model cannot be used for even static analyses such as hysteresis and displacement - pressure analyses.

On the other hand, the proposed model with Bouc-Wen model is in a good agreement with experimental results. In particular, the maximum displacement is almost same as the measured displacement. Thus hysteresis characteristics of the muscle can be completely expressed by introducing Bouc-Wen model. Then, it is suitable to set a hysteresis parameter $n$ as 1, because the hysteresis loop of the muscle has same trajectry regardless of cycles as shown in Fig. 4.8 and this phenomenon can be simulated when $n$ is set to 1.

In addition, the advantages of the model are parameter identification as mentioned in section 4.5. The five hysteresis parameters can be identified easily by comparing simulation with measured data. The other models proposed so far require: 1) Measurement of physical parameters of muscles, 2) Analysis based on experimental data to achieve feedforward control, and 3) Huge time and knowledge for parameter identification due to complexity of model structure. Therefore, the proposed model, which can be used easily and has simple structure, is suitable for control.

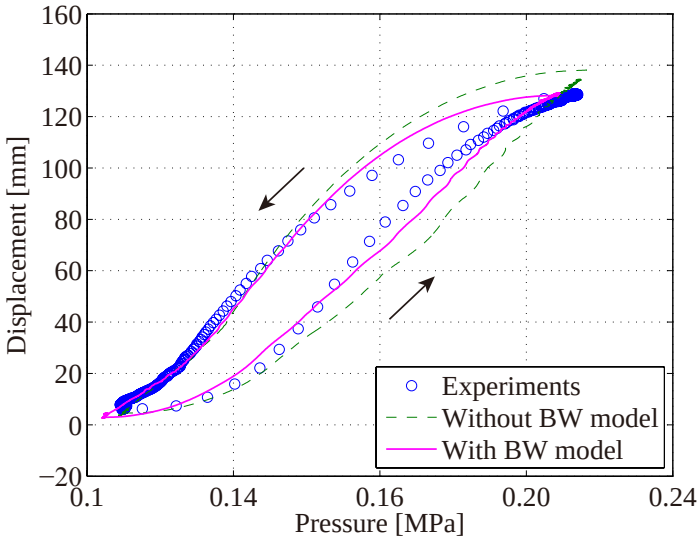


Fig. 4.9: Comparison of hysteresis loop

### 4.6.2 Analysis of load effect

Essential problem of the muscles is how to deal with loads connected with the muscles. The loads make contraction rate of the muscles smaller as shown in Fig. 1.3. Although previous discussions concern with the muscles under no-load condition, this section concerns with effect of loads for muscle models. Note that loads are connected with the bottom of the muscles and always force downward (Fig. 3.3).

Figure 4.10 shows experimental and simulation results of hysteresis loop when load 3.5 kgf connected with the muscle, where the hysteresis parameters of the proposed model are same as previous conditions in Table 4.2. Accuracy of both models, which are the identified model with Bouc-Wen model and the proposed model with Bouc-Wen model, are degraded by loads. In particular, the lower supply pressure is, the larger errors of the models are, because loads strongly affect on the lower supply pressure as shown in Fig. 1.3. Dynamics of the muscle is slower than the dynamics of supply pressure and then only restoring force of inner tube and weight of the muscle and loads work against the muscle during extension phase. Thus the proposed model, the input of which is supply pressure, cannot works well in lower pressure. This indicates the model identified under no-load condition cannot compensate the effect of loads.

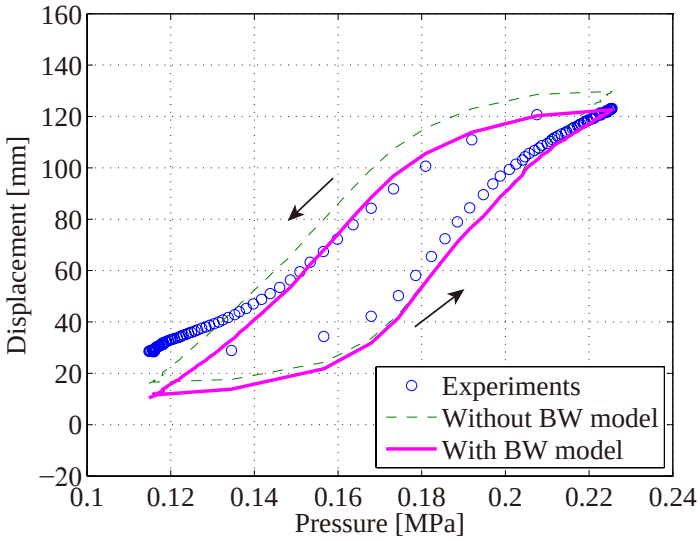


Fig. 4.10: Comparison of hysteresis loop with load: 3.5kgf

The McKibben muscles are generally used under loaded conditions. Thereby, identification under loaded conditions is suitable. Then hysteresis parameters of the Bouc-Wen model Eq. (4.25) are identified under loaded condition; with load 3.5 kg. Table 4.3 shows re-identified hysteresis parameters under loaded condition. Figure 4.11 shows hysteresis loop of the proposed model with re-identified hysteresis parameters. The proposed model has good agreement with experimental result by choosing the parameters appropriately when loads exist.

Table 4.3: Identified hysteresis parameters of proposed model: load 3.5 kgf

| Parameter | Value |
|---|---|
| $A$ | 0.965 |
| $\alpha$ | 0.980 |
| $\beta$ | 0.063 |
| $\gamma$ | 0.050 |
| $n$ | 1 |

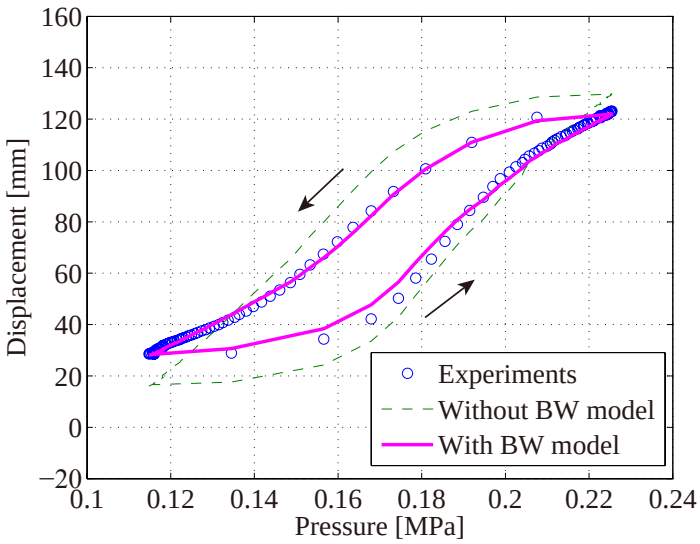


Fig. 4.11: Hysteresis loop of re-identified model with load: 3.5kg

Next, when a load connected with the muscle is changed from 3.5 to 7.0 kgf, accuracy of the proposed model is examined by comparing with experimental results. Figure 4.12 shows hysteresis loop of the proposed model under loaded condition; with load 7.0 kgf. Note that the parameters of

the muscle model are not changed (Table 4.3).

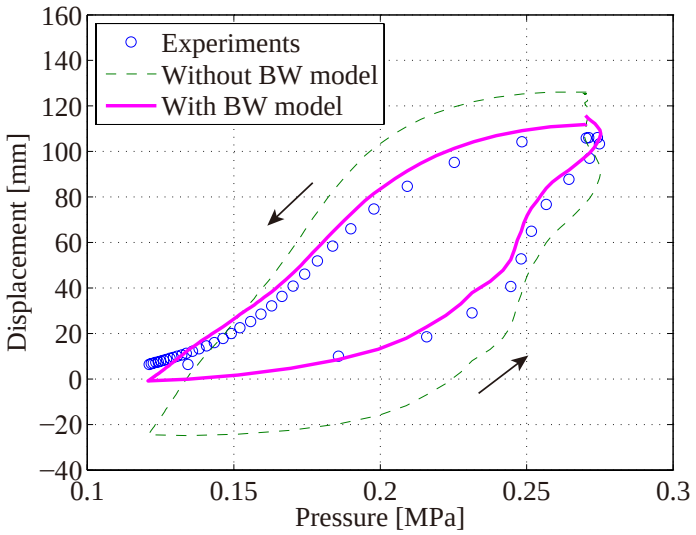


Fig. 4.12: Hysteresis loop of re-identified model with load: 7.0kgf

These results indicate when identification is conducted under loaded condition, the model has robustness for load changing. When loads are connected with the muscle, the load force always acts and pulls down the muscle. On the other hand, the restoring force of inner tube is dominant and correlation between supply pressure and displacement is poor at extension phase under no-load condition. Therefore, it is difficult to express behavior of the muscle for loads at that phase by using the proposed model, which is based on only input and output data. For this reason, identification under loaded condition is useful for the McKibben muscles.

# Chapter 5

# Controller design

## 5.1 Introduction

This chapter is concerned with controller design of tap water driven muscles. Purpose here is improvement of control performance of the muscles to expand their applications. In fact, the control performance of McKibben muscles is quite low due to their nonlinearities such as hysteresis. These muscles are, however, well known and they are used in fields not to be required high control performance. Then PID control is applied to the muscle systems. Conventional PID control cannot compensate the nonlinearities and it is difficult to use the muscles in various applications, which require precise control. To overcome this difficulty, some control laws have been applied: 1) $H_\infty$ control[7], 2) Gain scheduling control[9], 3) Adaptive backstepping control[67], 4) Sliding mode control[68], 5) Nonlinear PID control[69], and 6) Simple adaptive control[70].

The identified models of tap-water driven McKibben muscles are derived in Chap. 4. They are suitable for use of model-based controls for simplicity. In this chapter, two model-based controls that are MRAC and MPC are applied to the muscles. Adaptive control is an effective approach to compensate the effect of loads because it has robustness to disturbances. However, transient response is generally an essential problem of this control. That is, the control performance is unpredictable during parameter estimation process. In addition, the muscle parameters gradually change due to the material such as rubber tube and nylon sleeve. This means that the muscle is one example of the time-varying systems. Thus validation of the control performance for time-varying system is another purpose.

MPC is often used in process control[71]. It uses nominal models of plants to predict future outputs during a given time interval and to generate optimal inputs by minimizing an evaluation function. The evaluation function consists of error terms between reference trajectory and predicted outputs and input terms with proper weight. Moreover, MPC can take account of constraints for inputs and outputs. This is an advantage of it and the reason why MPC is often used.

MPC, however, cannot compensate effect of disturbances. Although accuracy of nominal models is important for control performance, conventional MPC is unsuitable when the parameters of the models are changed such as McKibben muscles. As mentioned before, the characteristics of the muscles is changed by loads. Thus compensation of disturbaces are a critical problem for the muscle displacement control. Therefore, we apply an adaptive parameter esitmation algorithm to MPC, that is adaptive model predictive control (AMPC).

Experiment of proposed controls shows control performance of them. Effect of loads and some parameters of the controller are also examined and discussed. In particular, key parameters of MPC and AMPC, which are coincident points and prediction horizon, are focused on.

## 5.2 PID control

PID control is a conventional control for muscle systems and generally only PI control is used. A purpose here is to find out its control performance by experiment. Figure 5.1 depicts block diagram of the PI controller. An input is applied voltage $u(t)$ for solenoid valves and an output is the muscle displacement $l(t)$.

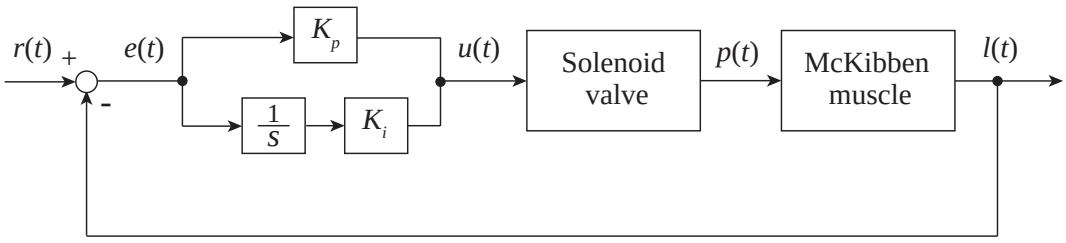


Fig. 5.1: Block diagram of PI control

### 5.2.1 Experiment of PI control

Figure 5.2 shows experimental result of PI control. Proportional and integral gains $K_p, K_i$ are chosen by trial and error; $K_p$ and $K_i$ are 0.65 and 12.12, respectively. Reference signal is sinusoidal wave; the frequency is 0.2 Hz, the amplitude is 25 mm, the offset is 95 mm. A sampling period for control is 0.01 s. Note that reference signal is set as low frequency such as 0.2 Hz to make the muscle displacement track the reference signal, especially extension phase because characteristics of rubber tube inside the muscle is dominant for the phase, contrary to contraction phase that characteristics of supply pressure is dominant. In other words, extension characteristics of the muscle is generally slower than contraction phase.

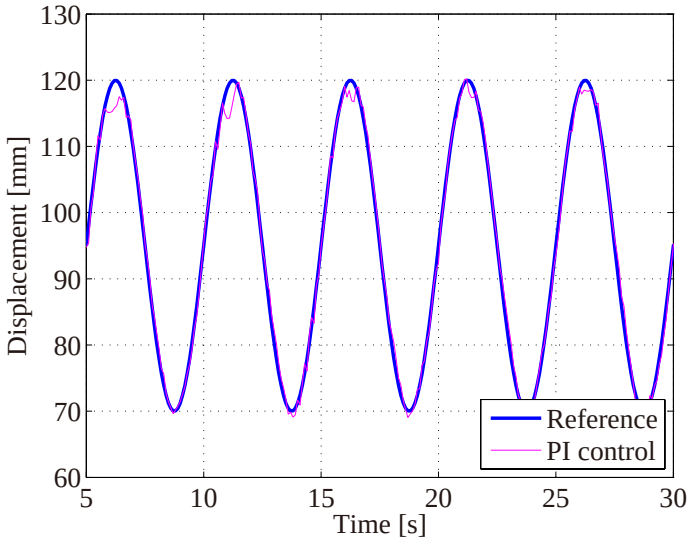


Fig. 5.2: Experimental result of PI control (sampling period: 0.01 s)

Next, experiment with sampling period 0.1 s is conducted. It is shown that the PI controller cannot make the muscle displacement track the reference signal. Figure 5.3 shows the result of PI control with sampling period of 0.1 s. This is carried out to compare the control performance of PI control with the one of other proposed model-based control such as MRAC and MPC.

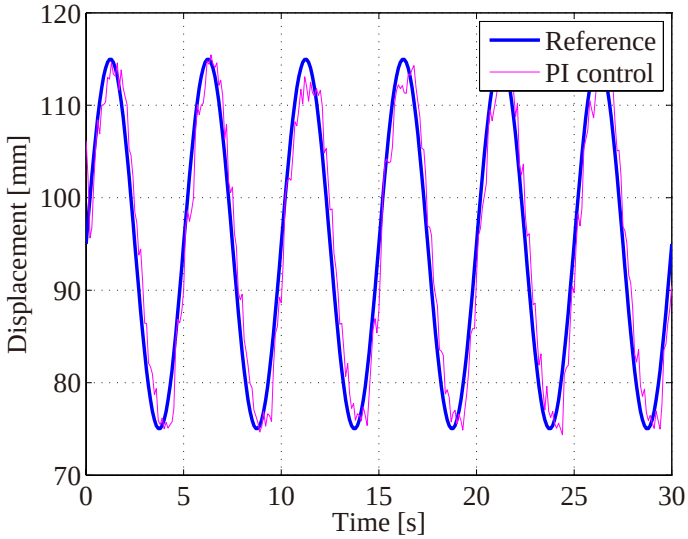


Fig. 5.3: Experimental result of PI control (sampling period: 0.1 s)

Following experiment examines the effect of loads connected with the muscle. Figures 5.4 and 5.5 show the experimental results of PI control with a load 3.5 kgf. Note that the gains are not changed in Fig. 5.4 but are changed in Fig. 5.5, and the frequency of reference signal is changed from 0.2 Hz to 0.1 Hz to show the difference plainly.

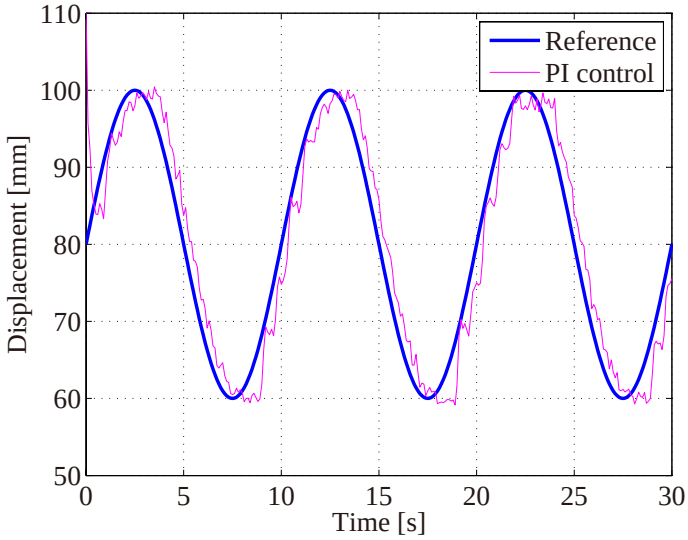


Fig. 5.4: Experimental result of PI control with a load: 3.5 kgf ($K_p = 0.65, K_i = 12.12$)

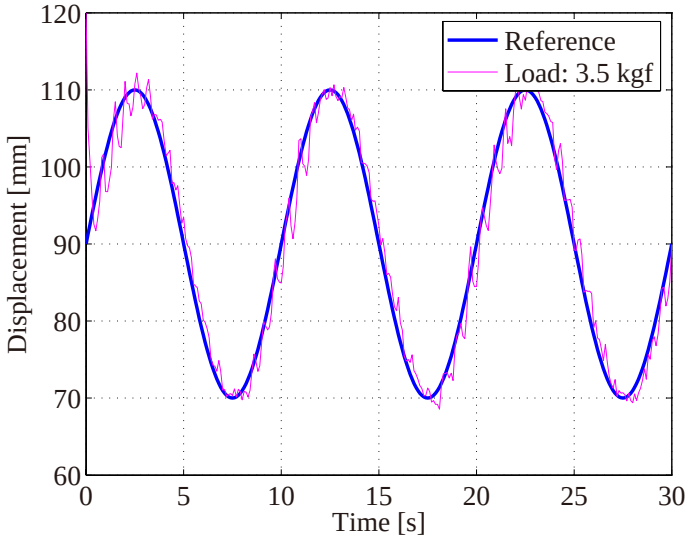


Fig. 5.5: Experimental result of PI control with a load: 3.5 kgf ($K_p = 1.363, K_i = 0.431$)

### 5.2.2 Discussion

The PI controller can control the muscle displacement when the proportional and integral gains are chosen adequately as shown in Figs. 5.2 and 5.3. Although relatively coarse sampling period 0.1s leads degradation of the control performance, especially reference signals are set to low frequency, 0.01 s as sampling period is available in application such as rehabilitation systems and robotics described in Chap. 3.

Figures 5.2 and 5.3 are special cases that no load is connected with the muscle. On the other hand, Figs. 5.4 and 5.5 show experimental results with a load. As seen in these figures, oscillation around the reference signal makes the control performance of PI control lower than the performance without loads. The load connected with the bottom end of the muscle pull the muscle down consistently. Thereby, extension characteristics of the muscle should be faster due to the load, and then the controller makes such oscillation because the gains of the controller are same. Thus, conventional PI control cannot compensate effect of loads. In addition, the larger loads are, the lower control performance of PI control is.

## 5.3 Adaptive control

This section shows experimental results of displacement control when MRAC is applied to the muscles. The applied algorithm of MRAC here is a projection algorithm[72]. Note that it is discrete-time deterministic adaptive control algorithm and objectives are single-input single-output systems. Although lots of adaptive control algorithms have been proposed, this simple algorithm is applied to compare with another model-based control, which is MPC.

### 5.3.1 Modified nominal muscle model

The nominal model derived in Chap. 4 should be modified to apply to displacement control. Although an input of the model is supply pressure $p(k)$ to make hysteresis analysis easy and the model simple, applied voltage for valves should be an input of the model for control purpose. Same method as Chap. 4, which is system identification method, is applied but input signal is changed from supply pressure to applied voltage for valves. As a result, following muscle model is obtained:

$$G_2(z) = \frac{L(z)}{U(z)} = \frac{0.2564z + 0.1995}{z^2 - 1.1209z - 0.2517} \tag{5.1}$$

where $U(z)$ is $z$-transformation of applied voltage for valves. Consideration of dynamics of valve makes the model second-order system. Figure 5.6 shows a comparison of measured and identified data by the model Eq. (5.1).

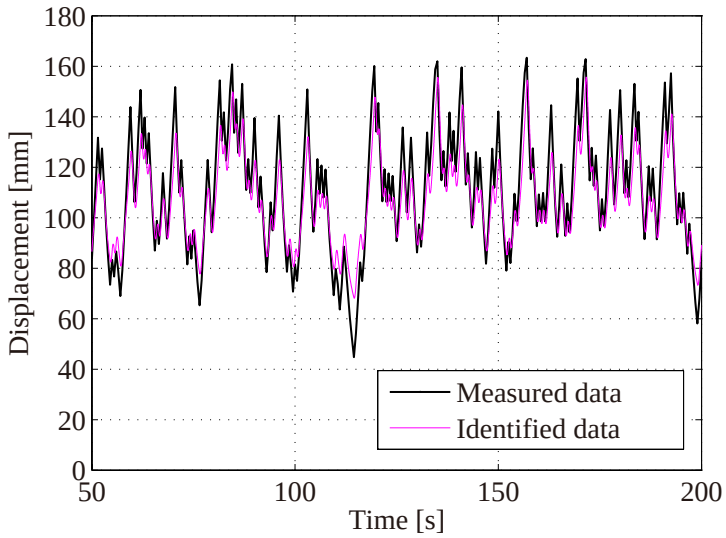


Fig. 5.6: Comparison of measured and identified data Eq. (5.1) (input: applied voltage for valves, output: muscle displacement)

In addition, state-space representation of the muscle model can be expressed as

$$\begin{aligned} l(k) &= 1.1209l(k-1) + 0.2517l(k-2) + 0.2564u(k-1) + 0.1995u(k-2) \\ &= \phi^T(k)\theta_0 \end{aligned} \tag{5.2}$$

where

$$\phi(k) = [l(k-1) \quad l(k-2) \quad u(k-1) \quad u(k-2)]^T \tag{5.3}$$

$$\theta_0 = [\theta_1 \quad \theta_2 \quad \theta_3 \quad \theta_4]^T \tag{5.4}$$

$$= [1.1209 \quad 0.2517 \quad 0.2564 \quad 0.1995]^T. \tag{5.5}$$

### 5.3.2 Methodology of MRAC (projection algorithm)

This algorithm generates inputs to make outputs, which are muscle displacement here, track outputs of a reference model. It means that the algorithm is one of the model reference adaptive controls.

Now we define output tracking error expressed as

$$\begin{aligned} e(k) &= l(k) - l^*(k) \\ &= \phi^T(k)\theta_0 - l^*(k). \end{aligned} \tag{5.6}$$

Althogh the tracking error being identically zero by choosing $u(k)$ to satisfy the following equation:

$$\phi^T(k)\theta_0 = l^*(k), \tag{5.7}$$

the following adaptive algorithm is applied because $\theta_0$ is essencially unknown[73].

$$\begin{aligned} \hat{\theta}(k) &= \hat{\theta}(k-1) + a(k)\phi(k-1)[1 + \phi^T(k-1)\phi(k-1)]^{-1} \\ &\quad \cdot(l(k) - \phi^T(k-1)\hat{\theta}(k-1)) \end{aligned} \tag{5.8}$$

$$\phi^T(k)\hat{\theta} = l^*(k+1) \tag{5.9}$$

where the gain constant $a(k)$ is chosen by:

$$a(k) = \begin{cases} 1 & \text{if [third component of right-hand side of Eq. (5.8)} \\ & \text{evaluated using } a(k) = 1] \neq 0, \\ \lambda & \text{otherwise where } \lambda \text{ is a constant in the interval } (\epsilon,\ 2-\epsilon), \\ & \lambda \neq 1 \text{ and } 0 < \epsilon < 1. \end{cases}$$

### 5.3.3 Experiment of MRAC: Projection algorithm

The experiment of MRAC is conducted to show its control performance, especially when some loads exist. Experimental conditions are same as previous conditions. A nominal model of the muscle is Eq. (5.2).

Figures 5.7 and 5.8 show experimental results of MRAC under no-load condition. Initial values of muscle displacement depend on the condition of muscle when the previous experiment was conducted.

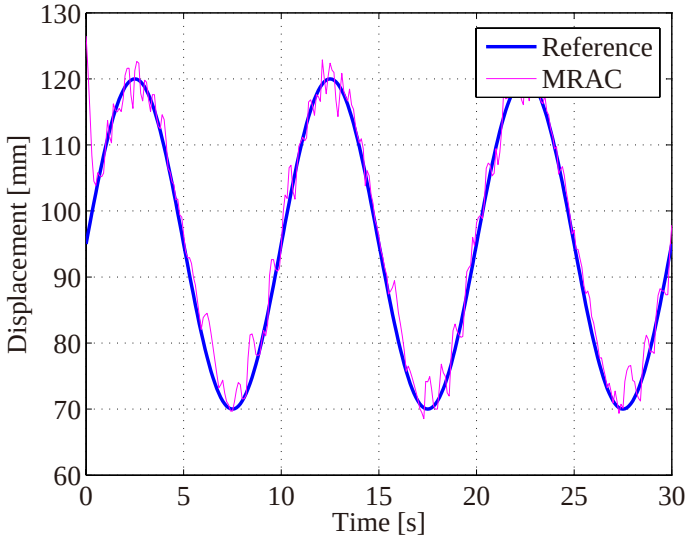


Fig. 5.7: Experimental result of MRAC

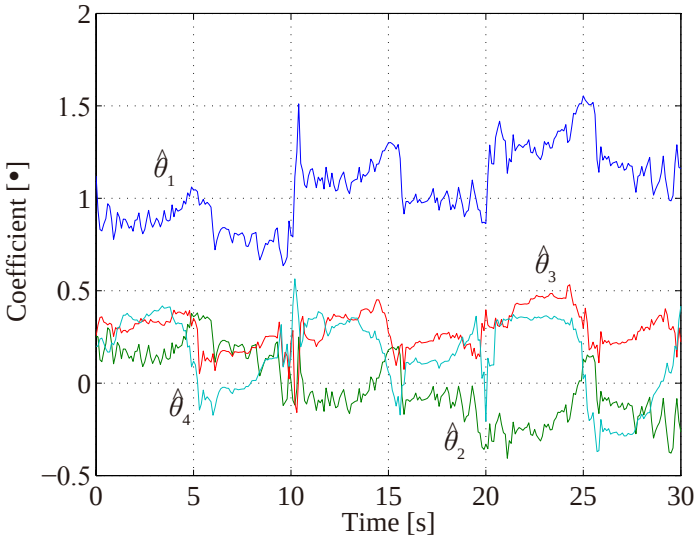


Fig. 5.8: Parameter estimation of MRAC

Next, experiment under loaded condition is conducted. Figures 5.9 and 5.10 show the experimental results.

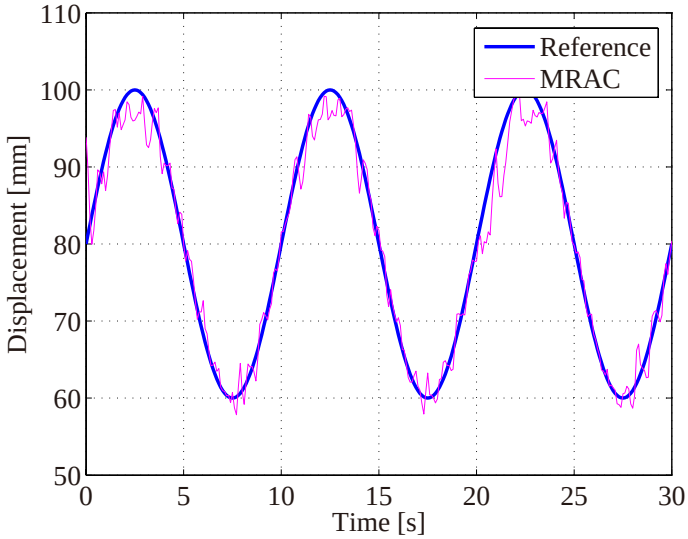


Fig. 5.9: Experimental result of MRAC (load: 3.5 kgf)

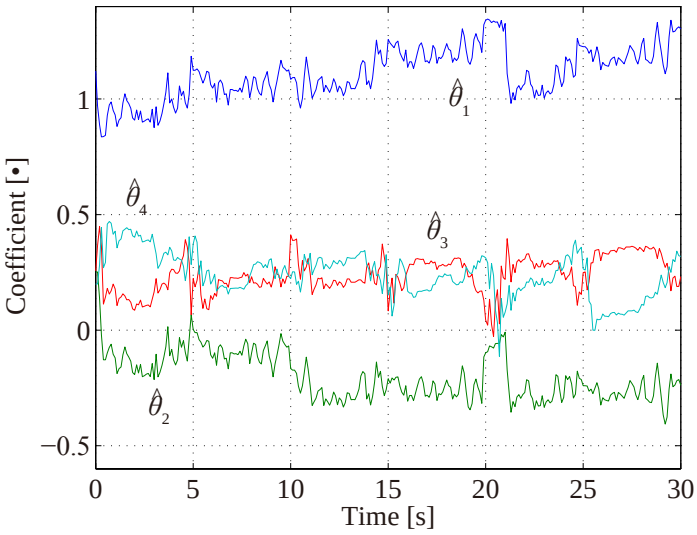


Fig. 5.10: Parameter estimation of MRAC (load: 3.5 kgf)

Note that amplitude of the reference signal is changed because characteristics of the muscle is varied by loads.

### 5.3.4 Discussion: MRAC (projection algorithm)

The experimental results show that MRAC can control the muscle displacement whether some loads exist or not. However, the control performance is not so high. This is caused by transient response of MRAC.

The characteristics of the muscle is varied by loads as mentioned before. In particular, when contract movement is switched from extension movement, the muscle parameters of the nominal model drastically changes. MRAC is one of resonable control methodologies to use for time-invariant systems because of its adaptive mechanism. However, transient response of parameter adaptation is an essential and critical problem of MRAC. In other words, the control performance of transient response of MRAC is not ensured. MRAC cannot work well for systems that its parameters are changed continuously.

As shown in Fig. 5.8, identified parameters of the nominal model are changed during experiment and are not converged to constant values because the characteristics of the muscle is changed as often as movement is switched and it is difficult to identify the parameters.

In addition, compared with conventional PI control, there are some fluctuations around 70 and 120 mm, which are switching points of movements in Fig. 5.7. The fluctuation in Fig. 5.9, which is the under loaded condition, is little bit smaller than the result under no-load condition. Moreover, comparison of Fig. 5.9 with Fig. 5.8 shows that the fluctuation ranges of identified parameters of the experiment under loaded condition are smaller than the ranges of the parameters of the experiment under no-load condition. It means that the pulling force of the load acts as an extension force of the muscle and the difference between contraction and extension movements becomes smaller.

## 5.4 Model predictive control (MPC): One coincident case

McKibben muscle systems can use relatively coarse sampling period for control because response of the muscles is generally slower than other actuators such as cylinders and motors. Moreover, performance improvement of PC makes MPC more attractive. Then MPC is applicable to the muscle systems. In general, MPC takes a lot of calculation time for prediction of outputs and optimal inputs. Applications of MPC to cylinder and motor controls are often inhibited by the problem of sampling period.

Unlike adaptive controls such as MRAC here, MPC not only introduces reference trajectory and makes outputs track the trajectory but also set arbitrary coincident points. Thus although both controls are model-based controls, the control performances during transient response differ from one another. MPC can control outputs during transient response as long as nominal models are well identified to the real objectives.

### 5.4.1 Methodology of MPC: One coincident case

Firstly, designers choose prediction horizon $H_p$ and then reference trajectory $r(k)$, which makes outputs track reference adequately as illustrated in Fig. 5.11. Figure 5.11 shows a case of one coincident point, which is the simplest case and predicted outputs coincide with reference trajectory at only $H_p$ steps later and then optimal input can be generated as a unique solution described later. Secondly, MPC calculates predicted outputs $\hat{y}(k|k)$ based on one-step-ahead estimation of nominal models. Finally, it generates optimal input $u(k|k)$ by minimizing evaluation functions. Note that expression $(k_1|k_2)$ means predicted value at time $k_1$ by calculating at time $k_2$. Although MPC can admit multiple coincident points on prediction horizon, it requires solutions of optimal problems such as quadratic programming and makes controllers complex[71].

To make controllers simple, we use only one coincident case at first. Note that the case imposes no constraints on inputs and outputs. If an optimal input is kept during prediction horizon, the input is uniquely decided. Predicted output $\hat{y}(k + H_p|k)$ is expressed as

$$\hat{y}(k + H_p|k) = \hat{y}_f(k + H_p|k) + S(H_p) \cdot \Delta\hat{u}(k|k) \tag{5.10}$$

where the first term of right-hand side indicates the free response that is obtained at $H_p$ steps later from present time $k$ when $u(k-1)$ is kept during $H_p$ steps and the second term indicates prediction of a step response at time $k$. $S(H_p)$ is the unit step response at $H_p$ steps later.

An optimal input difference $\Delta\hat{u}(k|k)$ can be expressed by difference between a present input and a predicted input as

$$\Delta\hat{u}(k|k) = \hat{u}(k|k) - u(k-1) \tag{5.11}$$

where $\hat{u}(k|k)$ is a predicted input at time $k$ and $u(k-1)$ is a present input.

A control purpose is to make predicted outputs coincide reference values at $H_p$ steps later and this is expressed as

$$\hat{y}(k + H_p|k) = r(k + H_p|k). \tag{5.12}$$

Substituting Eq. (5.12) into Eq. (5.10), input difference is rewritten by

$$\Delta\hat{u}(k|k) = \frac{r(k + H_p|k) - \hat{y}_f(k + H_p|k)}{S(H_p)}. \tag{5.13}$$

Thus optimal inputs can be obtained. Notice that this derivation assumes that model outputs coincide with plant outputs until present time $k$. Therefore, this routine is iterated every control steps.

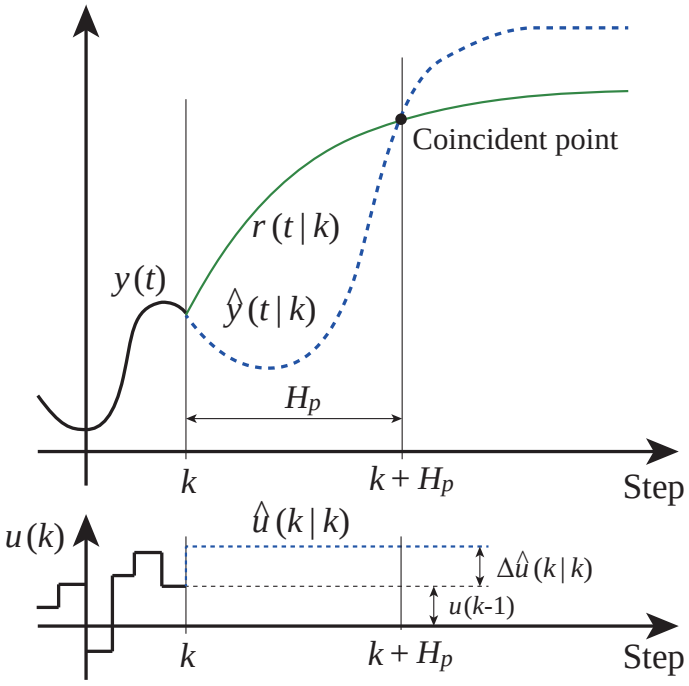


Fig. 5.11: Concept of MPC (one coincident case)

### 5.4.2 Experiment of MPC: One coincident point case

This section concerns with experiment of MPC for tap-water driven muscle systems described in Chap. 3. A nominal model of the muscle is Eq. (5.1), which is the re-identified model. Experimental

conditions are on Table 5.1 and a reference signal is sinusoidal wave same as previous experiment.

Table 5.1: Experimental conditions for MPC[71]

| Item | Value | Unit |
|---|---|---|
| sampling period | 0.01 | s |
| Prediction horizon | 4 | step |
| Coincident point | 1 | - |

Figures 5.12 and 5.13 show experimental result of MPC. Figures 5.14 and 5.15 depict reference signal and muscle displacement, and an input signal, respectively.

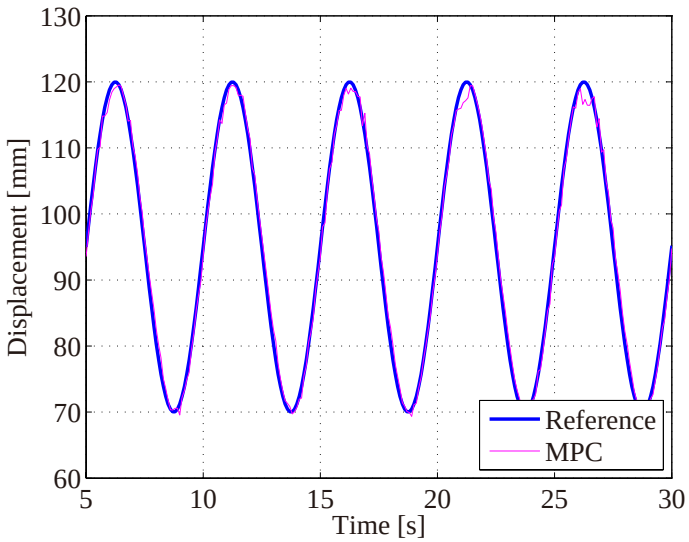


Fig. 5.12: Experimental result of MPC

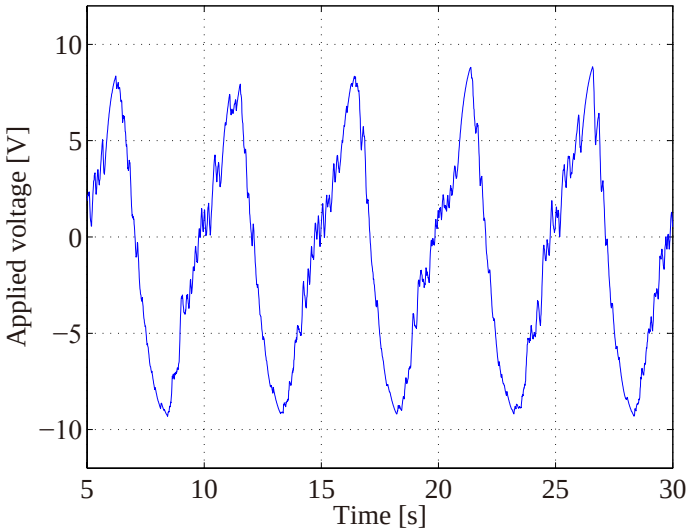


Fig. 5.13: Applied voltage for valve (MPC)

Following result shows the control performance of MPC when a load is connected with the muscle. Note that a nominal model of the muscle is also Eq. (5.1) and all experimental conditions listed in Table 5.1 are not changed.

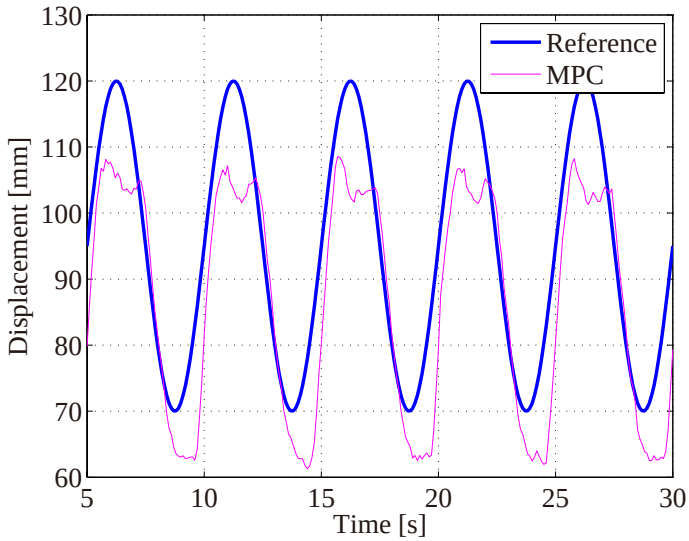


Fig. 5.14: Experimental result of MPC with load: 3.5 kgf

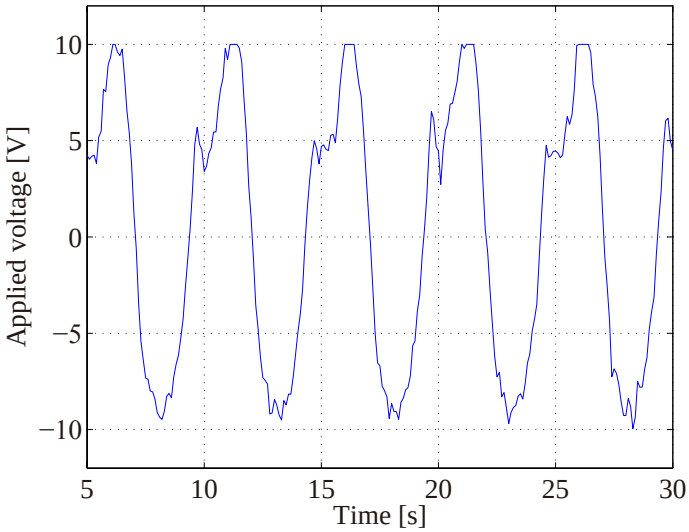


Fig. 5.15: Applied voltage for valve (Load: 3.5 kgf)

Saturation of applied voltage for the valves sometimes becomes a problem for prediction. Figures 5.16 and 5.17 show experimental result when the reference signal is changed; Amplitude 20 mm, offset 80 mm.

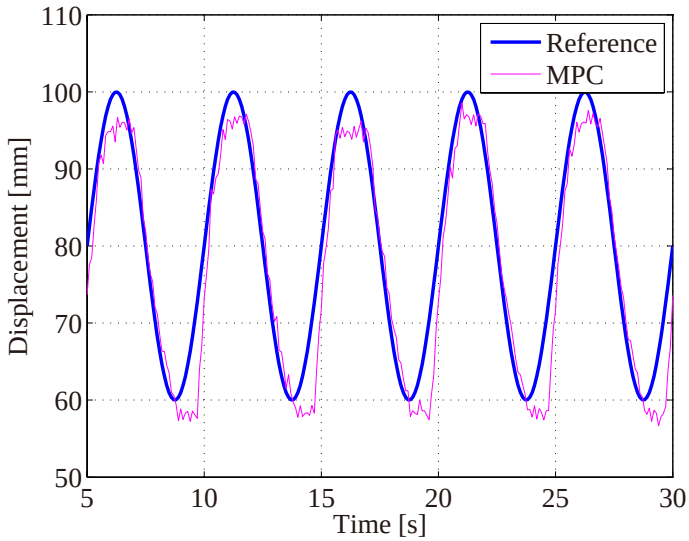


Fig. 5.16: Experimental result of MPC with load: 3.5 kgf

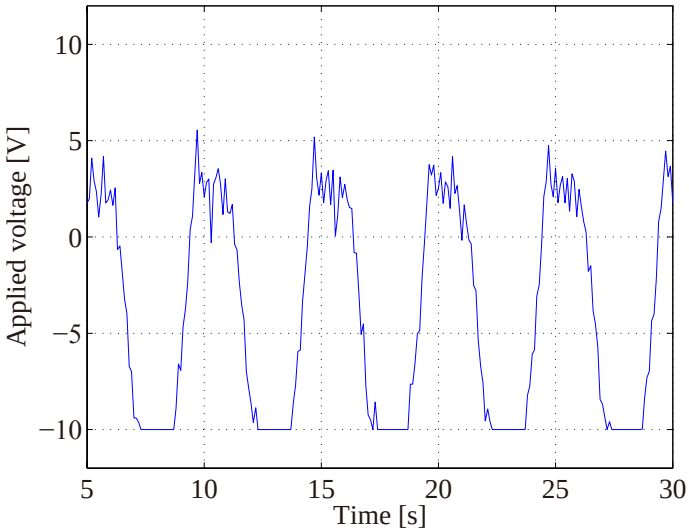


Fig. 5.17: Applied voltage for valve (Load: 3.5 kgf)

### 5.4.3 Discussion

This section describes experimental results and shows the control performance of PI control and MPC. Table 5.2 shows comparison of MPC with PI control with/without a load 3.5 kg.

Table 5.2: Comparison analysis of experimental results (PI vs. MPC)

| Control law | Mean abs. error [mm] | Max. abs. error [mm] |
|---|---|---|
| PI control | 1.588 | 4.370 |
| MPC | 1.176 | 3.973 |
| PI (with load) | 3.389 | 8.097 |
| MPC (with load) | 9.223 | 22.488 |

The result of MPC without the load shows that MPC have almost same control performance as conventional PI control, where the gains of PI control are chosen adequately. Both results show quite high performance. These are, however, the cases of no load.

On the other hand, when the load exists, the control performance of them are degraded, especially the performance of MPC drastically becomes worse. The performance of PI control can be improved by tuning the gains as shown in Fig. 5.5. However, to tune whenever loads change is not

practicable because loads connected with the muscle often change, for example, when the muscle is used as actuators of rehabilitation systems, loads are changed by body weight of patients. Thus tuning of the gains is difficult in practice.

Inaccuracy of prediction based on the nominal muscle model leads to the degradation of the performance of MPC. In other words, inappropriate predictions makes the performance worse because generation of inputs is based on predicted outputs by calculation of one-step-ahead estimation. Following equations indicate the nominal muscle model Eq. (5.1) and re-identified muscle model when the load is connected with the muscle:

$$G_2(z) = \frac{0.2564z + 0.1995}{z^2 - 1.1209z - 0.2517}, \qquad G_{2r}(z) = \frac{0.0051z + 0.1497}{z^2 - 1.1633z - 0.6872}. \tag{5.14}$$

Thus parameters of the muscle model are changed by the load. Then prediction using Eq. (5.1) can no longer work well and the controller generates ineligible inputs. Moreover, although the muscle becomes difficult to contract and easy to expand when loads are connected with the muscle, the model Eq. (5.1) cannot take account of it. Then the predicted outputs have offset as seen in Fig. 5.14. This is caused by parameter changing of muscle model and then we apply an adaptive parameter identification algorithm in next section, which is called recursive least squares (RLS) algorithm.

Figures 5.16 and 5.17 show that input signal is limited by saturation, which is based on rated voltage of the valves. The predictor in MPC here, however, cannot take into consideration of saturation. In other words, MPC assumes that the controller can take arbitrary inputs such as more than 10 V and less than -10 V.

## 5.5 Adaptive model predictive control (AMPC)

We apply an adaptive parameter estimation algorithm to the MPC in order to compensate parameter changing of the muscle when loads are connected with the muscle. The algorithm here is recursive least squares (RLS) algorithm[74]. This updates the parameters of the nominal muscle model Eq. (5.1). This section shows that RLS algorithm can compensate the parameter changing caused by loads. Moreover, the characteristics of the muscle changing momentarily due to materials such as

inner tube and sleeve can also be compensated by the algorithm.

RLS algorithm is combined with conventional MPC described previous sections. In particular, the nominal muscle model predicting outputs during prediction horizon is updated on real-time basis. Figure 5.18 shows block diagram of proposed controller including RLS algorithm.

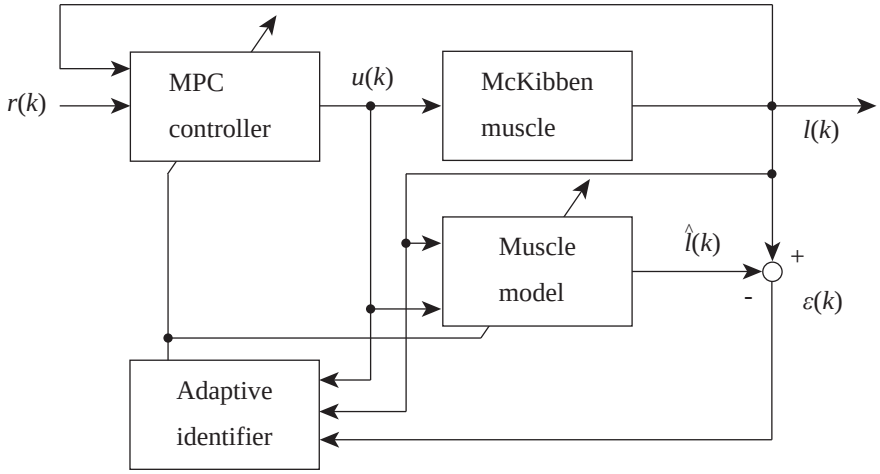


Fig. 5.18: Block diagram of MPC with RLS algorithm

Note that $r(k)$ is reference signals, $u(k)$ input signals, $l(k)$ muscle displacement, $\hat{l}(k)$ estimated muscle displacement, $\varepsilon(k)$ estimated error consisting of difference between $l(k)$ and $\hat{l}(k)$.

### 5.5.1 RLS algorithm

In general, algorithms that are used in system identification, for example least squares method, and based on obtained inputs and outputs are called off-line methods. These require all input and output data. Therefore, amount of calculation becomes larger and the algorithms are hard to be implemented on real-time basis.

Least square estimates based on input and output data at present time $k$ can be obtained by

$$\hat{\theta}(k) = \left( \sum_{i=1}^{k} \phi(i)\phi^T(i) \right)^{-1} \left( \sum_{i=1}^{k} \phi(i)y(i) \right) \tag{5.15}$$

where $\hat{\theta}(k)$ is estimated parameter vector, $\phi(k)$ regression vector consisting of inputs and outputs. Note that the detail of least squares method is introduced in Appendix B.

Then a covariance matrix $P(k)$ is expressed as

$$P(k) = \left( \sum_{i=1}^{k} \phi(i)\phi^T(i) \right)^{-1}. \tag{5.16}$$

Taking accout of inverse matrix of both side of Eq. (5.16) leads to

$$\begin{aligned} P^{-1}(k) &= \sum_{i=1}^{k-1} \phi(i)\phi^T(i) + \phi(k)\phi^T(k) \\ &= P^{-1}(k-1) + \phi(k)\phi^T(k). \end{aligned} \tag{5.17}$$

Same calculation also gives

$$\sum_{i=1}^{k} \phi(i)y(i) = \sum_{i=1}^{k-1} \phi(i)y(i) + \phi(k)y(k). \tag{5.18}$$

Substituting Eqs. (5.16)-(5.18) into Eq. (5.15), following equation is obtained

$$\begin{aligned} \hat{\theta}(k) &= P(k)\left( \sum_{i=1}^{k} \phi(i)y(i) \right) \\ &= P(k)\{P^{-1}(k-1)\hat{\theta}(k-1) + \phi(k)y(k)\} \\ &= \hat{\theta}(k-1) + P(k)\phi(k)\{y(k) - \phi^T(k)\hat{\theta}(k-1)\}. \end{aligned} \tag{5.19}$$

Applying matrix inversion lemma to Eq. (5.17),

$$P(k) = P(k-1) - \frac{P(k-1)\phi(k)\phi^T(k)P(k-1)}{1 + \phi^T(k)P(k-1)\phi(k)}. \tag{5.20}$$

The term $P(k)\phi(k)$ can be rewritten by using Eq. (5.20) as

$$\begin{aligned} P(k)\phi(k) &= \left\{ P(k-1) - \frac{P(k-1)\phi(k)\phi^T(k)P(k-1)}{1 + \phi^T(k)P(k-1)\phi(k)} \right\}\phi(k) \\ &= P(k-1)\phi(k)\left\{ 1 - \frac{\phi^T(k)P(k-1)\phi(k)}{1 + \phi^T(k)P(k-1)\phi(k)} \right\} \\ &= \frac{P(k-1)\phi(k)}{1 + \phi^T(k)P(k-1)\phi(k)}. \end{aligned} \tag{5.21}$$

Substituting Eq. (5.21) into Eq. (5.19),

$$\hat{\theta}(k) = \hat{\theta}(k-1) + \frac{P(k-1)\phi(k)}{1+\phi^T(k)P(k-1)\phi(k)}\varepsilon(k). \tag{5.22}$$

where $\varepsilon(k)$ is estimated error and difined by

$$\varepsilon(k) = y(k) - \phi^T(k)\hat{\theta}(k-1). \tag{5.23}$$

Consequently, RLS algorithm is expressed as

$$\begin{aligned}
\hat{\theta}(k) &= \hat{\theta}(k-1) + \frac{P(k-1)\phi(k)}{1+\phi^T(k)P(k-1)\phi(k)}\varepsilon(k) \\
\varepsilon(k) &= y(k) - \phi^T(k)\hat{\theta}(k-1) \\
P(k) &= P(k-1) - \frac{P(k-1)\phi(k)\phi^T(k)P(k-1)}{1+\phi^T(k)P(k-1)\phi(k)}
\end{aligned}$$

where initial value of $\hat{\theta}(k)$ is given by designers and also initial value of $P(k)$ is given to satisfy following equation;

$$P(0) = \zeta I. \tag{5.24}$$

where $\zeta$ is an arbitrary positive constant.

### 5.5.2 RLS algorithm with rectangular windows

Rectangular windows are usually used for RLS algorithm to apply the algorithm to time-varying system[75]. In general, an evaluation function can be expressed as

$$J(k) = \sum_{i=1}^{k} \varepsilon^2(i). \tag{5.25}$$

On the other hand, forgetting by using rectangular windows as shown in Fig. 5.19 can modify the evaluation function Eq. (5.25) as

$$J_r(k) = \sum_{i=k-L+1}^{k} \varepsilon^2(i). \tag{5.26}$$

This means that past data before the time $k - L + 1$ can be neglected and data included in the rectangular window are only used for estimation.

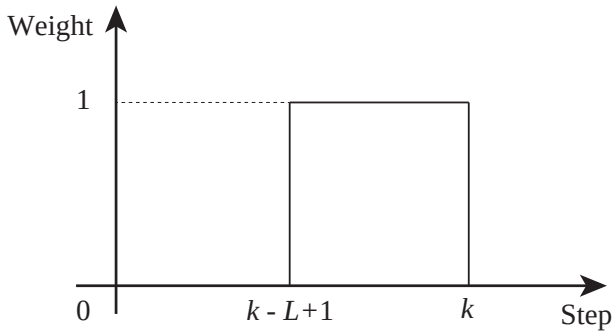


Fig. 5.19: Rectangular window

The modification gives following normal equations.

$$F(k)\hat{\theta}(k) = g(k) \tag{5.27}$$

where

$$F(k) = \sum_{i=k-L+1}^{k} \phi(i)\phi^T(i), \quad g(k) = \sum_{i=k-L+1}^{k} \phi(i)y(i) \tag{5.28}$$

Therefore, following equations can be obtained:

$$F(k) = F(k-1) + \phi(k)\phi^T(k) - \phi(k-L)\phi^T(k-L) \tag{5.29}$$

$$g(k) = g(k-1) + \phi(k)y(k) - \phi(k-L)y(k-L). \tag{5.30}$$

Then an assumption that

$$H(k) = F(k-1) - \phi(k-L)y(k-L) \tag{5.31}$$

rewrites Eq. (5.29) as

$$F(k) = H(k) + \phi(k)\phi^T(k). \tag{5.32}$$

Appling matrix inversion lemma to Eqs. (5.31) and (5.32), RLS algorithm with rectangular

windows can be obtained as

$$\begin{aligned}\hat{\theta}(k) &= \hat{\theta}(k-1)P(k)\phi(k)\{y(k)-\phi^T(k)\hat{\theta}(k-1)\} \\ &\quad -P(k)\phi(k-L)\{y(k-L)-\phi^T(k-L)\hat{\theta}(k-1)\} \qquad (5.33)\\ P(k) &= Q(k)-\frac{Q(k)\phi(k)\phi^T(k)Q(k)}{1+\phi^T(k)Q(k)\phi(k)} \qquad (5.34)\\ Q(k) &= P(k-1)+\frac{P(k-1)\phi(k-L)\phi^T(k-L)P(k-1)}{1+\phi^T(k-L)P(k-1)\phi(k-L)} \qquad (5.35)\end{aligned}$$

where $P(k) = F^{-1}(k)$ and $Q(k) = H^{-1}(k)$. Note that when $k - L = 1$, this algorithm is same as conventional RLS algorithm.

### 5.5.3 Experiment of AMPC

This section shows effectiveness of RLS algorithm by experiment. In the previous sections, the control performance of the MPC is degraded when there exists loads as seen in Table 5.2.

First of all, the nominal muscle model Eq. (5.1) is rewritten to express by using a parameter vector $\theta_0$ and a regression vector $\phi(k)$.

$$\begin{aligned}l(k) &= 1.1209l(k-1)+0.2517l(k-2)+0.2564u(k-1)+0.1995u(k-2)\\ &= \theta_0^T\phi(k) \qquad (5.36)\end{aligned}$$

where

$$\begin{aligned}\theta_0 &= [\theta_1 \quad \theta_2 \quad \theta_3 \quad \theta_4]^T\\ &= [1.1209 \quad 0.2517 \quad 0.2564 \quad 0.1995]^T, \qquad (5.37)\\ \phi(k) &= [l(k-1) \quad l(k-2) \quad u(k-1) \quad u(k-2)]^T. \qquad (5.38)\end{aligned}$$

RLS algorithm can estimate the parameter vector Eq. (5.37) on real-time basis. Then estimated parameter vector $\hat{\theta}(k)$ is used for prediction phase in MPC, which is calculation of one-step-ahead estimation. Note that transient state of parameter estimation and also control performance of the controller cannot be compensated.

AMPC can control the muscle displacement as same performance as conventional MPC when

no load is connected because the characteristics of the muscle are not changed. Figures 5.20 and 5.21 show the experimental results when a load 3.5 kgf is connected. Note that initial value of $P(k)$, that is $\zeta$, is $1 \times 10^3$ and other experimental conditions are same as in Table 5.1.

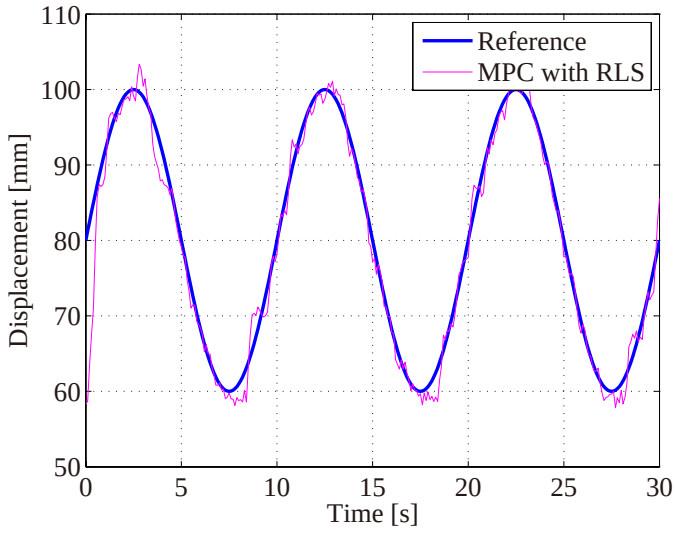


Fig. 5.20: Experimental result of AMPC

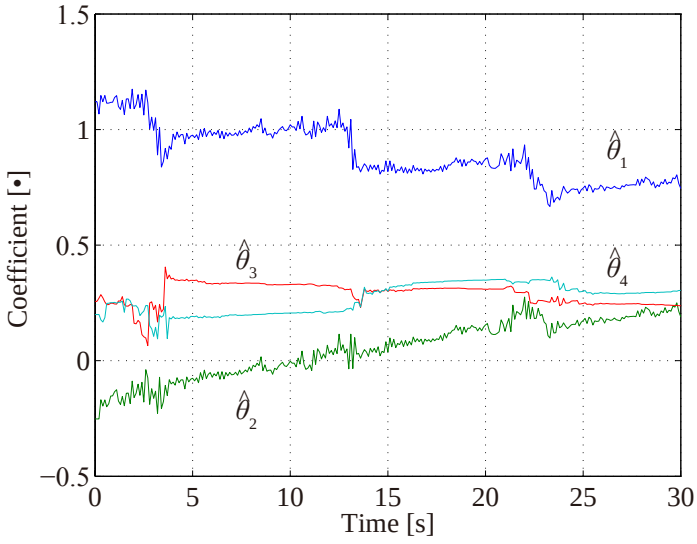


Fig. 5.21: Parameter estimation by RLS algorithm

Figure 5.22 shows a result of parameter estimation for long-term experiment. This experiment

is conducted to examine effectiveness of AMPC for time-varying system.

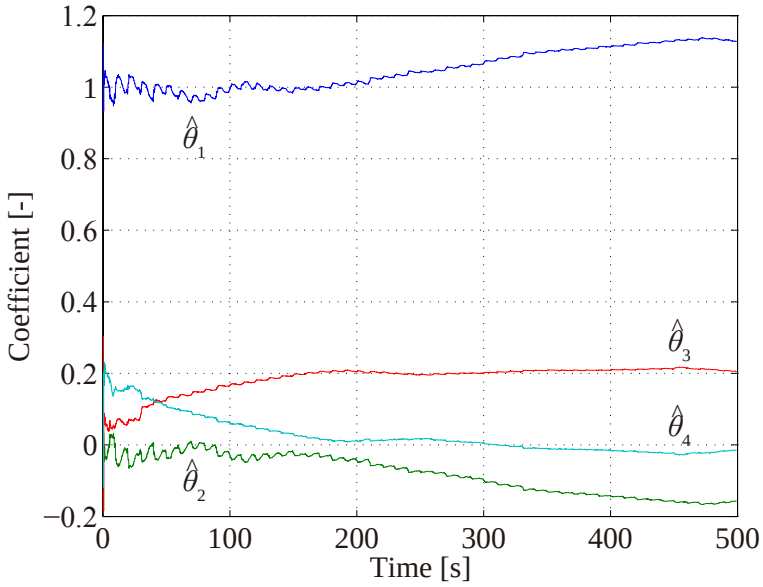


Fig. 5.22: Experimental result of AMPC

Figures 5.23 and 5.24 show the results of one-step-ahead estimation at the first 30 seconds and the last 30 seconds of the experiment, respectively.

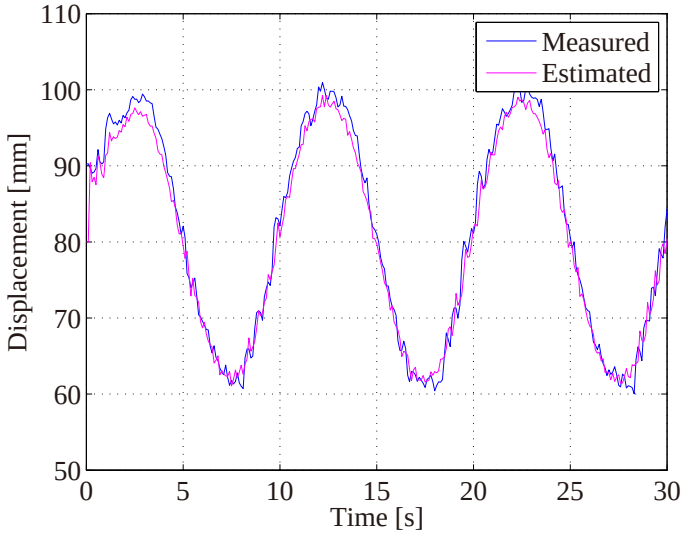


Fig. 5.23: One-step-ahead estimation at the first 30 seconds

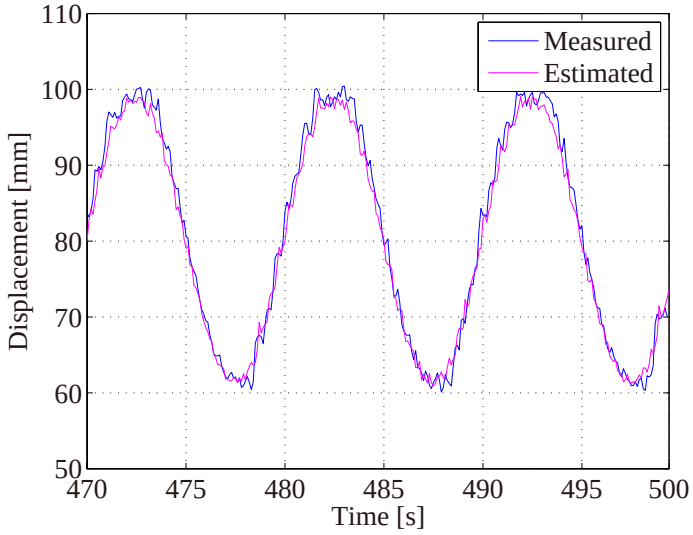


Fig. 5.24: One-step-ahead estimation at the last 30 seconds

### 5.5.4 Discussion

Experimental results described in Figs. 5.20 and 5.21 show that the RLS algorithm can compensate the effect of loads. The parameters of the nominal muscle model can be updated as shown in Fig. 5.21 and then the muscle displacement can track the reference trajectory as shown in Fig. 5.20. Thus taking account of the effect of loads as parameter changing, AMPC can control the displacement whenever there exists loads.

Moreover, when driving phases change, which are contraction and expansion phases, the RLS algorithm works well and the parameters of the muscle, especially $\hat{\theta}_1$ is drastically changed. This indicates that the characteristics of the muscle changes at the points.

On the other hand, Figs. 5.22-5.24 show the results of long-term experiment. When the characteristics of the muscle changes the parameters of the muscle also do. Although the changing of the parameters is small, the muscle can be treated as a time-varying system.

The RLS algorithm can also compensate the parameter changing of the time-varying system. One-step-ahead estimations shown in Figs. 5.23 and 5.24 are almost same but the parameters described in Fig. 5.22 has been changed. Therefore the algorithm can estimate the changing parameters of the muscle and the performance of one-step-ahead estimations are kept.

## 5.6 MPC: Multiple coincident points case

Previous section introduced the one coincident case for MPC. In the section, the controller can generate optimal input to make predicted output coincide the reference only at time $k + H_p$. Then optimal inputs can be chosen by calculating of free response and step response of nominal models. Note that the optimal inputs are unique solutions with assumption that the optimal inputs are kept during prediction horizon.

### 5.6.1 Methodology of MPC: Multiple coincident points case

MPC can also take multiple coincident points during prediction horizon[71]. When multiple coincident points are given, the controller cannot choose inputs in a same way as the one coincident case because equations to be solved are more than variables. Then approximate solutions are used, especially the least squares solutions.

The approximate solutions are solved by using an evaluation function. Generally, the evaluation function is defined as

$$V(k) = \sum_{i=0}^{H_p} ||\hat{y}(k+i|k) - r(k+i|k)||^2_{\mathcal{Q}(i)} + \sum_{i=0}^{H_u-1} ||\Delta\hat{u}(k+i|k)||^2_{\mathcal{R}(i)} \tag{5.39}$$

where $H_u$ is a control horizon, $\mathcal{Q}(i)$ a weight matrix for error between predicted outputs and reference, $\mathcal{R}(i)$ a weight matrix for inputs. Moreover, one coincident case can be considered by choosing some elements of $\mathcal{Q}(i)$ as zero.

Equation (5.39) can be rewritten by

$$V(k) = ||\mathcal{Y}(k) - \mathcal{T}(k)||^2_{\mathcal{Q}} + ||\Delta\mathcal{U}(k)||^2_{\mathcal{R}} \tag{5.40}$$

where

$$\begin{aligned} \mathcal{Y}(k) &= \begin{bmatrix} \hat{y}(k|k) \\ \vdots \\ \hat{y}(k+H_p|k) \end{bmatrix}, \quad \mathcal{T}(k) = \begin{bmatrix} r(k|k) \\ \vdots \\ r(k+H_p|k) \end{bmatrix}, \\ \Delta\mathcal{U}(k) &= \begin{bmatrix} \Delta\hat{u}(k|k) \\ \vdots \\ \Delta\hat{u}(k+H_u-1|k) \end{bmatrix} \end{aligned} \tag{5.41}$$

and weight matrices $\mathcal{Q}$ and $\mathcal{R}$ are given by

$$\mathcal{Q} = \begin{bmatrix} \mathcal{Q}(0) & 0 & \cdots & 0 \\ 0 & \mathcal{Q}(1) & \cdots & 0 \\ \vdots & \vdots & \ddots & \vdots \\ 0 & 0 & \cdots & \mathcal{Q}(H_p) \end{bmatrix}, \quad \mathcal{R} = \begin{bmatrix} \mathcal{R}(0) & 0 & \cdots & 0 \\ 0 & \mathcal{R}(1) & \cdots & 0 \\ \vdots & \vdots & \ddots & \vdots \\ 0 & 0 & \cdots & \mathcal{R}(H_u-1) \end{bmatrix}, \tag{5.42}$$

respectively. Predicted state variables $\hat{x}(k)(C\hat{x}(k) = \hat{y}(k))$ based on nominal models can be ob-

tained as

$$\begin{bmatrix} \hat{x}(k+1|k) \\ \vdots \\ \hat{x}(k+H_u|k) \\ \hat{x}(k+H_u+1|k) \\ \vdots \\ \hat{x}(k+H_p|k) \end{bmatrix} = \begin{bmatrix} A \\ \vdots \\ A^{H_u} \\ A^{H_u+1} \\ \vdots \\ A^{H_p} \end{bmatrix} x(k) + \begin{bmatrix} B \\ \vdots \\ \sum_{i=0}^{H_u-1} A^i B \\ \sum_{i=0}^{H_u} A^i B \\ \vdots \\ \sum_{i=0}^{H_p-1} A^i B \end{bmatrix} u(k-1)$$
$$+ \begin{bmatrix} B & \cdots & 0 \\ AB+B & \cdots & 0 \\ \vdots & \ddots & \vdots \\ \sum_{i=0}^{H_u-1} A^i B & \cdots & B \\ \sum_{i=0}^{H_u} A^i B & \cdots & AB+B \\ \vdots & \ddots & \vdots \\ \sum_{i=0}^{H_p-1} A^i B & \cdots & \sum_{i=0}^{H_p-H_u} A^i B \end{bmatrix} \begin{bmatrix} \Delta\hat{u}(k|k) \\ \vdots \\ \Delta\hat{u}(k+H_u-1|k) \end{bmatrix} \quad (5.43)$$

With definitions of

$$\Psi = \begin{bmatrix} A \\ \vdots \\ A^{H_u} \\ A^{H_{u+1}} \\ A^{H_p} \end{bmatrix}, \ \Upsilon = \begin{bmatrix} B \\ \vdots \\ \sum_{i=0}^{H_u-1} A^i B \\ \sum_{i=0}^{H_u} A^i B \\ \vdots \\ \sum_{i=0}^{H_p-1} A^i B \end{bmatrix}, \ \Theta = \begin{bmatrix} B & \cdots & 0 \\ AB+B & \cdots & 0 \\ \vdots & \ddots & \vdots \\ \sum_{i=0}^{H_u-1} A^i B & \cdots & B \\ \sum_{i=0}^{H_u} A^i B & \cdots & AB+B \\ \vdots & \vdots & \vdots \\ \sum_{i=0}^{H_p-1} A^i B & \cdots & B \end{bmatrix}, \quad (5.44)$$

an error equation can be obtained by

$$\varepsilon(k) = \mathcal{T}(k) - \Psi x(k) - \Upsilon u(k-1). \quad (5.45)$$

Eq. (5.40) is rewritten again by using Eqs. (5.43) and (5.44) as

$$\begin{aligned} V(k) &= ||\Theta\Delta\mathcal{U}(k) - \varepsilon(k)||^2_{\mathcal{Q}} + ||\Delta\mathcal{U}(k)||^2_{\mathcal{R}} \\ &= \varepsilon^T(k)\mathcal{Q}\varepsilon(k) - 2\Delta\mathcal{U}^T(k)\Theta^T\mathcal{Q}\varepsilon(k) + \Delta\mathcal{U}^T(k)[\Theta^T\mathcal{Q}\Theta + \mathcal{R}]\Delta\mathcal{U}(k). \end{aligned} \quad (5.46)$$

Considering following definitions;

$$\mathcal{G} = 2\Theta^T\mathcal{Q}\varepsilon(k), \quad \mathcal{H} = \Theta^T\mathcal{Q}\Theta + \mathcal{R}, \quad (5.47)$$

then the optimal input differences can be obtained by

$$\Delta\mathcal{U}(k)_{opt} = \frac{1}{2}\mathcal{H}^{-1}\mathcal{G}. \quad (5.48)$$

### 5.6.2 Modification of nominal model

A nominal model of the muscle is obtained by Eq. (5.1). When multiple coincident points are given, it is suitable to reduce the order of the nominal model because MPC makes lots of calculation of predicted output and optimal input as seen in the previous section 5.6.1. The order of denominator of the model expressing the dynamics of the model cannot be reduced and then the order of numerator of the model is reduced;

$$G_3(z) = \frac{L(z)}{U(z)} = \frac{0.1766z}{z^2 - 1.4406z + 0.4619} \quad (5.49)$$

Although fitting ratio of this model is less than the ratio of the previous model, the accuracy of one-step-ahead estimation is more than 95%. Note that sampling period is changed from 0.01 s to 0.1 s to gain enough calculation time for prediction within the sampling period. Then transforming Eq. (5.49) (transfer function) into state-space expression, we can obtain a following equation.

$$\begin{aligned} \mathcal{L}(k+1) &= \begin{bmatrix} 1.4406 & -0.4619 \\ 1 & 0 \end{bmatrix} \mathcal{L}(k) + \begin{bmatrix} 0.1766 \\ 0 \end{bmatrix} u(k) \\ &= A\mathcal{L}(k) + Bu(k) \end{aligned} \quad (5.50)$$

where $\mathcal{L}(k) = \begin{bmatrix} l(k) & l(k-1) \end{bmatrix}^T$ and

$$A = \begin{bmatrix} 1.4406 & -0.4619 \\ 1 & 0 \end{bmatrix}, \quad B = \begin{bmatrix} 0.1766 \\ 0 \end{bmatrix}. \tag{5.51}$$

Considering prediction horizon as 3 steps, a following equation is obtained,

$$\begin{aligned} \begin{bmatrix} \mathcal{L}(k+1) \\ \mathcal{L}(k+2) \\ \mathcal{L}(k+3) \end{bmatrix} &= \begin{bmatrix} A \\ A^2 \\ A^3 \end{bmatrix} \mathcal{L}(k) + \begin{bmatrix} B \\ (A+I)B \\ (A^2+A+I)B \end{bmatrix} u(k-1) \\ &+ \begin{bmatrix} B & 0 & 0 \\ (A+I)B & B & 0 \\ (A^2+A+I)B & (A+I)B & B \end{bmatrix} \begin{bmatrix} \Delta\hat{u}(k) \\ \Delta\hat{u}(k+1) \\ \Delta\hat{u}(k+2) \end{bmatrix}. \end{aligned} \tag{5.52}$$

Based on these equations and Eq. (5.48), optimal input difference can be obtained.

### 5.6.3 Experimental results of MPC: Multiple coincident points case

First of all, MPC using one coincident point has a problem. Figures 5.25 and 5.26 show experimental results of MPC using one coincident. Thus, when the sampling period of the experiment is coarse and the prediction horizon is longer, MPC using one coincident cannot work well and the muscle displacement also cannot track the reference because the inputs are chosen to coincide the predicted muscle displacement with the reference only at time $k+H_p$ and the controller cannot consider any other reference during prediction horizon such as $\hat{l}(k+1),\ \hat{l}(k+2),\ \cdots,\ \hat{l}(k+H_p-1)$. Although this problem may be prevented by a priori calculation based on nominal models, it is not practicable.

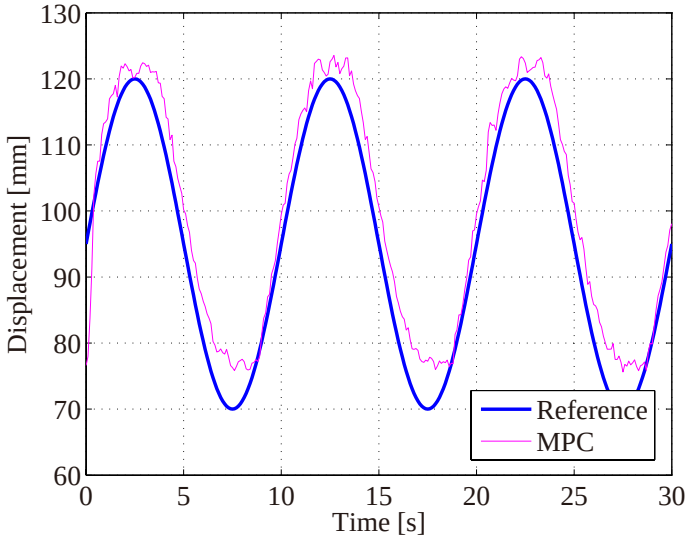


Fig. 5.25: Experimental result of MPC using one coincident point: 0.1 Hz ($H_p = 5$)

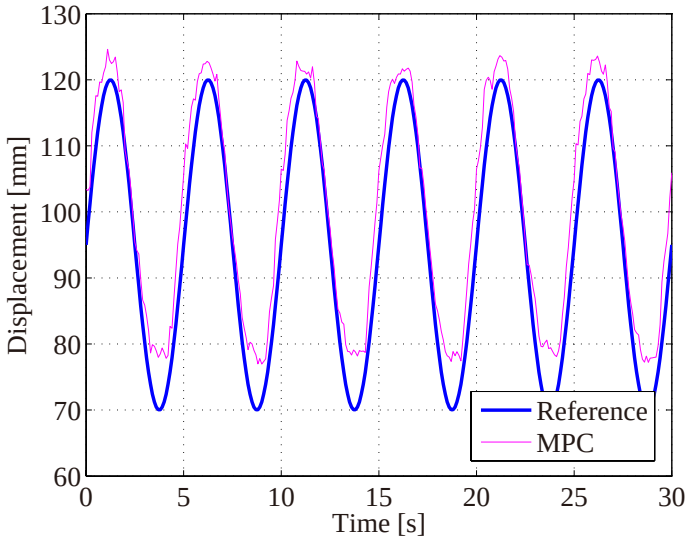


Fig. 5.26: Experimental result of MPC using one coincident point: 0.2 Hz ($H_p = 5$)

Next experiment shows the control performance of MPC using multiple coincident points. The nominal model of the muscle is same model as Eq. (5.50) and experimental conditions are follows: sampling period is 0.1 s, prediction horizon four step, and four coincident points. Note that Figs. 5.27 and 5.28 show the experimental results of 0.1 and 0.2 Hz as reference frequency, respectively.

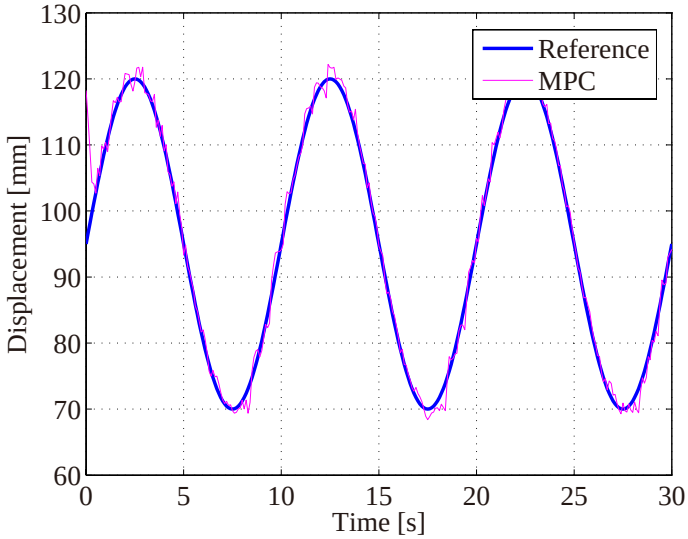


Fig. 5.27: Experimental result of MPC using four coincident points: 0.1 Hz ($H_p = 4$)

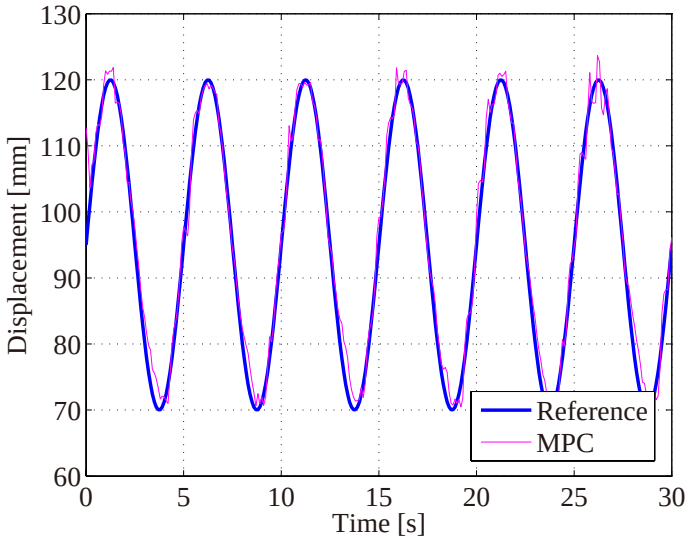


Fig. 5.28: Experimental result of MPC using four coincident points: 0.2 Hz ($H_p = 4$)

Changing prediction horizon from four to five steps shows following experimental results. Experimental conditions except for prediction horizon are same as previous experiment. Figs. 5.29 and 5.30 show the experimental results of 0.1 and 0.2 Hz as reference frequency, respectively.

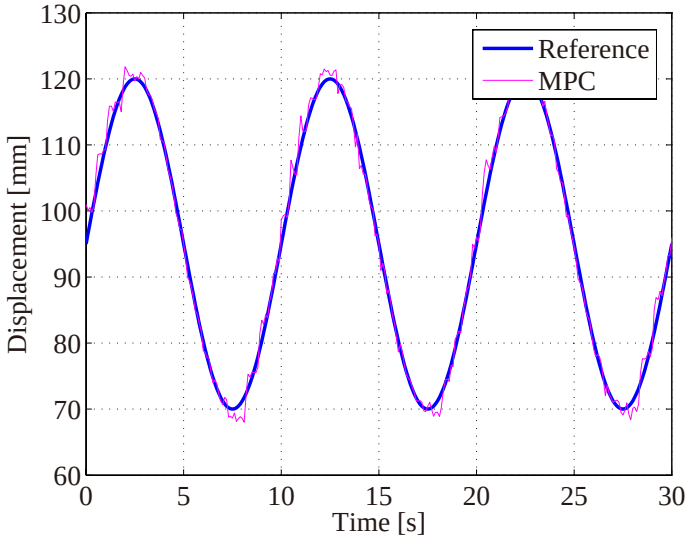


Fig. 5.29: Experimental result of MPC using five coincident points: 0.1 Hz ($H_p = 5$)

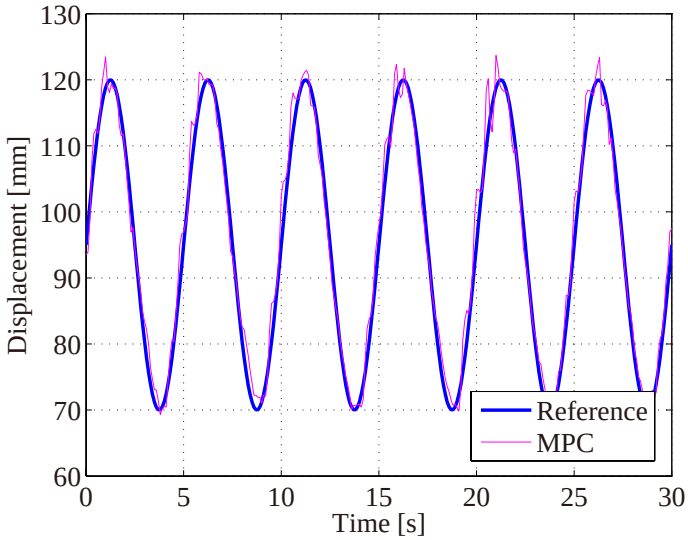


Fig. 5.30: Experimental result of MPC using five coincident points: 0.2 Hz ($H_p = 5$)

### 5.6.4 Experimental results of AMPC: Multiple coincident points case

AMPC contolller makes calculations of predicted outputs based on following equation:

$$\hat{\mathcal{L}}(k+1) = \begin{bmatrix} \hat{\theta}_1 & \hat{\theta}_2 \\ 1 & 0 \end{bmatrix} \mathcal{L}(k) + \begin{bmatrix} \hat{\theta}_3 \\ 0 \end{bmatrix} u(k). \tag{5.53}$$

Experiment here shows control performances of AMPC using multiple coincident points, of which numbers are four and five. This section shows the control performance when there exists loads. Figures 5.31 to 5.33 show the experimental results when load 3.5 kgf is connected with the muscle.

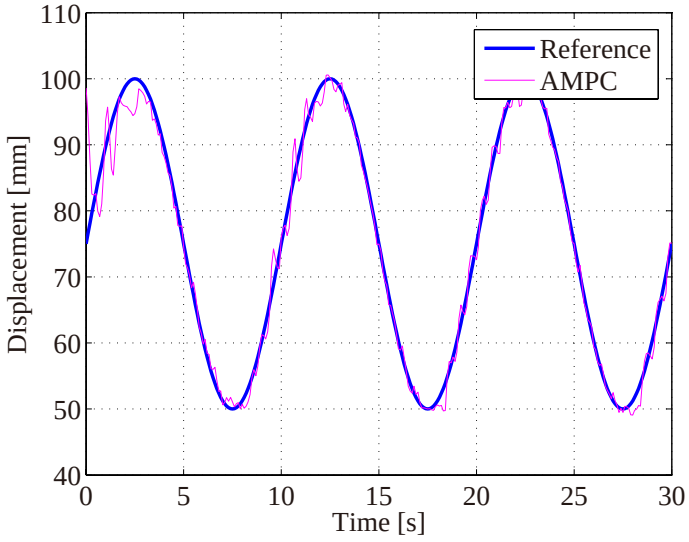


Fig. 5.31: Experimental result of AMPC: load 3.5 kgf (0.1 Hz, $H_p = 5$)

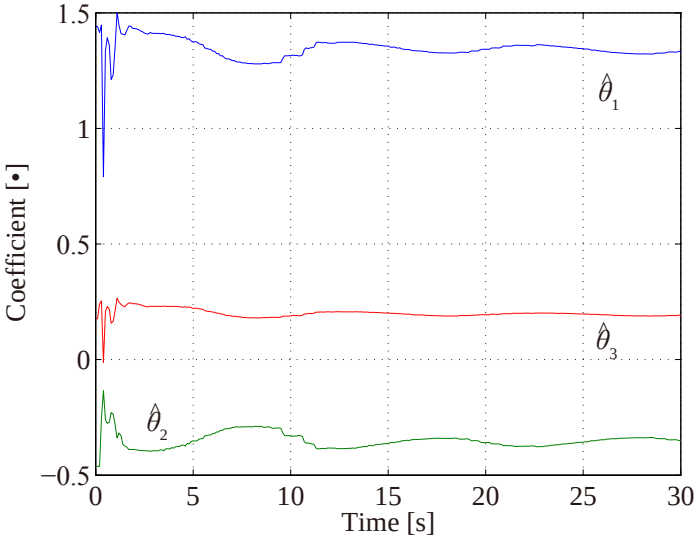


Fig. 5.32: Parameter estimation of AMPC: load 3.5 kgf (0.1 Hz, $H_p = 5$)

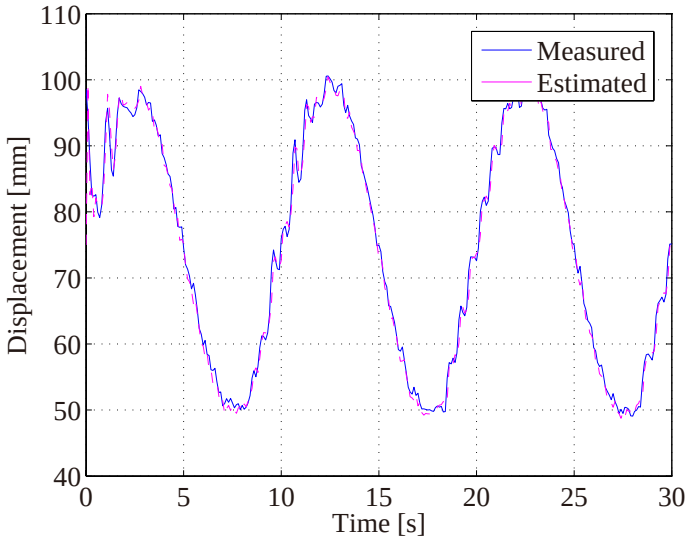


Fig. 5.33: One-step-ahead estimation of AMPC: load 3.5 kgf (0.1 Hz, $H_p = 5$)

Note that offset of reference trajectory is changed from 95 mm to 75 mm because a maximum contraction rate of loaded condition is smaller than the rate of no-load condition, and initial conditions of the parameters of the muscle model are Eq. (5.50).

Figure 5.33, which is the result of the one-step-ahead estimation based on the muscle model

with online parameter updating by RLS algorithm, is obtained by following equation:

$$\hat{l}(k) \quad = \quad \hat{\theta}_1 l(k-1) + \hat{\theta}_2 l(k-2) + \hat{\theta}_3 u(k-1). \tag{5.54}$$

Changing of reference frequency from 0.1 Hz to 0.2 Hz shows following experimental results.

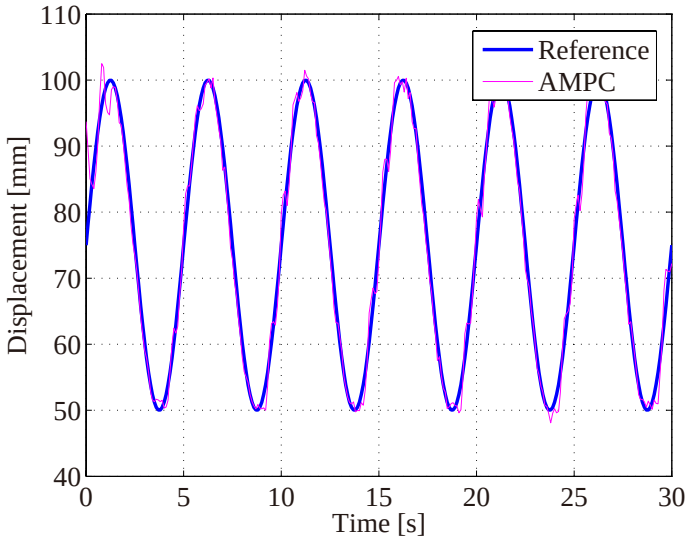


Fig. 5.34: Experimental result of AMPC using five coincident points: load 3.5 kgf (0.2 Hz, $H_p = 5$)

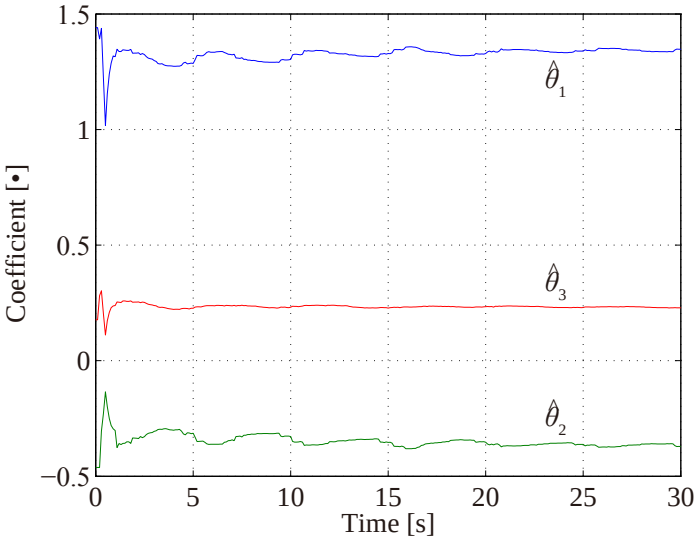


Fig. 5.35: Parameter estimation of AMPC: load 3.5 kgf (0.2 Hz, $H_p = 5$)

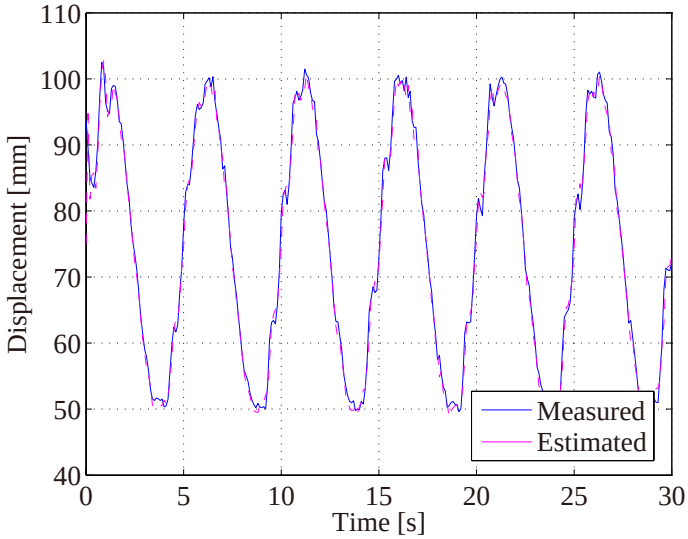


Fig. 5.36: One-step-ahead estimation of AMPC: load 3.5 kgf (0.2 Hz, $H_p = 5$)

In addition, experiment of higher-frequency reference, which is 0.3 Hz and 0.5 Hz, is conducted. Figures 5.37 to 5.42 show the experimental results of them. Notice that conventional MPC using one coincident point can absolutely not control the muscle displacement. Moreover, the control performance depends on the characteristics of the muscle such as time constant and time delay.

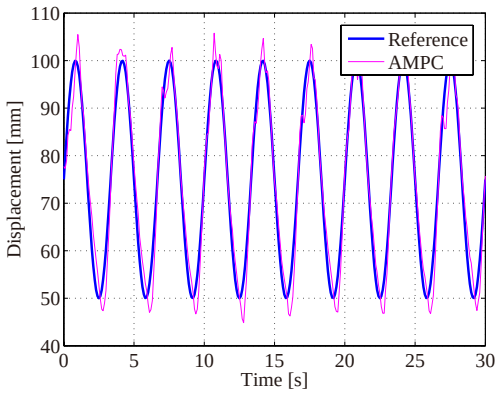


Fig. 5.37: Experimental result of AMPC: load 3.5 kgf (0.3 Hz, $H_p = 5$)

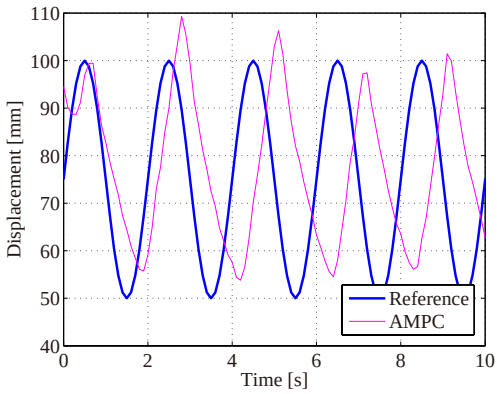


Fig. 5.38: Experimental result of AMPC: load 3.5 kgf (0.5 Hz, $H_p = 5$)

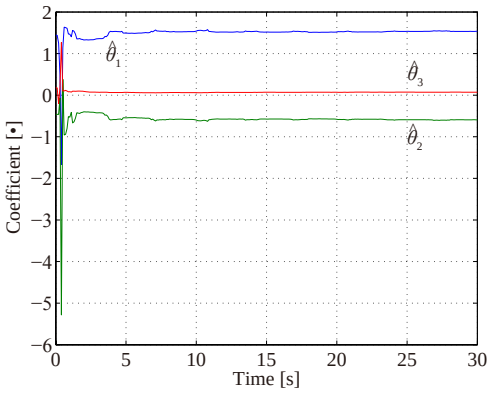


Fig. 5.39: Parameter estimation of AMPC: load 3.5 kgf (0.3 Hz, $H_p = 5$)

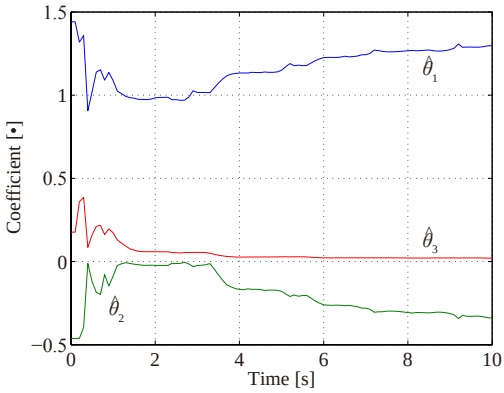


Fig. 5.40: Parameter estimation of AMPC: load 3.5 kgf (0.5 Hz, $H_p = 5$)

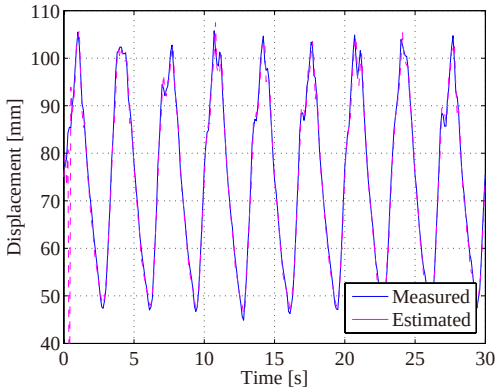


Fig. 5.41: One-step-ahead estimation of AMPC: load 3.5 kgf (0.3 Hz, $H_p = 5$)

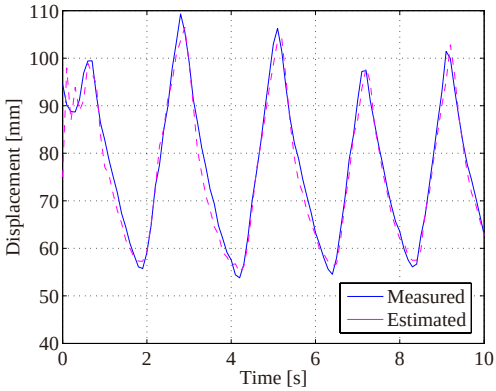


Fig. 5.42: One-step-ahead estimation of AMPC: load 3.5 kgf (0.5 Hz, $H_p = 5$)

### 5.6.5 Discussion

MPC using multiple coincident points is introduced here and experiment of MPC and AMPC using multiple coincident points are conducted with/without loads. As a result, the MPC can improve the problem of MPC using only one coincident point as described in Figs. 5.25 and 5.26.

The problem occurs when a sampling period is coarse and a prediction horizon is longer compared with the sampling period. Although accuracy of one-step-ahead estimation of the muscle model Eq. (5.36) is more than 95%, accuracy of the model is less than 80% at five steps later. Figure 5.43 shows the magnified view of the experimental result. For example, in the figure, muscle displacement at time $k$, which is $l(k)$, is measured and then to make the displacement track the

reference at 5 steps later, which is $r(k+5)$. Thereby, error between $l(k)$ and $r(k)$ still exists at that time. Thus, the model having identified error and MPC using only one coincident point leads degradation of control performance.

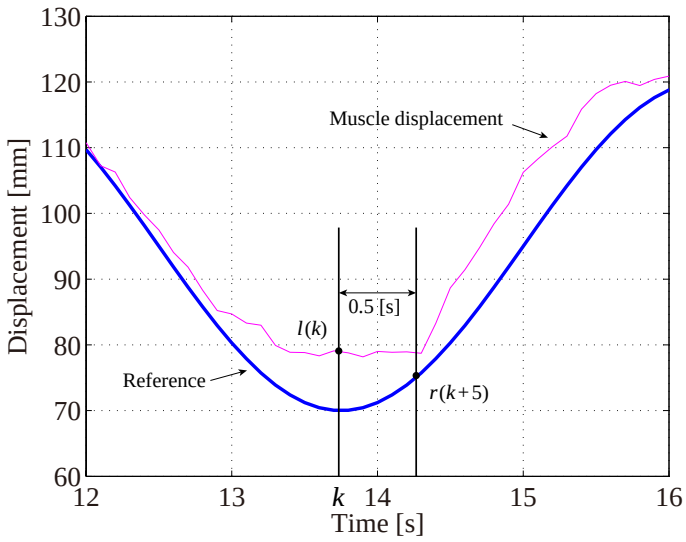


Fig. 5.43: Magnified view of experimental result (Fig. 5.25)

On the other hand, MPC using multiple coincident points can take account of all predicted output, which is predicted muscle displacement here, during prediction horizon. As described in Eq. (5.42), designers can choose the elements of the weight matrix $\mathcal{Q}$. If the weight of $\mathcal{Q}(1)$ is set to large, one-step-ahead estimated displacement is preferred. In this study, all the diagonal elements of the matrix $\mathcal{Q}$ are set to 1, which means all predicted displacement has same priority, and all the diagonal elements of the matrix $\mathcal{R}$ is set to 0.1.

In addition, using evaluation function, the control performance are not degraded when prediction horizon is changed from four steps to five steps as described in Figs. 5.27 to 5.30. In other words, although MPC using one coincident point has to consider the relation among a sampling period and prediction horizon and the characteristics of the muscle, MPC using multiple coincident points do not need to care such a condition.

Length of prediction horizon effects on the control performance of MPC. The performance can be higher when the length is longer but the amount of calculation is also larger. Designers have to pay attention to this matter.

Thus, compared with MPC using one coincident point, MPC using multiple coincident points achieves higher control performance and does not have the problem of one coincident point described before. However, there still exists the critical problem of loads. These results are only under the no-load condition. When loads exists, accuracy of the model is drastically degraded and MPC cannot work well whatever the number of coincident points are.

Then we apply the adaptive parameter estimation algorithm to the controller in same way as AMPC using one coincident point. AMPC can compensate the effect of loads as seen in Figs. 5.31 to 5.36. Although oscillation occurs at contraction phase, compared with experiment under no-load condition, the RLS algorithm can work and the parameters of the muscle model can be updated as described in Figs. 5.32 and 5.35. Moreover, one-step-ahead estimation based on the updated muscle model has good agreement with measured displacement in Figs. 5.33 and 5.36. Updated the parameters, the model-based controller generates appropriate inputs under the loaded condition.

Figures 5.37 to 5.42 show the experimental results of higher-frequency reference: 0.3 Hz and 0.5 Hz. Although AMPC cannot control when reference is 0.5 Hz, it depends on the characteristics of the muscle. As seen in Fig. 5.37, AMPC can control when the dynamics of the muscle is faster than the reference.

Incidentally, the dynamics of the muscle is related with the diameter of tubes connected with the muscle and orifice of the valves. In other words, flow rate of tap water and supply pressure depend on the dynamics of the muscle. Note that this concerns with only the contraction phase and extension phase depends on the characteristics of the rubber tube and the sleeve of the muscle because water inside the muscle is discharged in a moment and extension movement is dominated by them.

## 5.7 Comparative analysis on muscle model

We apply the identified model of the muscle as a nominal model. Although the model is linear and simple, the muscle must have nonlinearities such as hysteresis as mentioned before. Then we propose the modified model with BW model, which is a well-known hysteresis model in the field.

The objectives here are to compare the modified model with the identified model and evaluate them. The identified and modified models are Eq. (4.17) and Eq. (4.26) with identified hysteresis

parameters in Table 4.2. First, Fig. 5.44 shows the comparative result of both models on one-step-ahead estimation. Note that it is under no-hysteresis case, which is equivalent to $\alpha = 1$. Then Fig. 5.45 shows the time response of the muscle displacement control. There is some error around top and bottom points of sinusoidal wave.

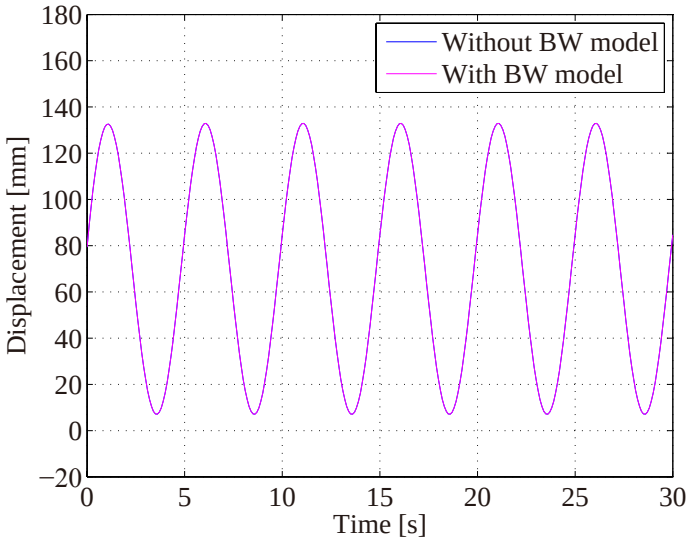


Fig. 5.44: Comparison of one-step-ahead estimation

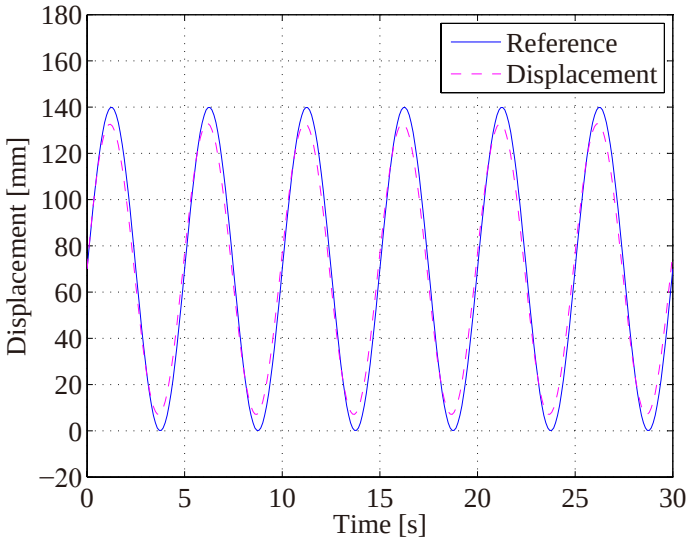


Fig. 5.45: Time response of displacement control (MPC)

Next, the hysteresis parameter $\alpha$ is set to 0.935 and then we compare the one-step-ahead estimation. Figures 5.46 and 5.47 show the simulation result of one-step-ahead estimation and time response, respectively.

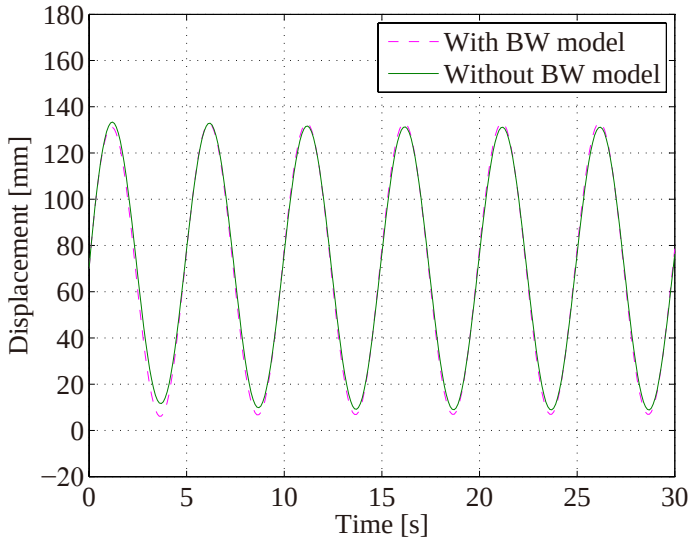


Fig. 5.46: Comparison of one-step-ahead estimation ($\alpha = 0.935$)

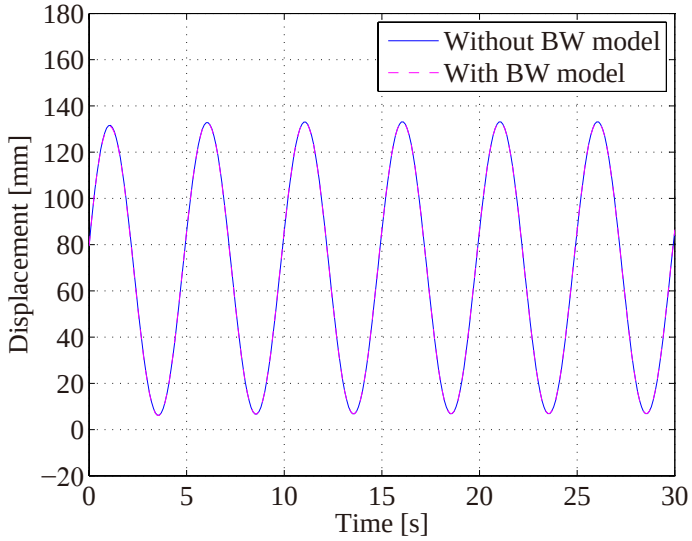


Fig. 5.47: Time response of displacement control ($\alpha = 0.935$)

Comapred with Fig. 5.44, there exists a little bit difference between indentified and modified

models. However, it is small and the time response of the muscle displacement is absolutely same tendency. In Figs. 5.48 and 5.49, the parameter $\alpha$ is set to 0.

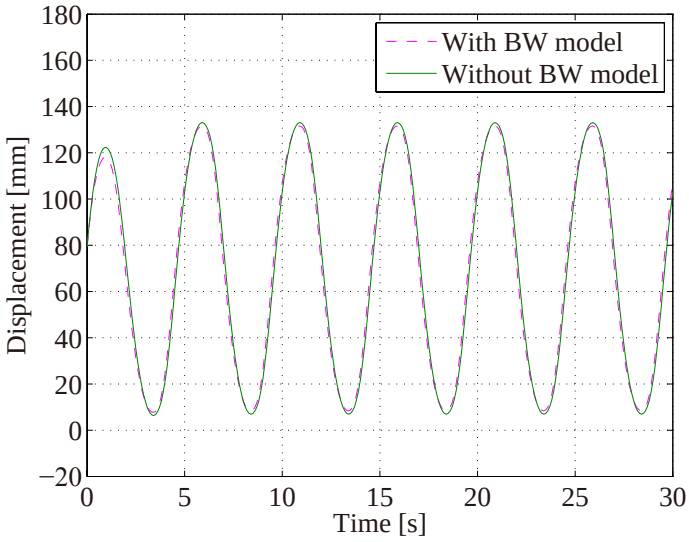


Fig. 5.48: Comparison of one-step-ahead estimation ($\alpha = 0$)

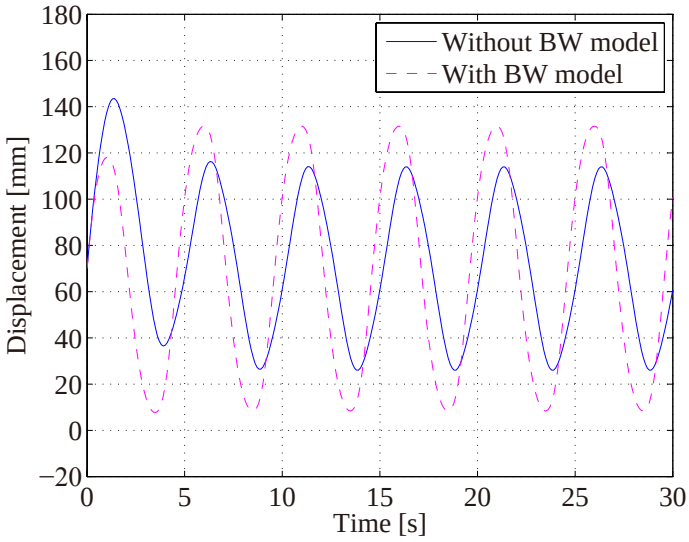


Fig. 5.49: Time response of displacement control ($\alpha = 0$)

Thus the time response of the modified model is different from the response of the identified model but its one-step-ahead estimation is almost same as the one-step-ahead estimation of identified

model. Thereby, the control performance of MPC does not depend on the BW model because MPC uses only the one-step-ahead estimation for generation of input signal.

In addition, we examine the effect of the reference frequency. Figures 5.50 and 5.51 show the simulation results of changing the reference frequency.

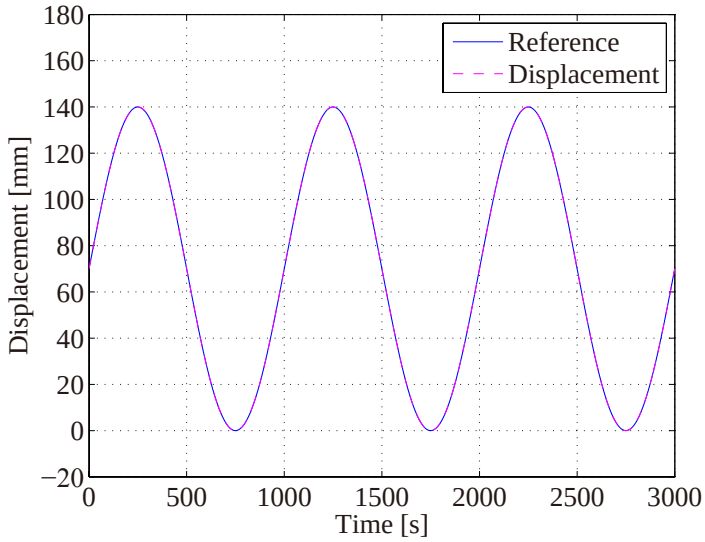


Fig. 5.50: Simulation results of 0.001 Hz as a reference frequency

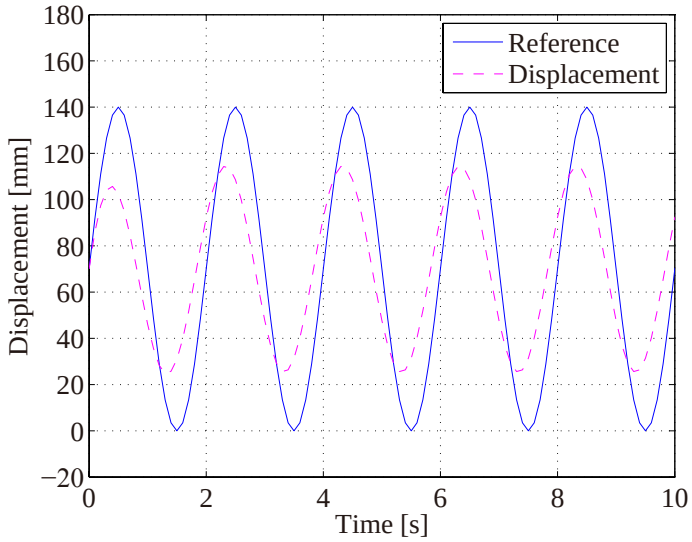


Fig. 5.51: Simulation results of 0.5 Hz as a reference frequency

As shown in the figures, effect of reference frequency is greater than the effect of hysteresis parameter $\alpha$. Therefore, the degradation of the control performance of MPC is caused by reference signal, which means that the considerable point here is transient characteristics of the muscle. This is the reason that we use the identified model without BW model. Note that this is only for MPC because MPC generally use one-step-ahead estimation of a nominal model.

## 5.8 Predictive On/Off control

Although On/Off valves are cheaper than servo or proportional valves, its control performance is lower than the performance of them. Taking account of the balance of cost and performance of whole systems, there is suitable to apply only On/Off valves. In general, two thresholds around reference, which are upper and lower one, are used to control. However, On/Off valves have been not usually used in the muscle dispacement control due to the performance. For this problem, concepts of MPC, which are one-step-ahead estimation and use of evaluation funtion, are applied to the conventional On/Off control.

In the conventional MPC controller, it is assumed that input signals can take arbitrary values within the rated input range: for example, servo valve can take arbitrary opening area of spool inside the valve and then can use arbitrary pressure or flow rate. However, On/Off control can take only “On” and “Off” signals. To overcome this difficulty, prediction only based on a nominal model and an evaluation function using least square error during given prediction horizon are introduced. The algorithm of the proposed controller is shown in Fig. 5.52.

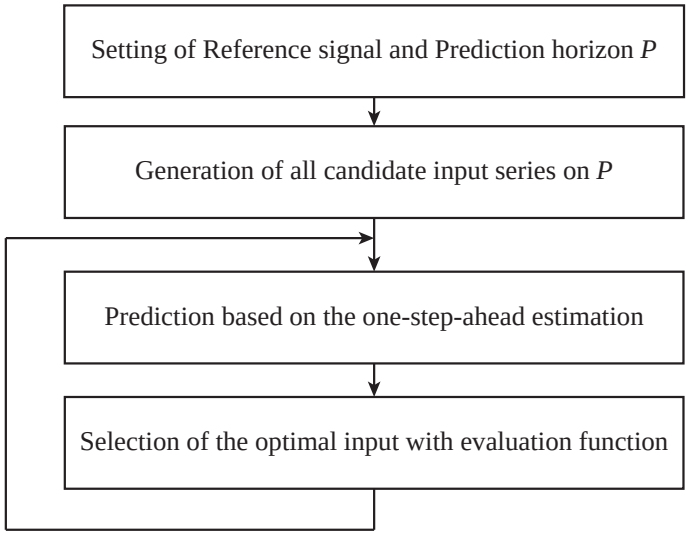


Fig. 5.52: Flow chart of the predictive On/Off control

### 5.8.1 Methodology of predictive On/Off control

Predictive On/Off control uses following equations. Note that the model is different from previous models because the proportional valves is exchanged to On/Off valves.

$$G_4(z) = \frac{L(z)}{U(z)} = \frac{0.3019}{z - 0.9276}. \tag{5.55}$$

Figure 5.53 shows the result of one-step-ahead estimation by the muscle model Eq. (5.55). It is obvious that accuracy of the model is more than 99% and the model can be used for a nominal model of predictive On/Off control.

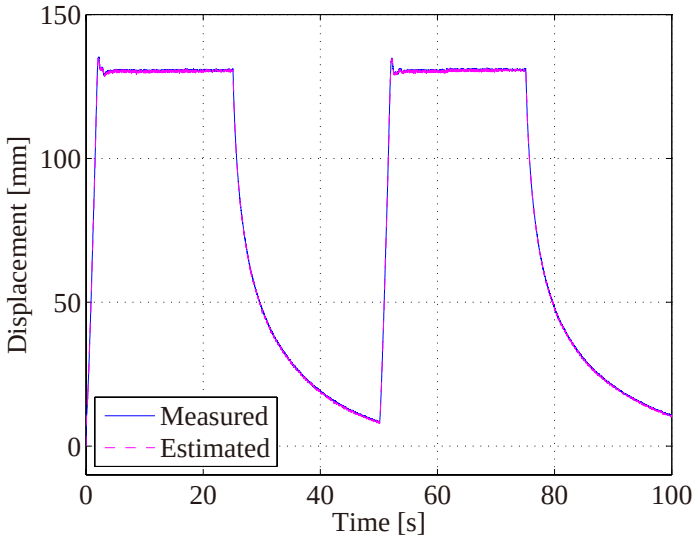


Fig. 5.53: Comparison result of the simulated displacement of the one-step-ahead estimation with the measured displacement

In addtion, we apply the proposed muscle model with Bouc-Wen model, that is,

$$\begin{cases} l(k) &= 0.3019u(k-1) - \phi_{hys}(l,w) \\ \phi_{hys}(l,w) &= -0.9276\{\alpha l(k-1) + (1-\alpha)w(k-1)\} \\ w(k+1) &= A\{l(k+1) - l(k)\} - \beta|l(k+1) - l(k)||w(k)|^{n-1} \\ & \quad -\gamma\{l(k+1) - l(k)\}|w(k)|^n + w(k) \end{cases} \tag{5.56}$$

**One-step-ahead estimation**

One-step-ahead estimation is used to get the predicted output. From Eq. (5.55), it can be obtained as

$$\hat{l}(k) = 0.9276l(k) + 0.3019u(k-1). \tag{5.57}$$

Then, following equation express one-step-ahead estimation of the proposed model with BW

model:

$$\begin{cases} l(k+1) &= 0.3019u(k) - \phi_{hys}(l,w) \\ \phi_{hys}(l,w) &= -0.9276\{\alpha l(k) + (1-\alpha)w(k)\} \\ w(k) &= A\{l(k) - l(k-1)\} - \beta|l(k) - l(k-1)||w(k-1)|^{n-1} \\ & \quad -\gamma\{l(k) - l(k-1)\}|w(k-1)|^n + w(k-1) \end{cases} \tag{5.58}$$

where the hysteresis parameters of the model are listed in Table 5.3.

Table 5.3: Identified hysteresis parameters of proposed model Eq. (5.58)

| Parameter | Value |
|---|---|
| $A$ | 10 |
| $\alpha$ | 0.98 |
| $\beta$ | 0.085 |
| $\gamma$ | -0.084 |
| $n$ | 1 |

Predicted outputs can be easily calculated by both equations bacause inputs for the valve is only "On" or "Off", which indicate here "10 V" and "-10 V", respectively.

**Evaluation function**

The predicted output series are used for the calculation of evaluation function in Eq. (5.59). The designer gives prediction horizon $P$, which is an integral multiple of the sample interval. Then the set $U_{in}$ of all On/Off combinations of the On/Off valve signals can be obtained at each step. Then an optimal input is chosen such that evaluation function is minimized:

$$J_p(k) = \sum_{i=k,\ u\in U_{in}}^{k+P} (l_{ref}(i) - \hat{l}(i))^2. \tag{5.59}$$

The proposed controller keeps the chosen input during one sampling interval and continues at each step.

### 5.8.2 Experiment of predictive On/Off control

To show the control performance of the proposed On/Off controller, some experiments are conducted. The sampling period of the experiment is set to 0.1 seconds. The predictive horizon is set to 0.4 seconds (4 steps). Figures 5.54 and 5.55 show experimental results of predictive On/Off control. Note that the results are compared with results of conventional On/Off control in the figures.

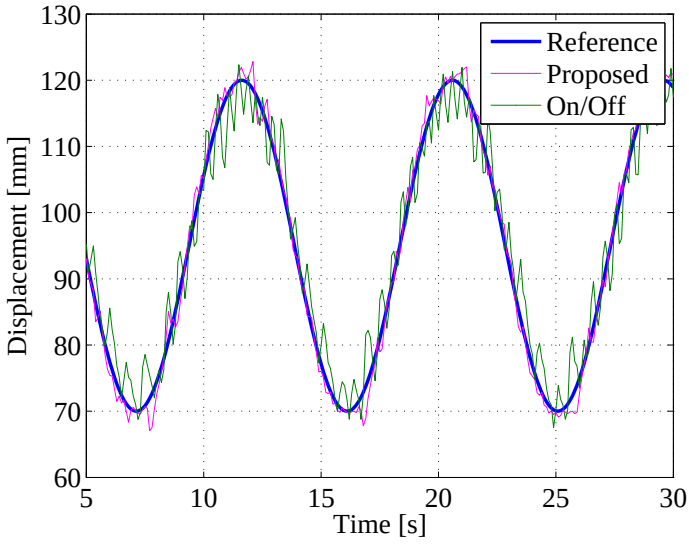


Fig. 5.54: Experimental result of predictive On/Off control

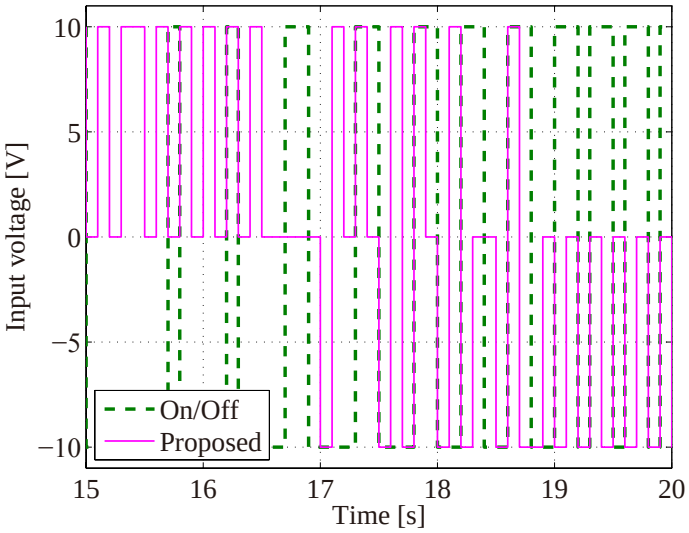


Fig. 5.55: Magnified view of input signal of predictive On/Off control (15 to 20 s)

### 5.8.3 Discussion

Proposed On/Off control based on one-step-ahead estimation and evaluation function is compared with conventional On/Off control, which uses upper and lower thresholds. Table 5.4 shows comparison analysis of the control methods. As seen in the table, the conventional On/Off control gives fluctuation between upper and lower thresholds. This is unavoidable in the case of conventional On/Off control. On the other hand, the proposed control can improve such a flucuation. Figure 5.56 shows the magnified view of Fig. 5.54. Additionally, it can reduce the mean error by half and the maximum error also can be reduced. Although noize of signals and sway of the muscle make the control performance of the proposed control degrade, it shows that prediction works well and undesireble switching can be reduced.

Table 5.4: Comparison analysis of experimental results

| Control method | mean abs. error [mm] | max. abs. error [mm] | Total "On" time [s] |
|---|---|---|---|
| Conventional ctrl. | 3.305 | 10.75 | 10 |
| Proposed ctrl. | 1.589 | 7.088 | 6.4 |

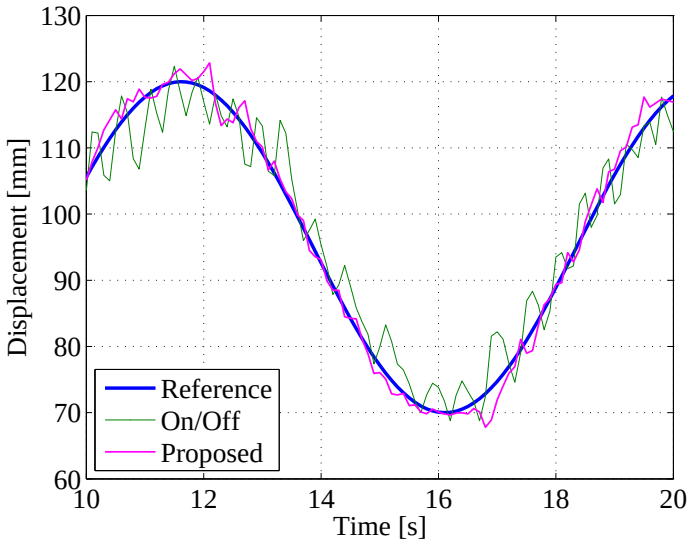


Fig. 5.56: Magnified view of Fig. 5.54 (10 to 20 s)

Total "On" time, which indicates the time when input signal for the valves is "On", is another considerable point. The input signal of the conventional On/Off control is turned to "Off" when measured displacement is over the upper threshold, and the signal is turned to "On" when it is under the lower threshold. This can lead to unnecessary switchings of the input signal. On the contrary, in the proposed control, undesirable switchings of the input signal for the valve can be reduced because the control can take account of the predicted muscle displacement and prevent unnecessary switching. In addition, the experimental setup can keep the internal pressure of the muscle by closing both valves $PV_1$ and $PV_2$, where the valves are not proportional valves but On/Off switching valves, and this can be considered in the algorithm of the proposed predictive On/Off control. Hence, the controller can use three input signals as shown in Table 5.5. Then there are $3^4$ input candidates to be considered bacause the prediction horizon here is set to 4 steps. By calculating evaluation function, the optimal input can be chosen. Additional input "Keep" can reduce frequent switching of the valves and then improve the control performance.

Table 5.5: Input signal of the proposed controller

| | $PV_1$ | $PV_2$ |
|---|---|---|
| Supply | On | Off |
| Discharge | Off | On |
| Keep | Off | Off |

The experimental result uses the modified muscle model Eq. (5.58), which contains Bouc-Wen hysteresis model. Figure 5.57 shows the comparison of Eqs. (5.55) and (5.56).

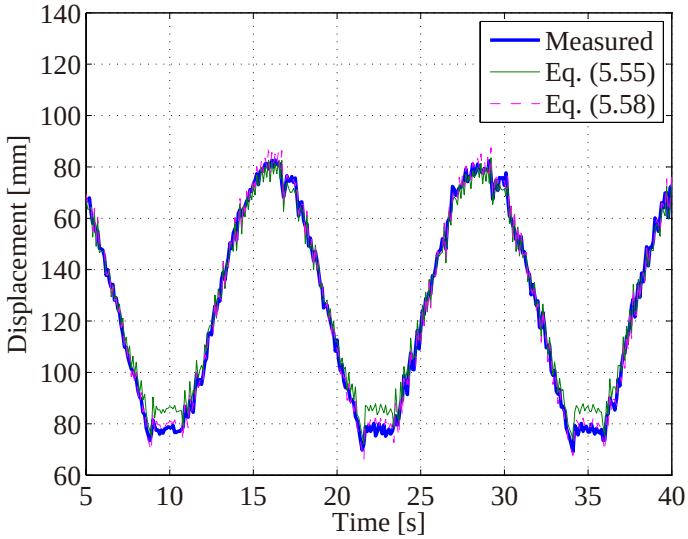


Fig. 5.57: Comparison of Eq. (5.55) and (5.56)

As seen in Fig. 4.9, there exists some difference between the simulated displacement by the identified muscle model and the measured displacement, especially. Thus improvement of the nominal model is important factor for the control performance of model-based control, and combination of identified muscle model and BW model is effective solution in the case of McKibben muscle.

# Chapter 6

# Estimation of muscle displacement

## 6.1 Introduction

In general, measurement devices such as stroke sensors and rotary potentiometers are required to control displacement of McKibben muscles. Use of such devices, however, may ruin the advantage of the muscles, especially high flexibility of the muscles. Moreover, when the muscles are used as actuators of gait-training orthoses, redundancy of the whole system is limited and then one of the advantages of the orthoses using the muscles may also be removed.

Although the control performances of the muscle using the proposed controls, which are MPC and AMPC, are shown in Chap. 5 and they are quite higher than conventional PI control, displacement control without displacement sensors is required for such orthoses. The measurement devices that we can use here are pressure sensors, flowmeters, and other flex sensors. These can be used for estimation of the muscle displacement because pressure sensors and flowmeters are installed on the circuit far from the muscle and flex sensors, which are flexible and thin, cannot inhibit muscle movement. Hence, measured data from these sensors can be used for displacement control of the muscle.

On the other hand, the muscle models derived in previous chapters, which are Eqs. (4.17), (4.26), (5.1), and (5.49), cannot be used for estimation of the muscle displacement. Although accuracy of one-step-ahead estimation is quite high as seen in Fig. 5.33, accumulated error cannot be compensated and there is no way to estimate and control. Thus, these models can be used as nominal models of MPC because prediction horizon is short but it is difficult to use them for

estimation.

In addtion, it is also difficult to estimate the muscle displacement when the adaptive parameter estimation algorithm such as RLS algorithm is used. Generally, the algorithm requires measured outputs to update the parameters of the model. However, it cannot be possible because the output cannot be measured directly. Hence, the adaptive algorithm, which is attractive when outputs can be measured, cannot solve the problem.

## 6.2 Estimation method I (flex sensor)

This section shows the application of a commercial flex sensor in order to measure the diameter of the muscle because there is a relationship between the diameter and the length of the muscle as described in Fig. 4.1 and also Eq. (4.1) and the muscle displacement can be estimated by the measured diameter. In this method, flex sensor is twisted around the muscle and covered with rubber tube. The lex sensor used in the experiment is shown in Fig. 6.1.

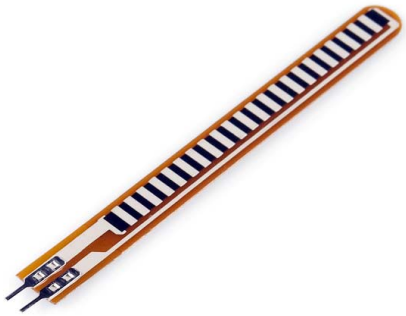

Fig. 6.1: Flex sensor (length: 2.2inch, spectrasymbol)

Resistance of the flex sensor changes depending on bentness when the sensor body is bent and then output voltage changes depending on the resistance. Figure 6.2 shows the result of calibration. Note that the sensor is wrapped around the center of McKibben muscle, not on the end of the muscle, and then a rubber tube covers on the sensor to prevent slipping of the sensor. As a result, relationship between resistance of flex sensor and McKibben diameter was shown as an approximately linear relation.

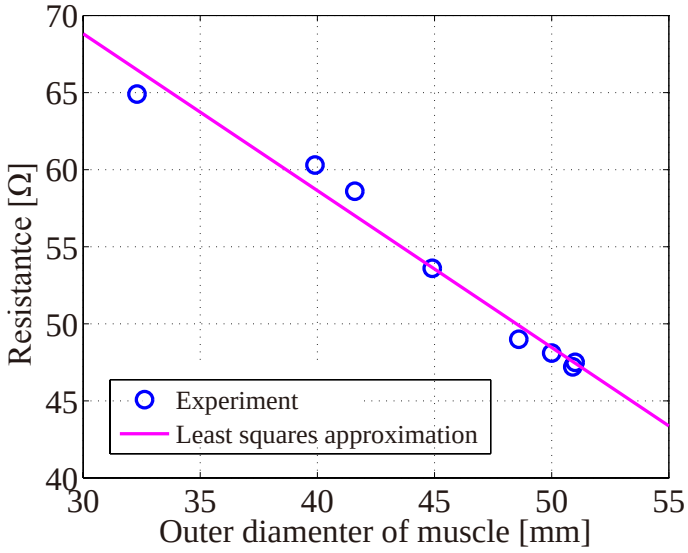


Fig. 6.2: Calibration of flex sensor

### 6.2.1 Experiment of estimation method I

This section shows the experimental result of the estimation method I (application of the flex sensor). The angle between a thread and axis $\gamma_m$ can be calculated via the muscle diameter in Eq. (4.1) because flex sensor measures changing of the resistance, which is related to the diameter. Then, the length of the muscle can be calculated with only the angle $\gamma_m$. After that, contraction rate, which is almost same as the muscle displacement, can be estimated via Eq. (3.2). Figures 6.3 and 6.4 show the estimation results with flex sensor. Note that the muscles used in these experiment are different from the muscle used in previous experiment in Chaps. 4 and 5.

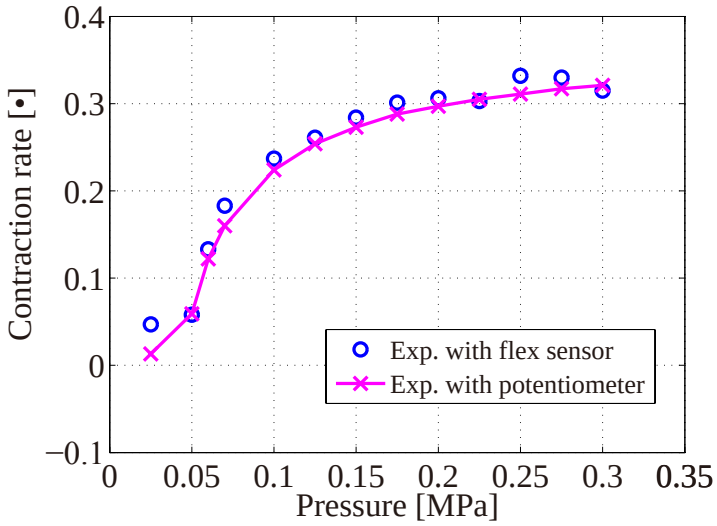


Fig. 6.3: Estimation results with flex sensor: 500 mm in natural length

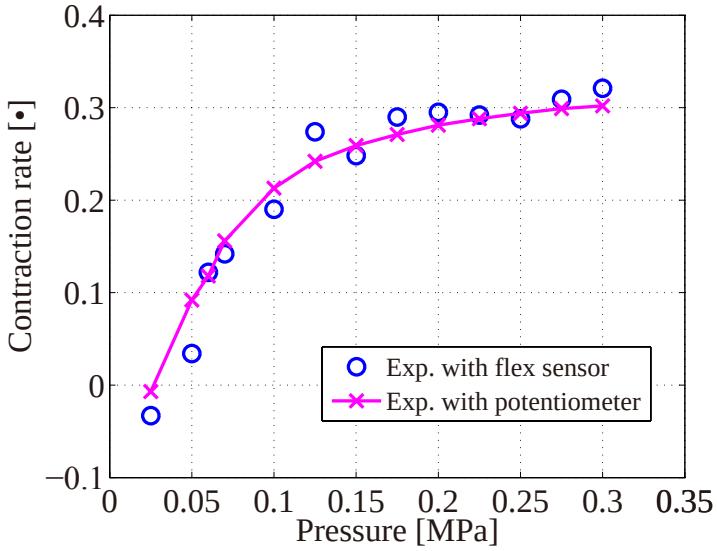


Fig. 6.4: Estimation results with flex sensor: 400 mm in natural length

### 6.2.2 Discussion: Estimation method I

Figures 6.3 and 6.4 show the experimental results of estimation method I, and the experimental results measured with potentiometer are also plotted on, in order to compare the validity of the estimation method I. The estimation leads to reduce a little accuracy of contraction rate. These results

are caused by following reason; 1) Flex sensor position, 2) Repetitive expansion and contraction action of muscle, and 3) Torsion of flex sensor covered with rubber tube.

However, the estimation with flex sensor has enough accuracy for underwater gait-training because, in general, underwater gait-training requires no high-accuracy operation. In addition, the purpose of this training is to move patient's lower limb to activate CPG as menthioned in the previous chapter. Moreover, the concepts of flame-less, flexible, and low-cost are more important issues than its performance from standpoint of rehabilitation. On the other hand, there are some problems for this method. In particular, the flex sensor position and the torsion of the sensor caused by repetitive operation are critical issues to control the gait-training orthosis. In addition, drastic performance degradation might be caused because the flex sensor is only covered with the rubber tube during experiment, not firmly fixed in axial axis. Therefore, improvement of measurement method with flex sensor is imperative matter.

## 6.3 Estimation method II (flowmeter)

This method uses a flowmeter to esitmate the muscle displacement. In peumatic McKibben muscles, related work[60] shows that displacement estimation of the muscles with flow rate can be possible. However, it requires consideration of compressibility of air and temperature dynamics and then the derivation method becomes complex. In particular, it is impossible to use the method in parallel with displacement control of the muscles.

On the other hand, in tap-water driven muscles, the estimation with flow rate should be easy and acculate because water as working fluid is incompressible and does not depend on temperature. Equation (6.1) shows relationship between the volume of the muscles and the inlet flow rate;

$$\Delta V = \int \Delta q dt. \tag{6.1}$$

where $V$ is the volume of the muscle, $q$ the inlet flow rate and then, from Eq. (4.1),

$$\Delta V = \frac{1}{4\pi m^2} l(b^2 - l^2) - \frac{1}{4}\pi D_0^2 L_0. \tag{6.2}$$

where $m$ the number of turns of a thread, and $D_0$ initial diameter of the muscles. Note that this

formulation is based on an assumption that the shape of the muscle is cylinder and conic shapes at the ends of the muscle are neglected. Substituting Eq. (6.1) into Eq. (6.2), the estimation obtained as

$$\int \Delta q dt = \frac{1}{4\pi m^2} l(b^2 - l^2) - \frac{1}{4}\pi D_0^2 L_0. \tag{6.3}$$

The muscle displacement, which consists of difference between the natural length of the muscle $L_0$ and the muscle length $l$ can be obtained by solving the equation for $l$ because $m$, $b$, $D_0$, $L_0$ are constant and inlet flow rate $q$ can be measured.

### 6.3.1 Experiment of estimation method II

Experimental setup shown in Fig. 3.3 is modified to measure inlet flow rate. Figure 6.5 shows modified experimental setup. A flowmeter (FD-M10AY, KEYENCE CORPORSTION) is set in the upper position of the muscle. The specification of the flowmeter is listed in Table 6.1. Note that the flowmeter can measure only one flow direction. Hence this section is concerned with only contraction phase and shows the accuracy of estimated muscle displacement by inlet flow rate during the phase.

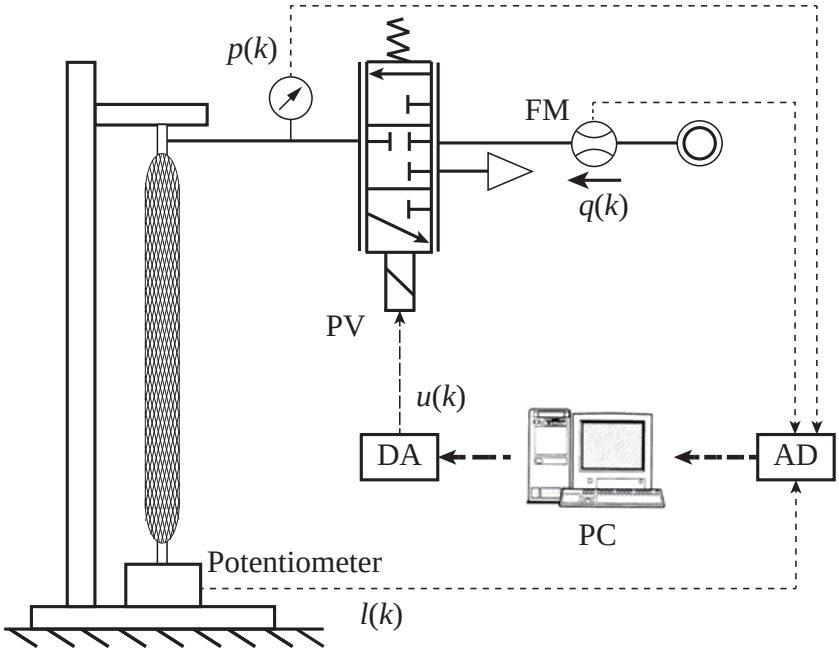


Fig. 6.5: Experimental setup for estimation method II

Table 6.1: Flowmeter (FD-M10AY, KEYENCE CORPORSTION)

| | |
|---|---|
| Working fluid | Water or non-corrosive liquid |
| Rated flow range | 0.5 to 10 L/min |
| Operation pressure range | Max. 1.0 MPa |
| Response time | Min. 0.5 s |
| Range of temperature | 0 to 85 °C (no freezing allowed) |
| Water proof | IP65 |

Table 6.2 shows the measured parameters of the muscle. Base on these parameters and Eq. (6.3), the muscle displacement can be estimated.

Table 6.2: Measured parameters of the muscle

| Parameter | Value | Unit |
|---|---|---|
| Natural length | 540 | mm |
| Thread length | 594 | mm |
| Diameter | 17 | mm |
| Turns of a thread | 5.4 | - |

Figures 6.6 and 6.7 show experimental result of inlet flow rate, where Figs. 6.6 and 6.7 are under the no-load and loaded conditions (3.5 kgf), respectively. The muscle displacement is estimated by integrated inlet flow rate, of which integral interval is from 0 to 2.5 s.

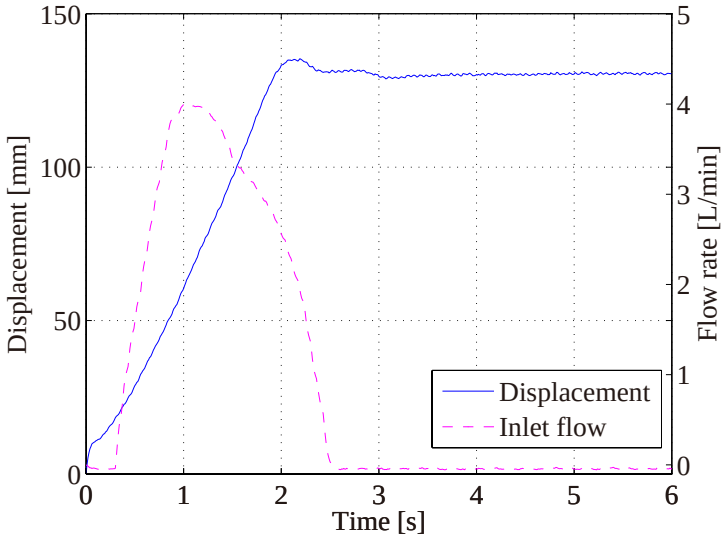


Fig. 6.6: Experimental result of flow rate and displacement (no load)

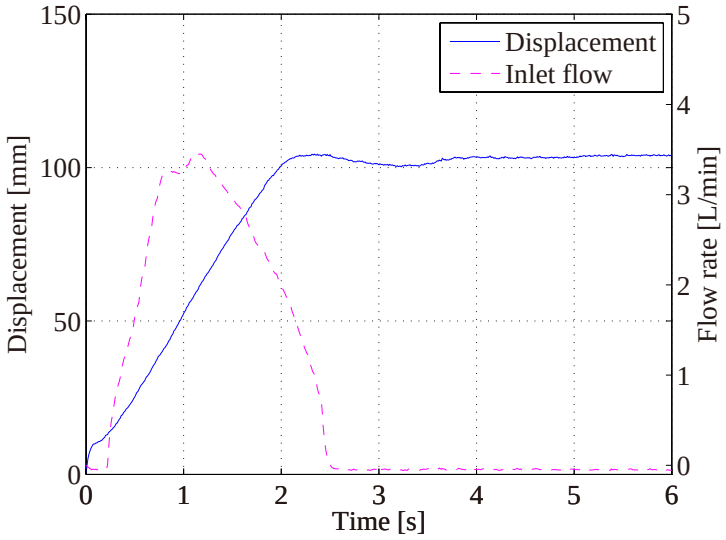


Fig. 6.7: Experimental result of flow rate and displacement (load: 3.5 kgf)

Figure 6.8 shows the estimated muscle displacement by Method II. Note that the estimated displacement has time delay caused by the response time of the flowmeter, which is 0.5 s as nominal value.

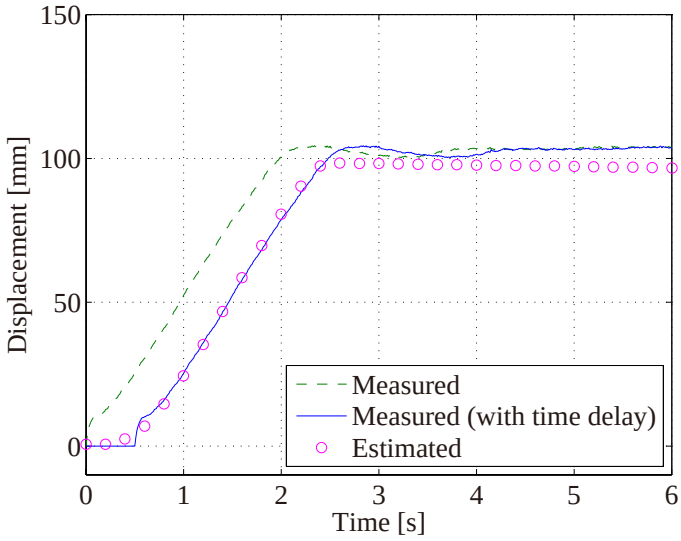


Fig. 6.8: Measured and estimated muscle displacement by Method II (load: 3.5 kgf): dot-line indicates the measured displacement without time delay, solid-line indicates the measured displacement with time delay (0.5 s)

Figure 6.9 shows experimental result of esitmation under no load condition, where the estimated displacement take account of the time delay of the flowmeter mentioned above.

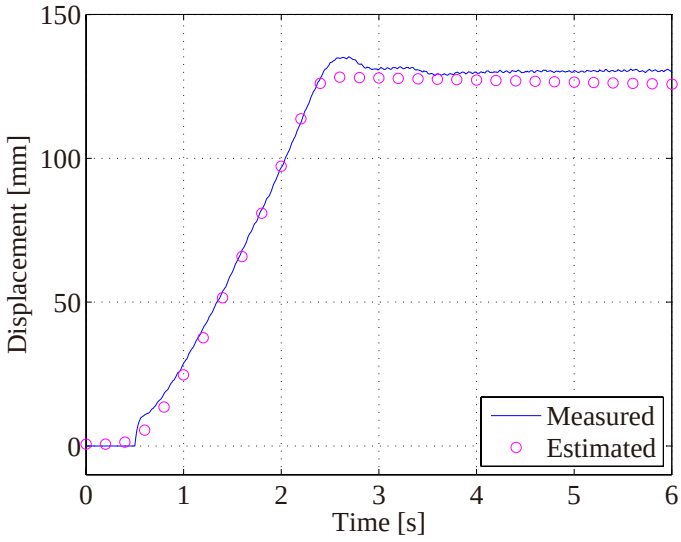


Fig. 6.9: Measured and estimated muscle displacement by Method II (no load)

### 6.3.2 Discussion: Estimation method II

This method requires pre-information such as natural length, thread length, and diameter of the muscle. However, these measurements can be easily obtained. In addition, the derivation method is only Eq. (6.3) due to the characteristics of water. Moreover, the method connects nothing with the muscle directly. These are quite attractive and can make sensorless displacement control possible, especially for actuators of gait-training orthoses. Therefore, the method is easy-to-use and relatively practicable.

The experimental results of the method as seen in Figs. 6.8 and 6.9 show that estimated displacement here has good agreement with measured displacement with/without a load, even during transient response. Thus use of flowmeter is suitable for displacement estimation of tap-water driven muscles. On the other hand, the accuracy of the method strongly depends on the performance of flowmeters. In particular, resolution and response time are important as shown in Fig. 6.8. Moreover, flowmeters are more expensive than pressure sensors and they in general can measure only one flow direction. Thus there exists some problems of flowmeters.

Supply pressure can also be easily measured and used for estimation. In fact, measured pressure can estimate the muscle displacement. However, there is a problem. Pressure difference between under no-load and loaded conditions are shown in Fig. 6.10.

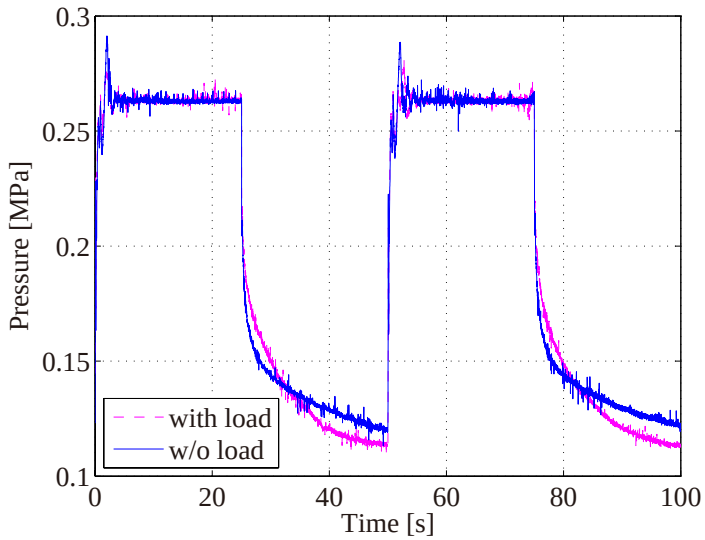


Fig. 6.10: Comparison of supply pressure: dot-line indicates under loaded condition and solid-line indicates under no load condition

As seen in the figure, the measured supply pressure under loaded condition is almost same as the pressure under no-load condition. As a result, it is obvious that estimation by supply pressure is difficult when some loads exist. As mentioned before, effect of loads cannot be neglected and it makes estimation by supply pressure impossible.

### 6.3.3 Displacement control (application of method II)

Conventional PI control with estimation method II, which uses flowmeters, can be applied to the muscle displacement control. Under constraints of flowmeters, the proposed control method can control only one direction. The experiment here shows the result of a constant reference of the muscle displacement: 100 mm. Figure 6.11 shows experimental result of the displacement control with estimation method II.

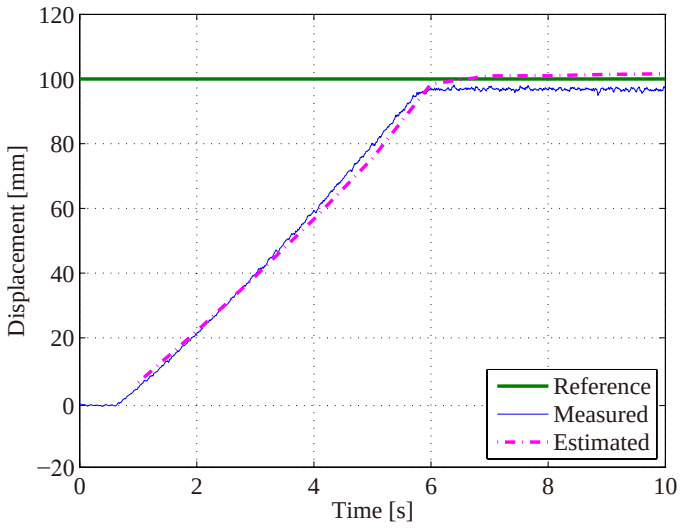


Fig. 6.11: Experimental result of displacement control with estimation method II

As a result, it is shown that the proposed method can make the muscle displacement track the constant reference. Figure 6.11 also shows the estimated muscle displacement. Although the measured displacement with the potentiometer connected with the end of the muscle is little bit smaller than the estimated displacement, this method can estimate not only steady-state response but also transient one of the muscle. Thus, it is possible to estimate the muscle displacement by the estimation method II.

However, the control performance of tracking control should be examined to validate the performance of the proposed method. In addition, repetitive operation also should be conducted because accumulated error must be larger and the performance might be degraded.

## 6.4 Modified estimation method II (flowmeter)

In this section, the experimental setup is modified again to be able to measure bidirectional flow, which is inlet flow through $FM_1$ and outlet flow through $FM_2$ shown in Fig. 6.12 and improve the response time of the flowmeter. Tables 6.3 and 6.4 show the specifications of the two flowmeters. Figure 6.13 shows relationship between muscle displacement and inlet and outlet flow. Inlet flow is larger than outlet flow shown in the figure due to the initial condition of the experimental circuit, which is not filled with water.

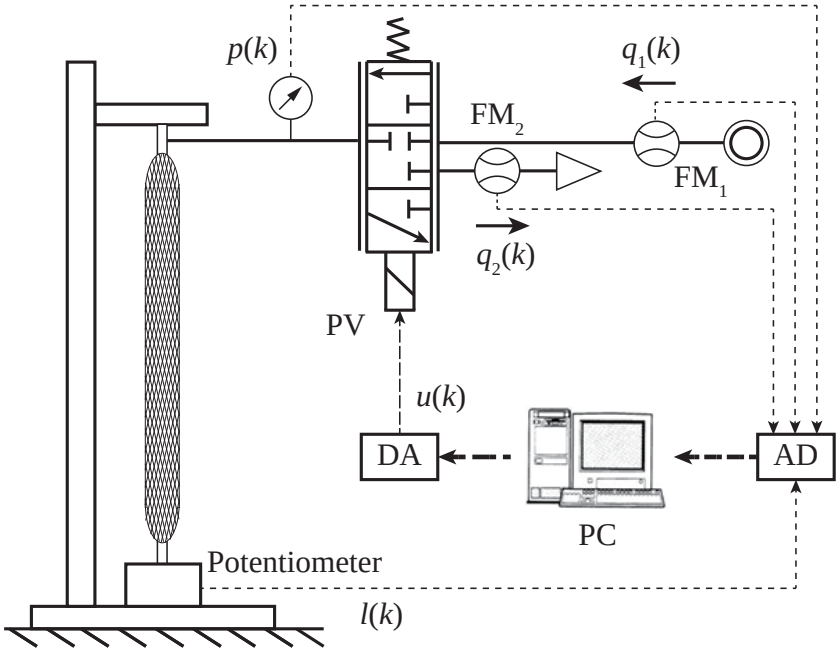


Fig. 6.12: Modified experimental setup using two flowmeters

Table 6.3: Flowmeter: $FM_1$ (NDV10-STD1, Aichi Tokei Denki Co., LTD.)

| | |
|---|---|
| Working fluid | Water |
| Rated flow range | 1 to 10 L/min |
| Operation pressure range | Max. 0.75 MPa |
| Pulse constant | 1.12 mL/P |
| Range of temperature | 0 to 40 °C (no freezing allowed) |
| Water proof | IP X4 |

Table 6.4: Flowmeter: $FM_2$ (OF10ZAT, Aichi Tokei Denki Co., LTD.)

| | |
|---|---|
| Working fluid | Water, kerosene, and oil |
| Rated flow range | 0.7 to 5 L/min |
| Operation pressure range | Max. 0.5 MPa |
| Max. frequency | 30 Hz |
| Range of temperature | -10 to 70 °C (no freezing allowed) |
| Water proof | IP X4 |

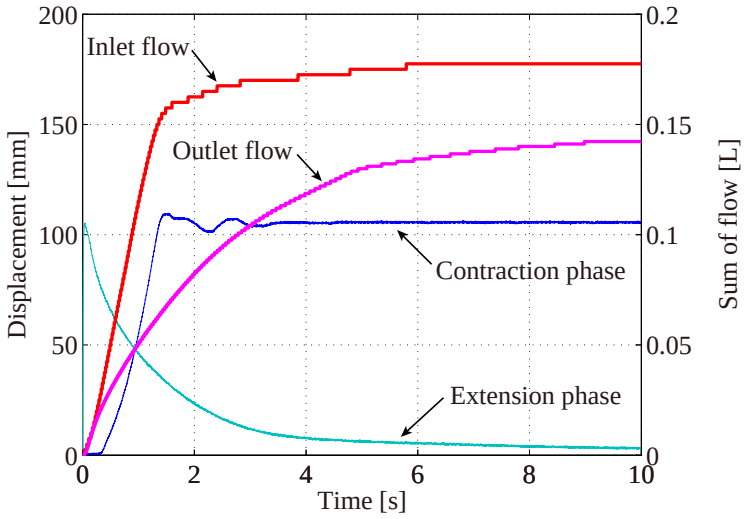


Fig. 6.13: Muscle displacement and inlet and outlet flow measured by $FM_1$ and $FM_2$

The characteristics between muscle displacement and muscle volume can be approximated as a second order polynomial[60].

$$l(k) = c_1 V^2(k) + c_2 V(k) + c_3 \tag{6.4}$$

where $c_i (i = 1, 2, 3)$ are constants. The sum of inlet and outlet flow is equivalent to the volume of the muscle. Then the equation can be rewritten by

$$l(k) = d_1 q^2(k) + d_2 q(k) + d_3. \tag{6.5}$$

where $q(k) = q_1(k) - q_2(k)$ and $d_i (i = 1, 2, 3)$ are constants.

Figure 6.14 shows the relationship in experiments. Note that there are two experimental results: 1) Under no-load condition, 2) Under loaded condition and the experiments, are carried out in five cycles. The important point here is that the hysteresis cannot be observed in the displacement - volume characteristics. Note that the initial condition of the volume is the volume when the muscle is filled with water at natural length. In addition, the solid line in the figure shows the approximated curve and is expressed as

$$l(k) = 5.687 q^2(k) - 0.2917 q(k) + 0.0046. \tag{6.6}$$

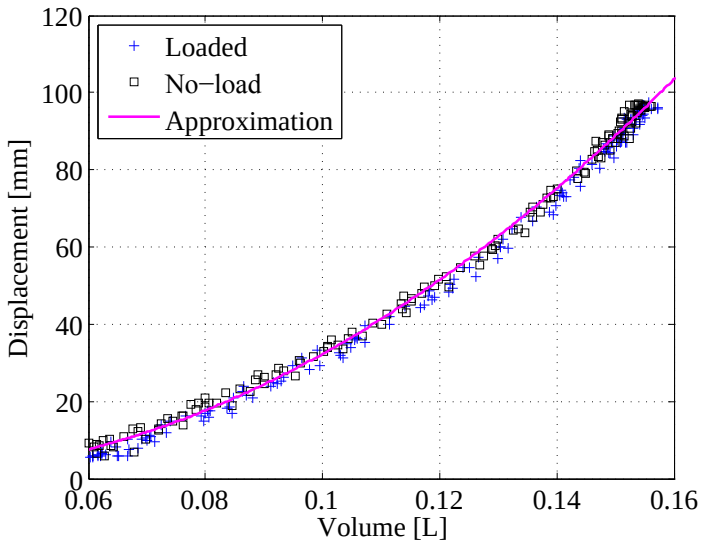


Fig. 6.14: Displacement - volume characteristics

### 6.4.1 Experiment of modified estimation method II

This section shows the experimental results of the modified estimation method II by using approximated curve Eq. (6.6). In the previous sections, we apply the estimation method at only contraction phase and then the experiment is the step response. The reference signal of the experiments here are rectangular and sinusoidal signals. Figures 6.15 and 6.16 show the experimenatal results.

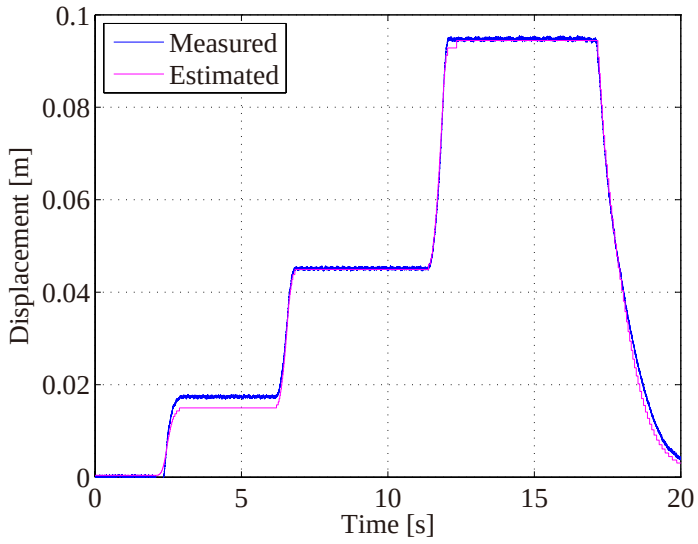


Fig. 6.15: Experimental result of estimation (rectangular signal)

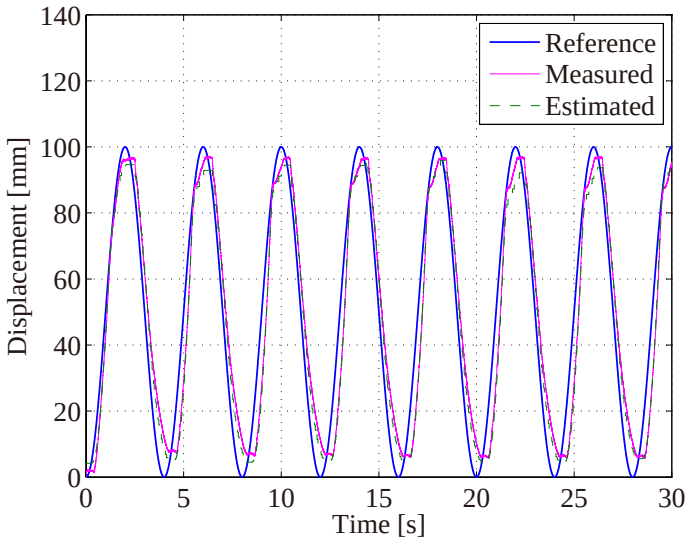


Fig. 6.16: Experimental result of estimation under loaded condition (sinusoidal signal)

The figures show comparison of the estimated muscle displacement with the measured displacement by linear potentiometer. Note that the reference signal in Fig. 6.16 is set to 0.25 Hz and the experiment is carried out under loaded condition (3.5 kgf). In addition, the muscle displacement can be estimated from measured volume based on Eq. (6.6) on real-time basis.

### 6.4.2 Discussion: Modified estimation method II

The experiments described in the previous section show the estimation capability of modified estimation method II. In particular, not only contraction but also extension phases are experimental objects because a couple of flowmeters $FM_1$ and $FM_2$ makes the experiments be possible.

Although the estimation capability is an important point in the experiments, there is an additional considerable point; that is loads connected with the muscle. In the estimation method II, we can examine the effect of loads on the estimation but it is only at the contraction phase. Then it is necessary to show the performance at the extension phase.

Figure 6.14 shows that there is a little bit effect on loads and also phases. Additionally, Figs. 6.15 and 6.16 show that the estimated displacement is in a good agreement with the measure displacement. Notice that there are some error between reference signals and measured and estimated displacement in Fig. 6.16 but it is not caused by the estimation process. However, when the reference signal is low frequency, which is equivalent to small flow rate, the flowmeter cannot measure the flow, especially less than 0.5 L/min.

### 6.4.3 Displacement control (application of modified method II)

Displacement control with estimated muscle displacement by modified estimation method II is carried out here to show its control performance. The control method is the same conventional PI control as the previous displacement control with estimation. In the experiments, reference signal is a sinusoidal wave; amplitude 50 mm, frequency 0.25 Hz, offset 50 mm, and phase shift $3/4\pi$.

Figures 6.17 and 6.18 show the experimental results. They are under no-load and loaded (3.5 kgf) conditions, respectively. Although the results seems to be same as the previous experiment, the estimated muscle displacement is used to control: the output error consists of the reference signal and the estimated displacement, not the reference signal and the measured displacement.

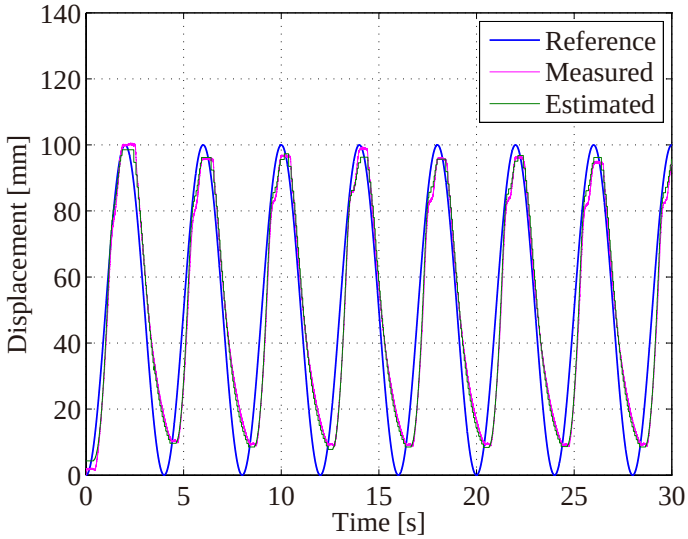


Fig. 6.17: Displacement control with estimation under no-load condition

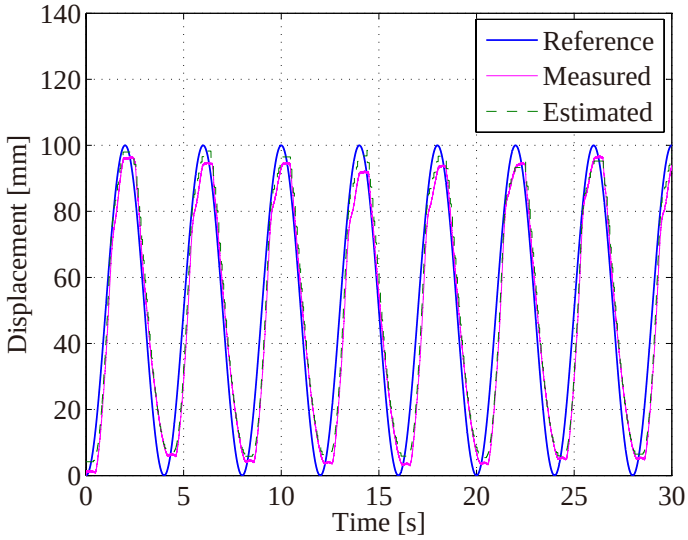


Fig. 6.18: Displacement control with estimation under loaded condition

The results of displacement control show that the muscle displacement can be controlled without the measured displacement and it means that we can control the muscle without any sensors to measure the displacement directly. Then displacement control with estimation is useful for rehabilitation devices because we can remove sensors and their cables, which are discarded things.

In addition, the modified method is feasible to estimate under loaded condition because hys-

teresis on the muscle displacement - volume characteristics is smaller than the hysteresis on the displacement - supply pressure characteristics as shown in Fig. 6.14. Although this method depends on the performance of flowmeter, especially rated range of flow rate, the estimated displacement is in a good agreement with the measure displacement and we can use the estimated displacement for control as well as the measured displacement.

# Chapter 7

# Conclusions

This dissertation is concerned with tap-water driven McKibben muscles, especially modeling and displacement control. Generally, McKibben muscles are driven by pneumatics. However, a driving source of the muscle here is only tap-water. In addition, noise and vibration problems of compressors generating compressed air can be solved. Moreover, 100% oil-free system can be realized because working fluid is water and no lubrication oil is used in the system. These suggests that application of McKibben muscles can be widely expanded.

The bottlenecks of McKibben muscles are control performance. Related work shows some applications of control methods such as $H_\infty$ control, adaptive control, and fuzzy control as mentioned in Chap. 5. Then some muscle models used in analysis of characteristics or model-based controls have also been derived. Although the models for analysis can express the muscle characteristics including nonlinearities such as hysteresis, they are usually static models and then cannot express dynamics of the muscles, and their structures are complex and cannot be used as nominal models of model-based controls. The model expressing statics of the muscles well cannot improve the control performance of the muscles. On the other hand, some derived models as nominal models of model-based control are simple and can express dynamics of the muscles. It is possible to improve the control performance of the muscles. However, most of them require lots of measurement of muscle parameters or are specialized only in certain muscles. Thereby, general versatility of the models may be lost.

The proposed method of modeling can solve these problems. Proposed method is based on linear system identification method. Although it requires some experiment, muscle model can be

obtained easily. In particular, the modeling of tap-water driven muscles by using linear system identification method is reasonable because water is incompressible fluid and then fitting percentage can be higher compared with pneumatic muscles. Note that the modeling of pneumatic muscles have to consider temperature dynamics and compressibility of air. In other words, although it is difficult to derive precise models of pneumatic muscles by using system identification method, it is possible to derive models of tap-water driven muscles. The derived model can be used as a nominal model of the muscle. However, it is not useful for hysteresis analysis because it is based on only the linear method. For this matter, we propose combination of a hysteresis model and the linear muscle model. In particular, Bouc-Wen hysteresis model is reasonable for the model because the structure of the derived model is transfer function and then it is easy to combine the hysteresis model. Moreover, hysteresis parameters of the model are intuitive to use and easy to tune.

Bouc-Wen model is usually used in modeling of magneto-rheological dampers. The models are based on structures of spring-mass-damper systems and added a virtual hysteresis state, which can express dynamics of hysteresis. The muscles are sometimes modeled as spring-mass-damper system whether driving source is pneumatics or water hydraulics. In addition, the structure of the derived model by system identification can be rewritten by state-space form and it almost same structure as spring-mass-damper systems.

Accuracy of the proposed model, which is combination of the linear muscle model and Bouc-Wen hysteresis model, is shown in Chap. 4, especially hysteresis analysis is focused on. As a result, the proposed model can express the static and dynamic characteristics under no-load condition. Nevertheless, the model whose parameters are tuned under no-load condition cannot compensate the effect of loads because the characteristics of the muscles strongly depend on load condition. Note that dominant components of the muscles characteristics are not supply pressure but the inner tube and the outer sleeve under no-load condition. On the other hand, under loaded condition, the dominant component is supply pressure.

The other experiment shows hysteresis analysis under loaded conditions. In the experiment, accuracy of the model identified under loaded condition (3.5 kgf) is validated under another loaded condition (7.0 kgf). Then the comparison of simulated and measured displacement shows that the model has good agreement with the actual muscle because characteristics of supply pressure is dominant under loaded conditions as mentioned before. Thus, it shows that the model has robustness

for loads.

The derived model is used as a nominal model of model-based control such as MRAC and MPC. Their control performances are compared with the performance of conventional PI control by experiment. Although the performance can be improved by tuning the gains of PI control appropriately, it cannot compensate the effect of loads. This is an essential problem of the muscles. For this problem, MRAC can compensate the effect but the control performance is degraded because the characteristics of the muscles is changed by movements, which are contraction and extension and then the adaptive algorithm always work. Generally, the control performance of MRAC cannot be ensured during transient response.

The control performance of MPC is almost same level as conventional PI control under no-load condition. This is because accuracy of the derived model is high and one-step-estimation can work well. However, the performance is degraded under loaded condition because the characteristics of the muscles is changed. Compared with the other control methods, MPC is strongly affected by loads. Then AMPC, which is MPC with RLS algorithm, is applied to the muscles. The proposed control can compensate the effect of loads by updating the muscle parameters. RLS algorithm is based on least squares method, and rectangular windows are used to implement an online parameter identification.

Additional improvement of MPC and AMPC is the number of coincident points. The simple way, which is only one point case, has a problem when prediction horizon is five steps. In other words, large prediction horizon affects on the control performance of MPC. Use of multiple coincident points can solve this problem although the structure of controller becomes more complex. Experimental results of MPC and AMPC with multiple coincident points show effectiveness of this approach and the control performance can be improved when the prediction horizon is set to five steps. Furthermore, when the frequency of the reference signal is higher, the controller can control the muscle as long as the muscles can track the reference signal. Note that it depends on the performance of valves, hydraulic circuits, and also pressure level of tap-water.

Predictive On/Off control based on the concepts of one-step-ahead estimation and evaluation function shows the possibility of improvement of the conventional On/Off control. Although the conventional On/Off control is attractive because the On/Off switching valves are cheaper than servo or proportional valves, its control performance is obviously lower than the performance of the

servo and proportional valves. In the proposed On/Off control, a nominal model derived by system identification and containing Bouc-Wen hysteresis model is used to predict the muscle displacement during prediction horizon and then optimal input can be chosen by using evaluation function. As a result, the proposed control can reduce the mean absolute error by half and total "On" time for the valves can also be reduced.

In Chap. 6, two estimation methods for the muscle displacement are proposed: 1) Estimation method I with flex sensor, and 2) Estimation method II with flowmeter. Although the method I can estimate the muscle displacement, there exists some problems such as position of the flex sensor, repetitive operation containing contraction and extension movement, and torsion of the flex sensor covered with rubber tube. On the other hand, the method II is reasonable for estimation of the displacement of tap-water driven McKibben muscles because it can be easily possible to implement. In addition, the control performance of the displacement control with estimation method II is shown by experiment. Although constant reference is used because of constraints of the flowmeter, it is shown that its accuracy is less than 5 mm.

Finally, achievements of this dissertation are as follows: 1) Modeling of the muscles with system identification method and application of Bouc-Wen hysteresis model, 2) Application of MPC with RLS algorithm and validation of its control performance, and 3) Estimated methods for displacement with flex sensors and flowmeters. The structure of the derived model is simple and the muscle paremeters including hysteresis paramenters can be easily tuned. Hence, the model is reasonable to use in model-based control. AMPC can control the muscle displacement under not only no-load but also loaded conditions. It is a great benefit that compensation of loads can be achieved because it is one of considerable problems of the muscles. Moreover, the proposed control can improve the control performance, although the control performance of the muscle in general is lower than any other actuators. The proposed estimation methods are useful for systems that require high flexibility and user friendliness such as rehabilitation devices.

# Bibliography

[1] Ministry of Health, Labour and Welfare: Annual Health, Labour and Welfare Report 2012-2013, 2013.

[2] C.P. Chou, and B. Hannaford, Measurement and modeling of McKibben pneumatic artificial muscles, Robotics and Automation, IEEE Transactions on Vol.12, No.1, pp.90-102, 1996.

[3] B. Tondu, and P. Lopez, Modeling and control of McKibben artificial muscle robot actuators, Control Systems, IEEE Vol.20, No.2, pp.15-38, 2000.

[4] X. Shen, Nonlinear model-based control of pneumatic artificial muscle servo systems, Control Engineering Practice Vol.18, No.3, pp.311-317, 2010.

[5] K. Ito et al., Robust control of water hydraulic servo motor system using sliding mode control with disturbance observer, SICE-ICASE, 2006. International Joint Conference. IEEE, 2006.

[6] D.G. Caldwell, G.A. Medrano-Cerda, and M.J. Goodwin, Braided pneumatic actuator control of a multi-jointed manipulator, Systems, Man and Cybernetics, 1993.'Systems Engineering in the Service of Humans', Conference Proceedings., International Conference on. IEEE, 1993.

[7] A. Pujana-Arrese et al., Modelling in Modelica and position control of a 1-DoF set-up powered by pneumatic muscles, Mechatronics, Vol.20, No.5, pp.535-552, 2010.

[8] J.H. Lilly, and L. Yang, Sliding mode tracking for pneumatic muscle actuators in opposing pair configuration, Control Systems Technology, IEEE Transactions on Vol.13, No.4, pp.550-558, 2005.

[9] D.W. Repperger, C.A. Phillips, and M. Krier, Controller design involving gain scheduling for a large scale pneumatic muscle actuator, Control Applications, 1999. Proceedings of the 1999 IEEE International Conference on. Vol.1. IEEE, 1999.

[10] D.W. Repperger, K.R. Johnson, and C.A. Phillips, Nonlinear Feedback Controller Design of A Pneumatic Muscle Actuator System, Proceedings of the American Control Conferenc e, San Diego, California, pp.1525-1529, 1999.

[11] H.I. Krebs et al., Overview of clinical trials with MIT-MANUS: a robot-aided neuro-rehabilitation facility, Technol Health Care, Vol.7, No.6, 1999.

[12] H. Barbeau, and S. Rossignol, Recovery of locomotion after chronic spinalization in the adult cat, Brain research, Vol.412, No.1, pp.84-95, 1987.

[13] A.M. Gordon et al., The variation in isometric tension with sarcomere length in vertebrate muscle fibres, The Journal of physiology, Vol.184, No.1, pp.170-192, 1966.

[14] M. Mori, and K. Suzumori, Development of very high force hydraulic McKibben artificial muscle and its application to shape-adaptable power Hand, IEEE, ICRA, 2009.

[15] H. Yoshinada et al., Seawater hydraulic actuator system for underwater manipulator, in Proc. 5th Int. Conf. Advanced Robot, vol.2, pp.1330-1335, 1991.

[16] M. Mori, and K. Suzumori, Development of Power Robot Hand with Shape Adaptability Using Hydraulic McKibben Muscles, IEEE ICRA, 2010.

[17] A.L. Behrman, and S.J. Harkema, Locomotor training after human spinal cord injury: a series of case studies, Physther, Vol.80, pp.688-700, 2000.

[18] M.A. Mat Dzahir, T. Nobutomo, and S.I. Yamamoto, Development of body weight support gait training system using pneumatic mckibben actuators-Control of Lower Extremity Orthosis, Engineering in Medicine and Biology Society (EMBC), 35th Annual International Conference of the IEEE, 2013.

[19] Y.L. Park et al., Design and control of a bio-inspired soft wearable robotic device for ankle-foot rehabilitation, Bioinspiration & biomimetics, Vol.9, No.1, 2014.

[20] T. Noritsugu, and T. Tanaka, Application of rubber artificial muscle manipulator as a rehabilitation robot, Mechatronics, IEEE/ASME Transactions on Vol.2, No.4, pp.259-267, 1997.

[21] G.S. Sawicki, K.E. Gordon, and D.P. Ferris, Powered lower limb orthoses: applications in motor adaptation and rehabilitation, Rehabilitation Robotics, 2005. ICORR 2005. 9th International Conference on. IEEE, 2005.

[22] T. Tsuji et al., Development of Rehabilitation Support Robot with Guidance Control Based on Biarticular Muscle Mechanism, IEEJ Journal of Industry Applications, Vol.3, No.4, pp.350-357, 2014.

[23] M.A. Mat Dzahir, and S.I. Yamamoto, Recent Trends in Lower-Limb Robotic Rehabilitation Orthosis: Control Scheme and Strategy for Pneumatic Muscle Actuated Gait Trainers, Robotics, Vol.3, No.2, pp.120-148, 2014.

[24] H. Kobayashi, H. Nozaki, and T. Tsuji, Development of power assist system for caregiver by muscle suit, Mechatronics and Automation, 2007, ICMA 2007, International Conference on. IEEE, 2007.

[25] H. Kobayashi et al., Development of a muscle suit for the upper body-realization of abduction motion, Advanced robotics, Vol.18, No.5, pp.497-513, 2014.

[26] G. Andrikopoulos, G. Nikolakopoulos, and S. Manesis, A survey on applications of pneumatic artificial muscles, Control & Automation (MED), 2011 19th Mediterranean Conference on. IEEE, 2011.

[27] K. Narioka, and K. Hosoda, Motor development of an pneumatic musculoskeletal infant robot, Robotics and Automation (ICRA), 2011 IEEE International Conference on. IEEE, 2011.

[28] R.A. Cooper, Rehabilitation engineering applied to mobility and manipulation, CRC Press, 2010.

[29] D. Beckers, and M. Buck, Activities of Daily Living, PNF in Practice. Springer Berlin Heidelberg, pp.293-300, 2014.

[30] WHOQOL group, The World Health Organization quality of life assessment (WHOQOL): position paper from the World Health Organization, Social science & medicine, Vol.41, No.10, pp.1403-1409, 1995.

[31] Ministry of Health, Labour and Welfare, Survey on persons with physical disability, 2006.

[32] D.A. Umphred et al., Neurological rehabilitation, Elsevier Health Sciences, 2013.

[33] A. Wernig et al., Laufband therapy based on 'rules of spinal locomotion' is effective in spinal cord injured persons, Eur J Neurosci Vol.7, pp.823-9, 1995.

[34] V. Dietz et al., Laufband therapy based on 'rules of spinal locomotion' is effective in spinal man, Lancet, Vol.344, pp.1260-1263, 1994.

[35] V. Dietz et al., Locomotor activity in spinal cord in paraplegic patients, Ann Neurol, Vol.37, pp.574-582, 1995.

[36] A.L. Behrman, and S.J. Harkema, Locomotor training after human spinal cord injury: a series of case studies, Physther, Vol.80, pp.688-700, 2000.

[37] E.J. Protas et al., Supported treadmill ambulation training after spinal cord injury: a pilot study, Arch Phys Med Rehabil, Vol.82, pp.825-831, 2001.

[38] G. Colombo et al., Treadmill training of paraplegic patients using a robotic orthosis, Journal of Rehabilitation Research and Development Vol.37, No.6, pp.693-700, 2000.

[39] V. Dietz, R. Müller, and G. Colombo, Locomotor activity in spinal man: significance of afferent input from joint and load receptors, Brain Vol.125, pp.2626-2634, 2002.

[40] S. Grillner, P. Wallen, and L. Brodin, Neuronal network generating locomotor behavior in lamprey: Circuitry, transmitters, membrane properties and simulations, Annual Review of Neurosience, Vol.14, pp.169-199, 1991.

[41] N. Kojima, K. Nakazawa, and H. Yano, Effects of limb loading on the lower-limb electromyographic activity during orthotic locomotion in a paraplegic patient, Neuroscience Letters, Vol.274, pp.211-213, 1999.

[42] H. Kakou et al., Walking assist robot and its clinical application, Journal of University of Occupational and Environmental Health, Vol.31, No.2, pp.207-218, 2009.

[43] K. Hachisuka et al., A prototype walking assist robot and its clinical application for stroke patients with severe gait disturbance. In: Ring. H, Soroker. N. (Eds), Advances in Physical and Rehabilitation Medicine, Monduzzi Editore, Bolobna, pp.23-26, 2003.

[44] S. Yamamoto et al., Development of pneumatic gait assist system, Complex Medical Engineering, CME 2007. IEEE/ICME International Conference on, pp.1337-1340, 2007.

[45] T. Miyoshi et al., Robotic gait trainer in water:Development of an underwater gait-training orthosis, Disability and Rehabilitation, Vol.30, pp.81-87, 2008.

[46] T. Miyoshi et al., Functional roles of lower-limb joint moments while walking in water. Clinical Biomechanics, Vol.20, pp.194-201, 2005.

[47] C.P. Chou, and B. Hannaford, Static and dynamic characteristics of McKibben pneumatic artificial muscles, Robotics and Automation, 1994. Proceedings., 1994 IEEE International Conference on. IEEE, 1994.

[48] B. Hannaford, and J. Winters, Actuator properties and movement control: biological and technological models, Multiple muscle systems. Springer New York, pp.101-120, 1990.

[49] H.F. Schulte, The characteristics of the McKibben artificial muscle, The application of external power in prosthetics and orthotics Vol.874, pp.94-115, 1961.

[50] D.H. Chen et al., Study on Shorting Mechanics of McKibben Actuator, Transactions of the Japan Society of Mechanical Engineers. A, Vol.74, pp.442-449, 2008 *in Japanese*.

[51] D.B. Reynolds et al., Modeling the dynamic characteristics of pneumatic muscle." Annals of Biomedical Engineering Vol.31, No.3, pp.310-317, 2003.

[52] S. Davis, and D.G. Caldwell, Braid effects on contractile range and friction modeling in pneumatic muscle actuators, The International Journal of Robotics Research Vol.25, No.4, pp.359-369, 2006.

[53] T. Vo-Minh et al., Cascade position control of a single pneumatic artificial muscle-mass system with hysteresis compensation, Mechatronics Vol.20, No.3, pp.402-414, 2010.

[54] T. Vo-Minh et al., A new approach to modeling hysteresis in a pneumatic artificial muscle using the Maxwell-slip model, Mechatronics, IEEE/ASME Transactions on Vol.16, No.1, pp.177-186, 2011.

[55] T. Kosaki, and M. Sano, Control of a Parallel Manipulator Driven by Pneumatic Muscle Actuators Based on a Hysteresis Model, Transactions of the Japan Society of Mechanical Engineers. C, Vol.75, No.759, pp.3011-3018, 2009 *in Japanese*.

[56] T. Kagawa, T. Fujita, and T. Yamanaka, Nonlinear model of artificial muscle, Transactions of The Society of Instrument and Control Engineers, Vol.29, No.10, pp.1241-1243, 1993 *in Japanese*.

[57] F. Soeiro et al., Stochastic and hybrid methods for the identification in the Bouc-Wen model for magneto-rheological dampers, Journal of Physics: Conference Series. Vol.135, No.1, IOP Publishing, 2008.

[58] P. Ge, and M. Jouaneh, Modeling hysteresis in piezoceramic actuators, Precision engineering, Vol.17, No.3, pp.211-221, 1995.

[59] K. Kadota et al., Estimation of contraction force from the volume of isothermalized pneumatics artificial rubber muscles, Transactions of the Japan fluid power system society, Vol.42, No.1, pp.1-6, 2011.

[60] K. Kadota et al., Estimation of contraction rate from the volume of isothermal pneumatic rubber muscles, Transactions of the Japan fluid power system society, Vol.40, No.2, pp.17-21, 2009.

[61] R. Bouc, Modèle mathématique d'hystérésis, Acustica, Vol.24, No.3, pp.16-25, 1971.

[62] L. Ljung, System identification, Birkhäuser Boston, 1998.

[63] Y.K. Wen, Method for random vibration of hysteretic systems, Journal of the Engineering Mechanics Division, Vol.102, No.2, pp.249-263, 1976.

[64] F. Ikhouane, and J. Rodellar, Systems with hysteresis: analysis, identification and control using the Bouc-Wen model. John Wiley & Sons, 2007.

[65] F. Ikhouane, V. Mañosa, and J Rodellar, Dynamic properties of the hysteretic Bouc-Wen model, Systems & control letters, Vol.56, No.3, pp.197-205, 2007.

[66] S. Erlicher, and N. Point, Thermodynamic admissibility of Bouc-Wen type hysteresis models, Comptes rendus Mècanique, Vol.332, No.1, pp.51-57, 2004.

[67] W.T. Reutzel, and C.D. Rahn, Adaptive backstepping control of a McKibben actuator driving an inertial load, ASME 2002 International Mechanical Engineering Congress and Exposition. American Society of Mechanical Engineers, 2002.

[68] P. Carbonell, Z.P. Jiang, and D.W. Repperger, Nonlinear control of a pneumatic muscle actuator: backstepping vs. sliding-mode, Control Applications, 2001.(CCA'01). Proceedings of the 2001 IEEE International Conference on. IEEE, 2001.

[69] J. Zhong et al., One Nonlinear PID Control to Improve the Control Performance of a Manipulator Actuated by a Pneumatic Muscle Actuator, Advances in Mechanical Engineering 2014, 2014.

[70] Y. Fudaba et al., Simple adaptive control synthesis enhanced by scaling and its application to positioning control of antagonist-type pneumatic actuation mechanism, Transactions of the Institute of Systems, Control and Information Engineers, Vol.22, No.10, pp.350-356, 2009 *in Japanese*.

[71] J.M. Maciejowski, Predictive control: with constraints. Pearson education, 2002.

[72] G.C. Goodwin, P.J. Ramadge, and P.E. Caines, Discrete time stochastic adaptive control, SIAM Journal on Control and Optimization, Vol.19, No.6, pp.829-853, 1981.

[73] G.C. Goodwin, and K.S. Sin, Adaptive filtering prediction and control. Courier Dover Publications, 2013.

[74] A.H. Sayed, and T. Kailath, A state-space approach to adaptive RLS filtering, Signal Processing Magazine, IEEE, Vol.11, No.3, pp.18-60, 1994.

[75] J. Jiang, and Y. Zhang, A revisit to block and recursive least squares for parameter estimation, Computers & Electrical Engineering, Vol.30, No.5, pp.403-416, 2004.

[76] A. Visintin, Differential models of hysteresis. Vol.1. Berlin: Springer, 1994.

# Appendix A

# Bouc-Wen hysteresis model

The Bouc-Wen hysteresis model is introduced by Bouc[61]. Consider Fig. A.1, where $\mathcal{F}$ is a force and $x$ a displacement, it is shown that $\mathcal{F}$ corresponding to the point $x = x_0$ is not a function because there are four values of $\mathcal{F}$. Thereby, the force at the instant time $t$ depends not only on the displacement at the time $t$ but also on the past values of the displacement. An assumption is introduced as follows:

**Assumption 1** *Figure A.1 remains the same for all increasing functions $x(\cdot)$ between $0$ and $x_1$, for all decreasing functions $x(\cdot)$ between the values $x_1$ and $x_2$, etc*[64].

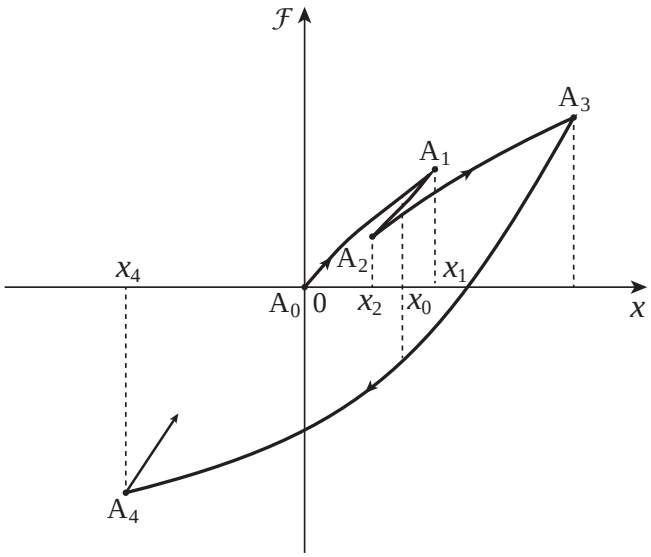


Fig. A.1: Force vs. displacement for a hysteresis

Note that Assumption 1 is called the rate-independent property[76]. The form of the functional $\mathcal{F}$ is described as

$$\frac{d\mathcal{F}}{dt} = g\left(x, \mathcal{F}, \mathrm{sign}\left(\frac{dx}{dt}\right)\right)\frac{dx}{dt}. \tag{A.1}$$

Consider the following equation

$$\frac{d^2x}{dt^2} + \mathcal{F}(t) = u_{BW}(t) \tag{A.2}$$

for some given input $u_{BW}(t)$ and initial conditions. Although Eqs. (A.1) and (A.2) can describe hysteretic oscillators completely, it is difficult to obtain the solution of Eq. (A.1) because of the nonlinearities of the function $g$. Then, an application of a variant of the Stieltjes integral to define the functional $\mathcal{F}$:

$$\mathcal{F}(t) = \mu^2 x(t) + \int_{t_1}^{t} F_{BW}(V_s^t)dx(s) \tag{A.3}$$

where $t_1 \in [-\infty, +\infty)$ is the time instant, which is given after the displacement and the force are defined. The term $V_s^t$ is the total variation of $x$ in the time interval $[s, t]$. The functional $\mathcal{F}$ is chosen to satisfy some mathematical properties. Equation (A.4) is an example given in Reference[61]:

$$\mathcal{F}(t_2) = \sum_{i=1}^{N} A_i e^{-\alpha_i t_2} \tag{A.4}$$

where $A_i$ are shown in Fig. A.1 and $\alpha_i > 0$ $(i = 1, \ldots, N)$. Equations (A.2)-(A.4) can be written by

$$\frac{d^2x}{dt^2} + \mu^2 x + \sum_{i=1}^{N} Z_i = u_{BW}(t) \tag{A.5}$$

$$\frac{dZ_i}{dt} + \alpha_i \left|\frac{dx}{dt}\right| Z_i - A_i \frac{dx}{dt} = 0 \qquad i = 1, \ldots, N. \tag{A.6}$$

Equations (A.5) and (A.6) show the Bouc-wen hysteresis model. Although the details of the model is described in Reference[61], the extension of the equations describing restoring forces with hysteresis can be expressed as

$$\dot{z} = \begin{cases} -\alpha|\dot{x}|z^n - \beta\dot{x}|z^n| + A\dot{x} & \text{for } n \text{ odd} \\ -\alpha|\dot{x}|z^{n-1} - \beta\dot{x}z^n + A\dot{x} & \text{for } n \text{ even.} \end{cases} \tag{A.7}$$

# Appendix B

# Least squares method

Consider an evaluation function for parameter estimation, the following equation is defined as

$$J_N(\theta) = \frac{1}{N}\sum_{k=1}^{N} h(k, \theta, \varepsilon_p(k, \theta)) \tag{B.1}$$

where $h(k, \theta, \varepsilon_p(k, \theta))$ is a positive scalar function expressed as

$$\varepsilon_p(k, \theta) = y_p(k) - \hat{y}_p(k|\theta). \tag{B.2}$$

Considering linear regression models such as ARX and FIR models, the predicted error can be given by

$$\varepsilon_p(k, \theta) = y_p(k) - \hat{y}_p(k|\theta) = y_p(k) - \theta^T \phi(k). \tag{B.3}$$

By choosing the function $h$ as follows

$$h(k, \theta, \varepsilon_p(k, \theta)) = \varepsilon_p^2(k, \theta), \tag{B.4}$$

the evaluation function for parameter estimation can be expressed as

$$J_N(\theta) = \frac{1}{N}\sum_{k=1}^{N} \varepsilon_p^2(k, \theta) = \frac{1}{N}\sum_{k=1}^{N} y_p(k) - \hat{y}_p(k|\theta)^2. \tag{B.5}$$

Equation (B.5) is written by

$$J_N(\theta) = \theta^T R(N)\theta - 2\theta^T f(N) + c(N). \tag{B.6}$$

where $R(N)$ is an $m \times m$ matrix, $f(N)$ an $m \times 1$ vector, and $c(N)$ a scalar, and they are given by

$$R(N) = \frac{1}{N}\sum_{k=1}^{N} \phi(k)\phi^T(k) \tag{B.7}$$

$$f(N) = \frac{1}{N}\sum_{k=1}^{N} \phi(k)y^T(k) \tag{B.8}$$

$$c(N) = \frac{1}{N}\sum_{k=1}^{N} y^2(k) \tag{B.9}$$

respectively, where $m$ is the number of unknown parameters.

Derivative of Eq. (B.6) with respect to $\theta$ gives minimalized $J_N(\theta)$, that is,

$$\nabla J_N(\theta) = 2R(N)\theta(N) - f(N) = 0. \tag{B.10}$$

Thus, the following equation called normal equation can be given:

$$R(N)\hat{\theta}(N) = f(N). \tag{B.11}$$

Then, batch least squares method can be expressed as

$$\begin{aligned} \hat{\theta}(N) &= R^{-1}(N)f(N) \\ &= \left(\sum_{k=1}^{N} \phi(k)\phi^T(k)\right)^{-1}\left(\sum_{k=1}^{N} \phi(k)y(k)\right). \end{aligned} \tag{B.12}$$